Low-temperature mica schists of Anglesey, U.K: cold subduction on the margin of Avalonia

Thesis submitted in accordance with the requirements of the University of Adelaide for an Honours Degree in Geology

Larissa Joy Collins

November 2017

THE UNIVERSITY of ADELAIDE

LOW-TEMPERATURE MICA SCHISTS OF ANGLESEY, UK: COLD SUBDUCTION ON THE MARGIN OF AVALONIA

RUNNING TITLE: COLD SUBDUCTION ON THE MARGIN OF AVALONIA

ABSTRACT

Anglesey in North Wales is considered to contain the oldest exposures of lawsonite-glaucophane blueschist in the world, marking the first appearance of lawsonite in the geological record, and heralding the emergence of truly modern subduction thermal regimes. The blueschists formed in the late Neoproterozoic during subduction beneath Avalonia. Interlayered within the blueschist unit are rare lenses of garnet-bearing metapelite that form part of a lithological association with more voluminous garnet-free metapelites. Detrital U-Pb zircon geochronology of the metapelites indicates that deposition of the protolith occurred ~630-590 Ma ago. The dominant detrital zircon ages correspond to the age of arc magmatism along the inferred margin of Avalonia, suggesting that the bulk of the detritus was derived from erosion of the arc. The presence of less abundant older zircons that range in age up to 2Ga, suggest that the arc was built on an ancient continental margin. This suggestion is supported by Nd isotopic compositions of the metapelites, which indicate derivation from an evolved source. The rare garnet metapelites contain the metamorphic assemblage garnet-muscovite-chlorite-albite-quartz-titanite-rutile-pyrite in which coronas of rutile surround titanite. Phase equilibria forward modelling of the metapelites indicates a prograde burial path that culminated with conditions around 400-450°C, at pressures of 10-12kbar. These conditions give an average thermal gradient of around 40°C/kbar, which is comparatively warm for lawsonite-bearing rocks. This suggests the Anglesey

lawsonite-bearing blueschists record the onset of global subduction thermal regimes in the late Neoproterozoic that can stabilise lawsonite, rather than simply being a fortuitous preservation of widely developed refrigerated metamorphic rock systems.

KEYWORDS

Anglesey, lawsonite, blueschist facies metapelite, geochronology, phase equilibria forward modelling

TABLE OF CONTENTS

LIST OF FIGURES AND TABLES

INTRODUCTION

Metamorphic rocks are a profound record of the secular evolution of the lithosphere's geothermal gradient regime, and consist of new mineral assemblages whose formation records heat loss over time. Metamorphic minerals, such as garnet, rutile, titanite and muscovite record the pressure and temperature of formation which can be modelled using phase equilibria forward modelling, as well as the derived P-T conditions which effectively record geothermal gradients. Around 600 million years ago, records of high pressure, low temperature blueschist facies metamorphism emerge, interpreted to result from the process of subduction, a hydrous process that enables a subducting slab to descend to depths and pressures high enough to create a cold geothermal gradient, (Tsujimori *et al.,* 2006; Tsujimori and Ernst, 2014).

An intriguing factor in the geological record of blueschist metamorphism is that blueschist facies rocks are not found older than the late Neoproterozoic (Gibbons and Mann,1983; Liou *et al*., 1990; Maruyama and Liou, 1998; Brown, 2006; Brown, 2008; Brown, 2010; Palin and White, 2015). Does this record represent a secular evolution of heat loss, or simply a preservation issue? (Maruyama and Liou, 1998). Stern, (2008) attributes the lack of ancient blueschists to a changing geothermal gradient throughout the Archean. In contrast, Palin and White (2015) suggest changes in oceanic crustal composition and not geothermal gradient are the biggest factor in the occurrence of post-Neoproterozoic blueschist. Geothermal gradient plays a large part in the preservation of blueschist facies metamorphism and only a handful of Precambrian blueschist terranes exist, and that Anglesey, Wales (Fig. 1) is one of those (Liou *et al.,*

1990). However, the geochronology and geological background in Anglesey are lacking in detail (Dallmeyer and Gibbons, 1987; Asanuma *et al.,* 2015; Asanuma *et al.,* 2017).

Anglesey, Wales (Fig. 1) is thought to be home to the oldest lawsonite- bearing blueschists in the world (Gibbons and Mann, 1983; Tsujimori *et al.,* 2006). Blueschist facies metamorphism occurs under low geothermal gradients, from 150-350°C/GPa, as part of high pressure low temperature (HPLT) regimes (Brown, 2008; Palin and White, 2015). Lawsonite is a calcium- aluminium hydrosilicate, only stable under low geothermal gradients, characteristic of cold subduction (Gibbons and Mann, 1983; Kawai *et al.,* 2006; Tsujimori *et al.,* 2006; Tsujimori and Ernst, 2014 ; Asanuma *et al.,*2017). The emergence of lawsonite at this time suggests that through the Precambrian the geothermal gradient evolved to produce lawsonite-bearing mineral assemblages, or enabled better preservation; either way implying a significant change in the Earth's thermal regime in that there are no recorded blueschist belts prior to 700 Ma (Brown, 2008; Tsujimori and Ernst, 2014).

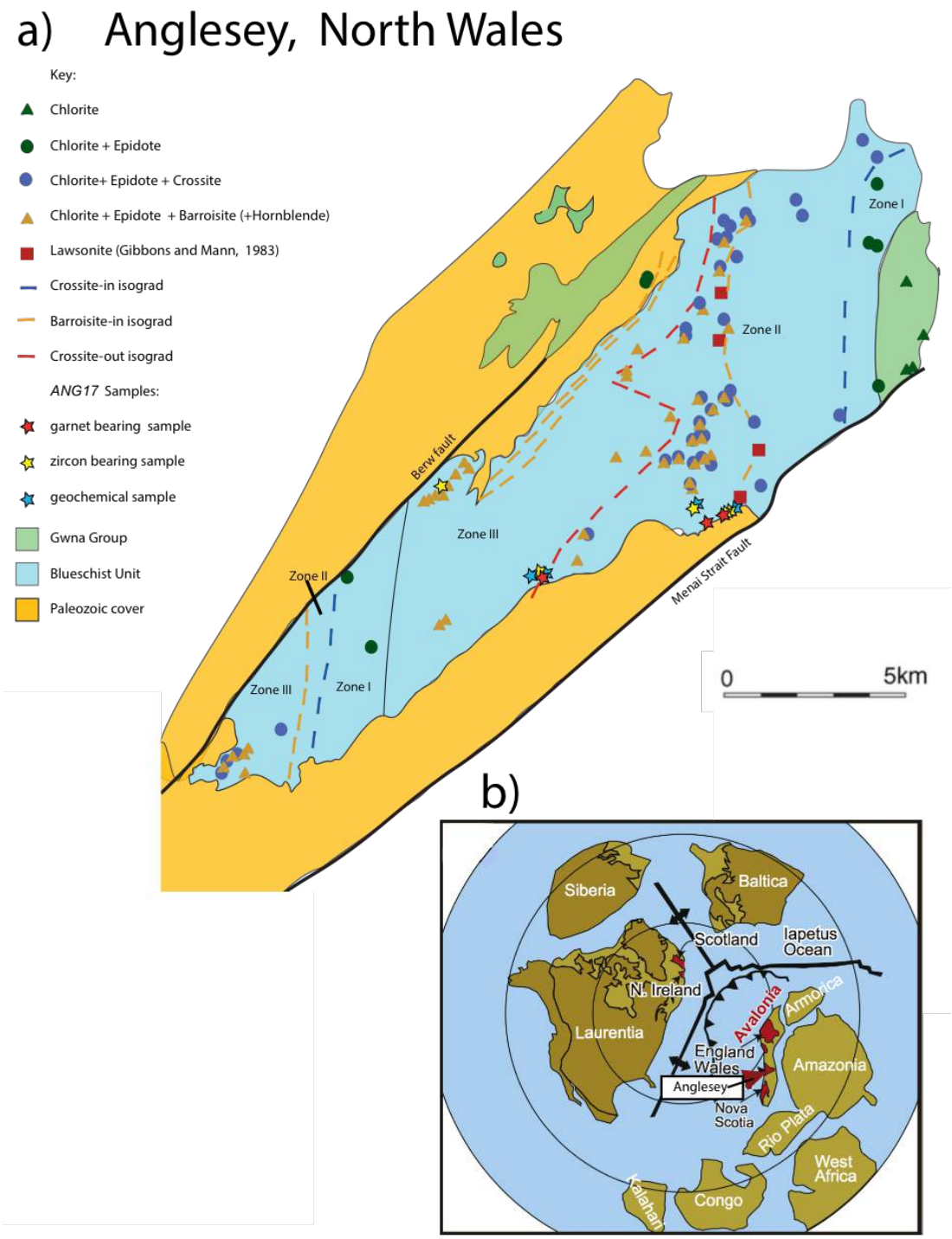

Figure 1: Location map of Anglesey, Wales. Stars illustrate where samples were obtained. Map modified from Kawai *et al*., (2006) and Kawai *et al,* (2007) with the addition of the lawsonite isograd from Gibbons and Mann, (1983). Figure 1b) shows the location of Anglesey and most of the United Kingdom on the margin of Avalonia in the Neoproterozoic to Early Cambrian, and their role in the amalgamation and assembly of Gondwana, modified after Asanuma, *et al.,* (2017) and Santosh , *et al.,* (2014).

The focus of this study is to examine garnet-bearing metapelites that are interlayered with the blueschists. These rocks have not been previously examined in detail and offer an avenue to explore the conditions of formation of the blueschist belt.

Provided that the interbedded pelites record the same metamorphic characteristics as the blueschists, the metapelites should effectively record the P-T conditions of the Anglesey blueschist belt. Based on this logic, the pelites will be used to obtain an overall P-T estimate of the evolution of both the metapelite and blueschist unit. This hypothesis will be tested through the use of U-Pb detrital zircon geochronology and εNd isotopes to determine the source region and protolith of the Anglesey mica schists, as well as phase equilibria forward modelling to determine if the pelitic schists did actually form under cold conditions in the Neoproterozoic. The detrital geochronological data will also support or refute the hypothesis that the metapelites are indicative of an autochthonous subduction setting, contrasting the interpretation that Anglesey was part of an allochthonous subduction terrane transported by a strike-slip fault (Gibbons and Mann, 1983; Gibbons, 1983). The primary aim of this thesis is to investigate the tectonic, petrographic and paleogeographic relationships of the metapelites to the Anglesey blueschist belt using mineral equilibria modelling and U-Pb detrital zircon spectra to better understand the evolution of the blueschist facies metamorphism and also the geological context into the secular evolution of Earth.

GEOLOGICAL SETTING AND BACKGROUND

Anglesey in North Wales, (Fig. 1), is home to the oldest known lawsonite-bearing blueschists (Brown, 2008; Tsujimori and Ernst, 2014). A characteristic mineral of

blueschist facies metamorphism, lawsonite is stable at very low temperatures and thus diagnostic of a HPLT regime (Gibbons and Mann, 1983; Strachan, 2012). Gibbons and Mann, (1983) showed that the blueschists with interbedded metapelites outcrop in 3 main units, the Central unit, the Aethwy unit and the Lleyn unit, where the Lleyn unit is likely an analogue of the Aethwy unit, as the ages and lithological units are similar (Gibbons and Horak, 1990; Strachan, 2012; Asanuma *et al*., 2015; Asanuma *et al.,* 2017). The majority of these schists are blueschist-imprinted-on-greenschist facies, where the blueschists overprints indicate a local tectonic control on the preservation of the HPLT metamorphism (Gibbons and Mann, 1983).

The Anglesey Blueschist Unit extends on a NE-SW trend for 5 x 25 kilometres, on the island of Anglesey bound by the steeply-dipping Berw and Menai Strait faults (Fig. 1; Kawai *et al.,* 2006; Kawai *et al.,* 2007) and barroisite/crossite rich lenses within the blueschist unit have an Ar-Ar metamorphic age of ~560-550Ma, interpreted as the cooling age (Liou *et al*., 1990; Kawai *et al.,* 2006; Kawai *et al.,* 2007; Asanuma *et al.,* 2015). Table 1 provides a summary of existing geochronology across Anglesey. Lleyn Peninsula in the southwest of the island shows the continuation of the blueschist unit (Gibbons and Mann,1983; Maruyama and Liou, 1998; Kawai *et al.,*2006; Kawai *et al*., 2007; Asanuma *et al.,* 2015). Paleogeographic reconstructions suggest that throughout the Neoproterozoic, Anglesey sat on the border of Western Gondwana, on a microcontinent called Avalonia (Fig. 1b; Gibbons and Horak, 1996). Avalonia was accreted in the early Paleozoic, and Anglesey is suggested to have rifted off (Stern, 2005; Stern, 2008).

The Anglesey blueschist unit occurs mainly as mafic, micaceous fine-grained schists with minor metabasite lenses (Gibbons and Mann, 1983; Gibbons, 1983; Asanuma *et al.,* 2017). The three metamorphic zones within the blueschist unit are mica schists, phengite schists, and epidote-glaucophane blueschists (Gibbons, 1983; Kawai *et al.,* 2006; Treagus, 2007; Asanuma *et al.,* 2015). Zones I, II and III are defined by mineral isograds, where zone I is defined by epidote-chlorite metabasites, zone II is crossite-epidote, and zone III is barroisite-epidote, each zone separated by the crossite and barroisite isograds (Fig. 1; Gibbons, 1983; Asanuma *et al.,* 2015). Lawsonite (Fig. 1) is present in zone II and appears to follow a series of ductile shear zones and separated by a large fault through the middle of Anglesey (Dallmeyer and Gibbons, 1987; Kawai *et al.,* 2006). The Anglesey blueschists consist of fine-grained, foliated rock, containing epidote, glaucophane, amphibole schist; both barroisite and crossite, with quartz, chlorite, sphene, hematite, magnetite, with lawsonite (Dallmeyer and Gibbons, 1987; Gibbons and Mann, 1983; Gibbons, 1983; Kawai *et al.,* 2006; Kawai *et al.,* 2007).

Blueschists are thought to form only by subduction, based on the association between ancient subduction mélanges and blueschist facies metamorphism (Brown. 2008; Sizova *et al.,* 2010). Blueschist terranes require more than just simple crustal thickening to achieve cold geothermal gradients, (Stern, 2005; Brown, 2008; Sizova *et al.,* 2010). Controls on the rate of cold subduction are the thermal regime, age of slab, density and indirectly composition (Stern, 2005;Brown, 2008; Sizova *et al.,* 2010). Brown (2008) argues that multiple studies suggest that the dehydration of the slab is controlled by the thermal structure of the subduction zone as a function of age and plate velocity, which

in may explain how the subduction zone may be significantly cooler at depth where older oceanic lithosphere is subducted, in comparison to subducting younger lithosphere.

One way of achieving a colder geothermal gradient is through water being carried into the mantle wedge by lawsonite in a modern cold subduction zone (Maruyama and Okamoto, 2006; Brown, 2008). However, Zheng *et al*., (2016) argue that the breakdown hydrous minerals such as chlorite is more commonly responsible for hydrating the downgoing slab and lowering the temperature under comparatively higher thermal gradients. A commonly accepted interpretation is that the Anglesey blueschists represent an accretionary paleo-subduction zone. The Anglesey Blueschist unit was part of a shallowly dipping slab, exhumed from ~ca. 35km to an upper crustal depth of ~6km into an accretionary complex to the north west of Anglesey (Kawaii *et al*., 2007).

Bias in the geological record could provide a caveat to this interpretation; the lack of blueschist facies and high-pressure metamorphism to ultra-high-pressure metamorphism (HPM-UHPM) prior to the Neoproterozoic may be due to preservation issues, or overprinting (Brown, 2008). Brown, (2008) also suggests that HPM-UPHM metamorphism under low-to-intermediate geothermal gradients is an analogue for modern subduction in early stages of subduction-to-collision accretionary orogenesis.

Brown (2008), speculates that there is a close relationship between the age of metamorphic belts characterized by extreme metamorphism and the supercontinent cycle, reflected in how subduction-to-collision accretionary orogenesis records the amalgamation of continental lithosphere into supercontinents via metamorphism. A lot

of controversy surrounds whether the Anglesey blueschist unit was part of a subduction-accretion orogenic system, also known as 'Pacific' or 'Cordilleran' type, formed mainly in periods of plate convergence, or a subduction-collision orogenic system; also known as 'Himalayan' type, formed under ocean closure in assembly of supercontinents (Nance *et al.* 2002; Brown, 2006; Kawaii *et al*., 2007; Liou *et al.,* 2010). Brown (2006) also suggests that the two types may over-print on each other, making it hard to distinguish which regime the Anglesey blueschists formed in. The mode of subduction is disputed as to whether the subduction regime is autochthonous or allochthonous, each having a different signature on the rocks in the form of detrital zircon provenance; allochthonous arcs giving a comparatively unimodal detrital signal, where autochthonous arcs would result in more evolved detritus as eroded arc material would have more opportunity to mix with older sources from erosion of the basement to the arc.

Table 1: Summary of previous geochronological work across Anglesey Island and the neighbouring Lleyn Peninsula.

	Age	Geochronological Method	Reference
Blueschist Unit	566±11 Ma 549±10 Ma 545±10 Ma 530 ±10 Ma	K-Ar (Minimum depositional age; metamorphic ages)	Asanuma *et al., (2017).*
	586-582 Ma 574-565 Ma 560-550 Ma	Ar-Ar (cooling age)	Dallmeyer and Gibbons, (1987)
Penmynydd Schists (part of the blueschist unit)	560-550 Ma	Ar-Ar (metamorphic cooling age)	Dallmeyer and Gibbons, (1987)
Central Shear Zone	575±11 Ma 578±11 Ma	K-Ar (Minimum depositional age; metamorphic ages)	Asanuma *et al.,* (2017)
Gwna Group (Anglesey Island)	571 ±20 Ma 878 ± 43 Ma 550 ± 24 Ma	U-Pb LA-ICP-MS (weighted average/maximum depositional ages reported)	Asanuma *et al.,* (2017)
Gwna Group	608-601 Ma 564-539 Ma		Asanuma *et al.,* (2015)

(Lleyn Peninsula)			
New Harbour Group	474 ±9 Ma	K-Ar (Minimum depositional age; metamorphic ages)	Asanuma *et al.,* (2017)
South Stack Group	501 ±10 Ma	U-Pb SIMS (maximum depositional age reported)	Collins and Buchan, (2004)

ANALYTICAL METHODS

Bulk rock geochemistry

Whole rock geochemical analyses were provided for samples *ANG13a* and *ANG13b*, through the use of Wavelength Dispersive X-ray Fluorescence (WD-XRF) spectrometry. This process was undertaken at the Department of Earth and Environment, Franklin and Marshal College, Lancaster, PA, USA. Major elements analysed were SiO_2, TiO_2, Al_2O_3, Fe_2O_3 (total), MnO, MgO, CaO, Na_2O, K_2O, P_2O_5, FeO and Fe_2O_3, analysed on fused disks prepared by using a lithium tetraborate flux. The amount of ferric to ferrous iron content was determined by titration.

Zircon U-Pb geochronology

Samples were crushed, sieved, separated and mounted using magnetic and heavy liquid techniques. Zircon mineral separates were mounted separately in epoxy resin then polished and carbon coated prior to cathodoluminescence imaging on the Scanning Electron Microscope. Scanning Electron Microscopy was conducted using the FEI Quanta 600 MLA Scanning Electron Microscope with a Gatan Cathodoluminesence detector in order to image the surface of the carbon coated zircon mounts before LA-ICP-MS. This was done at Adelaide Microscopy.

U-Pb LA-ICP-MS

Detrital zircons from the 79-400 μm and >79μm fractions of samples ANG8, ANG12a, ANG12b, ANG17, ANG18, and ANG20 were analysed through Laser Ablation-Inductively Coupled Plasma-Mass Spectrometry. Radiogenic U-Pb isotopic data were collected using LA-ICP-MS on mounted detrital zircon grains, using the Agilent7500cx NewWave 213nm Nd:YAG laser at Adelaide Microscopy. Methodology followed that of Payne *et al.,* (2006). The zircon signal acquisition was taken with 30 seconds background measurement and sample ablation, and measured against the known GJ, Plesovice and 91500 zircon standards. Ablation size was 30micron at 5Hz with 29% fluency. Zircon isotopic data was reduced using Iolite and IgorPro software (Paton , *et al.,* 2011). All errors are at 2σ unless otherwise mentioned.

Garnet *ε*Nd isotopes

Garnets were separated from the crushed aggregate by SelFrag, magnetic separation and hand picking. Samples *ANG13a ANG13b*, *ANG15a* and *ANG16* were sent away to Curtin University where they underwent SelFrag, a mineral separation technique that collects aggregate grains intact. This was necessary as the fine-grained nature of the garnet made for difficulties in their separation. Fractions of pure garnet as well as whole rock powders of the aforementioned samples were provided to David Bruce, who underwent Thermal Ionisation Mass Spectrometry to determine the *ε*Nd concentrations. Methodology followed that of Payne, *et al.,* (2006), modified to account for a 12ohm amplifier. Nd isotopes of garnet were measured on a 12Ω amplifier, where whole rock was measured with an 11Ω amplifier, carried out on a Isotopx Phoenix Thermal Ionisation Mass Spectrometer. 100 ratios were taken at a minimum, and then corrected

to a set $^{146}Nd/^{144}Nd$ ratio of 0.7219. The standard used was JNdi-1 TIMS reference material.

LA-ICP-MS maps of garnet

Two thin sections containing garnet (ANG13b and ANG15a) were analysed using LA-ICP-MS on the Agilent 7700s Resonetics 193nm laser to determine the trace element abundance. Several garnets from both thin sections were analysed by transect, and one from each thin section was mapped in rasters. Spot sizes on the transects were 29μm, and the spot size for the maps were 51μm rasters. The standards used were NIST-612 and GSD. Iolite was used to reduce the data, using Si as the index element and to create the trace element images (Paton, *et al.,* 2011).

Electron probe microanalyses methods

Elemental compositions of garnet were obtained by a Cameca SXFive electron microprobe at Adelaide Microscopy. For each analysis, a beam of 20nA was set, and a correction method was applied, and measurements of SiO_2, ZrO_2, TiO_2, ZnO, Al_2O_3, FeO, MnO, MgO, CaO, Ce, P_2O_5, Na_2O, K_2O and Cl were collected from Wavelength Dispersive Spectrometers (WDS). The probe was calibrated using an andradite crystal prior to analyses, using Fe and Al standards.

Phase equilibria forward modelling

Pressure-temperature pseudosections

P-T pseudosections for samples *ANG13b* and *ANG15a* were calculated using THERMOCALC, a phase-equilibrium modelling program (Powell & Holland, 1988).

THERMOCALC v. 3.40 was used, with an internally consistent thermodynamic dataset 'ds6' of Holland and Powell, (2011). Pseudosections were calculated in the MnNCKFMASHTO (MnO-Na_2O-CaO-K_2O-FeO-MgO-Al_2O_3-SiO_2-H_2O-TiO_2- Fe_2O_3) system (White *et al.,* 2014). The following activity-composition models were used; garnet, chlorite, plagioclase and biotite (White *et al.,* 2014), muscovite (Smye *et al.,* 2010) and stilpnomelane, (Holland and Powell, 2011). Whole-rock XRF analyses from the EPMA were recalculated with an apatite-removing correction. Apatite is not able to be modelled using THERMOCALC, and its presence as a peak mineral would significantly affect the rock Ca content. Thus, apatite was removed through converting the wt% amount of P_2O_5 to a molar amount, normalised by the total to get the proportion of P_2O_5 in a bulk composition. This number was then multiplied by 3.33, on the assumption that an ideal apatite formula is $10CaO{:}3P_2O_5$. This gave the proportion of CaO hosted in apatite, and was then subtracted from the original proportion of CaO. Pyrite, another peak mineral, is unable to be modelled by THERMOCALC and as such left out. The presence of pyrite indicates a more reduced system, which affects the proportion of Fe_2O_3 converted to FeO. The presence of phengite suggests a hydrous mineral assemblage, as well as the interbedded-lawsonite-bearing blueschists, thus H_2O was set to excess. Prior to the calculated P-T pseudosections, temperature- oxidation (T-Mo) diagrams were started to better constrain the peak assemblage g-chl-mu-ru-q-sph-ab. The stability of the assemblage over a large range of temperatures led to an average composition (x) taken from the middle of the peak field to start the pseudosections.

Phase abundance contours

TCInvestigator, a Matlab-based software, was used to create the 'normalised' phase abundance contours of the modelled P-T pseudosections (Pearce *et al.,* 2015). The

modal proportions of garnet, chlorite, albite, phengite, titanite rutile and quartz were calculated.

RESULTS

Samples

Table 2: Sample descriptions and localities (WGS84, 30u)

Sample	*Location (UTM) WGS84,30u*	*Description*	*Analysis*
ANG8	0413755, 5897440	Rock sample	Detrital Zircon U-Pb Geochronology
ANG12a	0416603, 5895749	Rock sample	Detrital Zircon U-Pb Geochronology
ANG12b	0416603, 5895749	Rock sample	Detrital Zircon U-Pb Geochronology
ANG13a	0416510, 5895766	Rock sample	Garnet Sm-Nd Geochronology,
ANG13b	0416510, 5895766	Rock sample, Thin section	Garnet Sm-Nd Geochronology, Trace Element mapping, Phase Equilibria forward modelling
ANG15a	0416667, 5895692	Rock sample, Thin section	Garnet Sm-Nd Geochronology, Trace Element mapping, Phase Equilibria forward modelling
ANG16	0416673, 5895731	Rock sample	Garnet Sm-Nd Geochronology
ANG17	0420539, 5297058	Rock sample	Detrital Zircon U-Pb Geochronology
ANG18	0420539, 5297058	Rock sample	Detrital Zircon U-Pb Geochronology
ANG20	0420914, 5897320	Rock sample	Detrital Zircon U-Pb Geochronology

Petrography

ANG13B

Sample *ANG13b* is a garnet-bearing quartz-mica schist, interpreted to have formed from an interbedded metapelite within the Anglesey Blueschist Belt. *ANG13b* contains peak garnet, chlorite, phengite, quartz, albite, titanite, rutile, apatite and pyrite. Fine grained garnet, up to 0.5mm, (Fig. 2a; 2c) contains quartz, chlorite and titanite inclusions. Rutile partially replaces titanite, a reaction texture shown in (Fig. 2g), and in places is intergrown with chlorite (Fig. 2a). Quartz, muscovite and chlorite demonstrate small scale folding, and show a foliation (Fig. 2b). Pyrite is partially replaced by limonite.

Retrograde chlorite also grows post-garnet, as shown by the foliation wrapping around garnet.

ANG15A

Sample *ANG15a* is also a garnet-bearing quartz-mica schist, and has similar mineralogy as *ANG13b*, with the absence of apatite. Peak minerals in *ANG15a* are garnet, chlorite, quartz, muscovite, albite, titanite, rutile, and pyrite. Furthermore, rutile is shown to overgrow titanite, as shown in *ANG13b* (Fig. 2g). Rare zircons are present in the matrix, (Fig. 2d), and are ~50μm in length. Comparably to *ANG13b,* fine grained garnets appear up to ~0.5mm, and define a foliation (Fig. 2e). The foliation is defined by quartz, muscovite and albite (Fig. 2f).

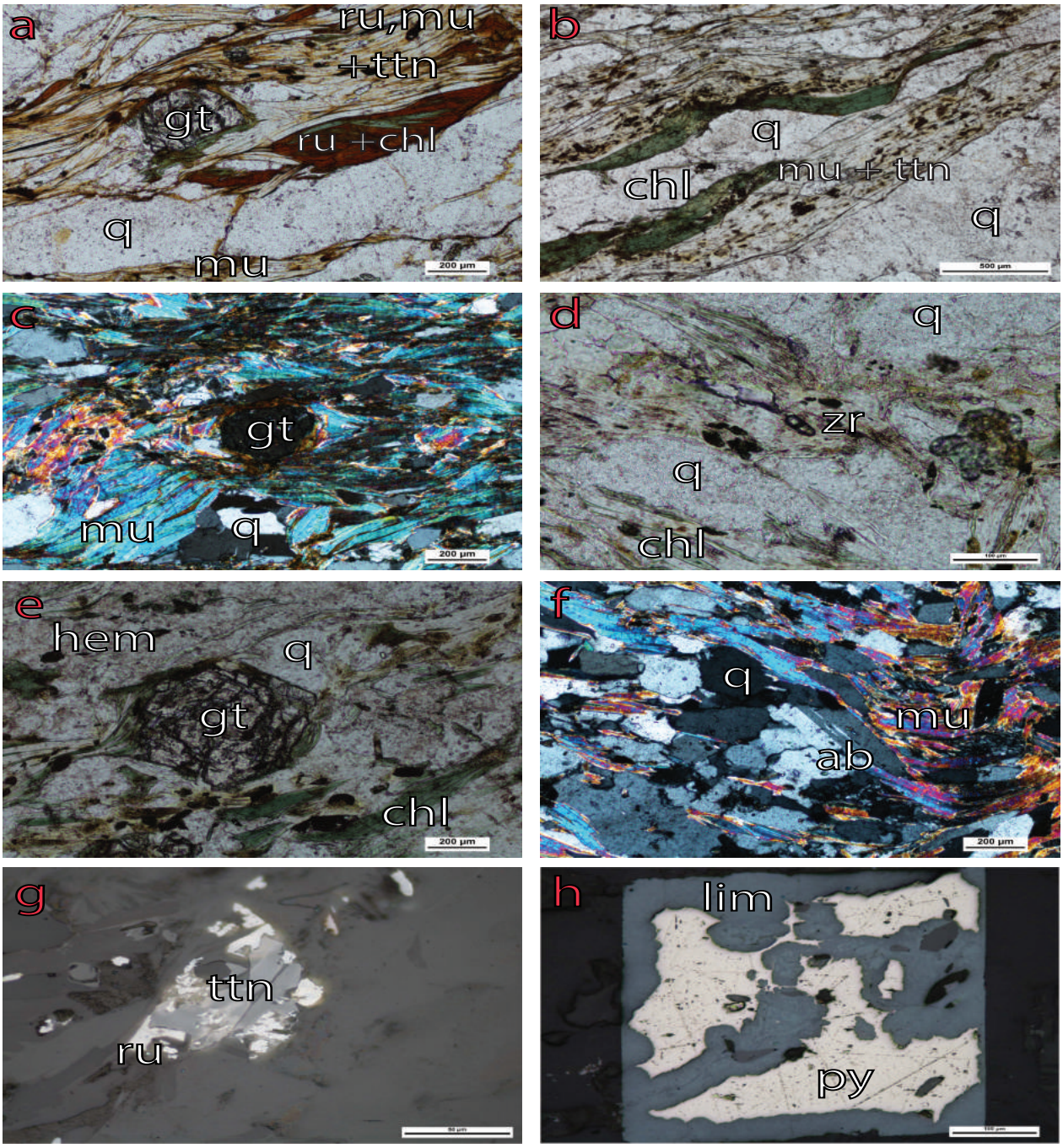

Figure 2: Photomicrographs of thin sections *ANG13b* and *ANG15a*. A) *ANG13B* in PPL; Garnet wrapped by the foliation between muscovite (phengite), quartz and chlorite. Rutile coexists with chlorite. B) *ANG13B* in PPL shows the foliated chlorite, quartz and mica with titanite inclusions. C) *ANG13B* in XPL displaying how garnet is wrapped by the foliation. D) *ANG15a* in PPL showing a zircon in situ, as well as the similarity between samples. E) *ANG15a* in PPL showing garnet and chlorite foliation, and the oxides contained to the mica. F) *ANG15a* in XPL, displaying albite and quartz veins, and muscovite. G) *ANG13b* in reflected light, showing rutile replacing titanite. H) *ANG15a* in reflected light, showing relict pyrite being replaced by limonite.
Abbreviations: ab: albite, chl: chlorite, gt: garnet, lim: limonite, mu: muscovite, py: pyrite, q: quartz, ru: rutile, ttn: titanite, zr: zircon.

Zircon U-Pb geochronology

Detrital zircon mounts were analysed for U-Pb geochronology using LA-ICP-MS, on samples *ANG8, 12a, 12b, 17, 18* and *20.* The small size of the zircon made finding enough grains to mount difficult, as the few zircons present were mostly <79μm, which is why the decision was made to mount the <79μm fraction for samples *12a, 12b, 18* and 20, as well as the >79μm of samples *8, 12a, 12b, 17*. Ideally, the spectra from both sized fractions of all samples would be included, but the nature of the few, small zircon made this challenging. Full data table and standard information can be found in Appendix A. Following Asanuma *et al.,* (2017), probability density estimates were calculated using the $^{207}/^{206}$ Pb ages for analyses older than 1000 Ma, and the ^{206}Pb/^{238}U ages for analyses younger than 1000 Ma.

ANG8

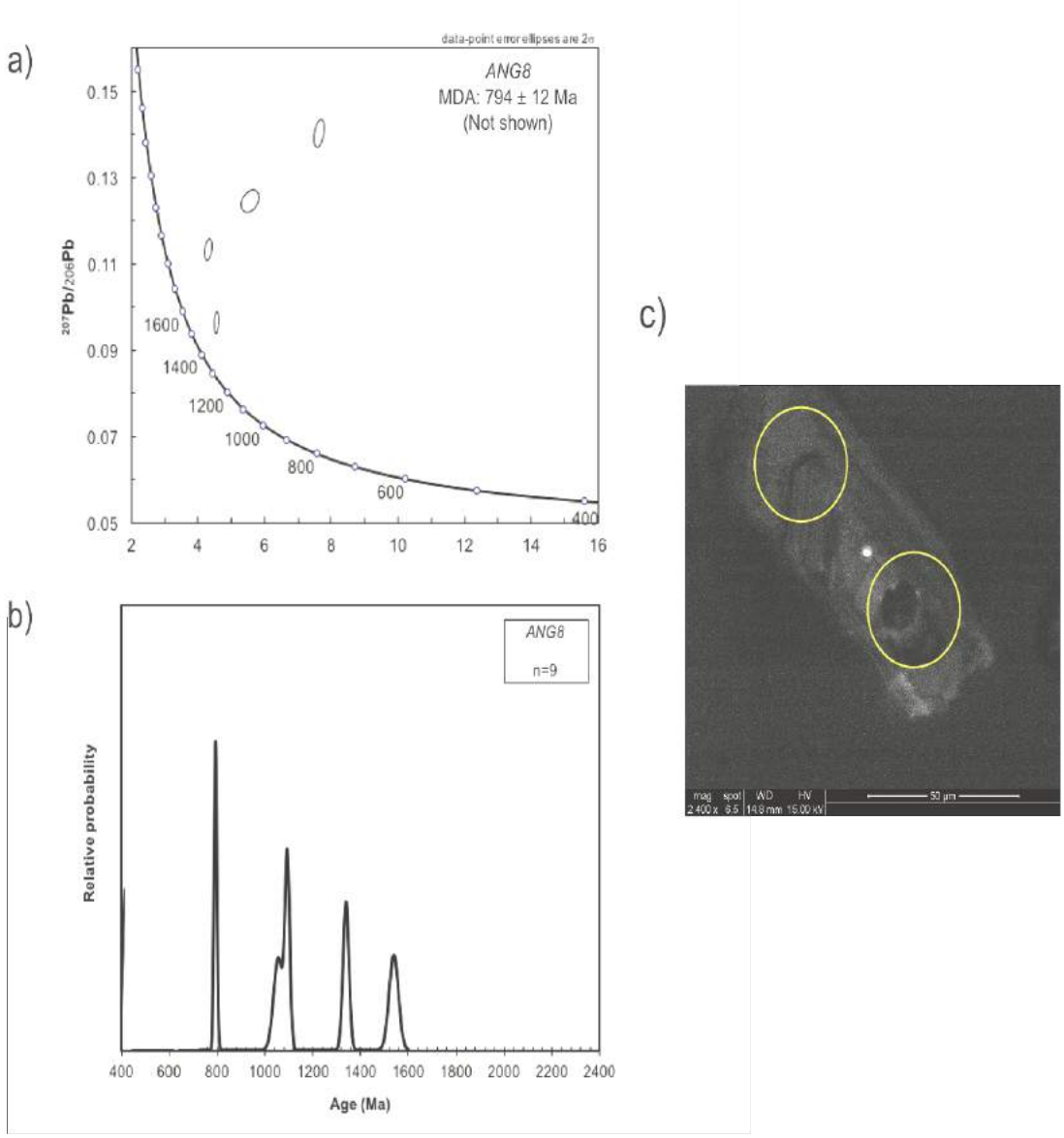

Figure 3: U-Pb analyses of *ANG8*. *a*) Terra-Wasserburg plot of 4 analyses within 30% concordance. b) Probability density estimate, showing a peak at ~631.1 ± 9.3Ma. c) Cathodolumiscence image of a zircon, showing scaled 30µm laser spots of the youngest zircon of *ANG8*.

4 analyses within ± 30% concordance were used to create Fig. 3, although Fig. 3a presents a lead-loss trend between 1600-400Ma. The maximum depositional age (MDA) of *ANG8* is 794 ± 12 Ma, constrained by the youngest concordant detrital zircon of the population. The dominant peak of Fig. 3b is the MDA, but this sample has such low concordance it is not a good representative of the sample.

ANG12a

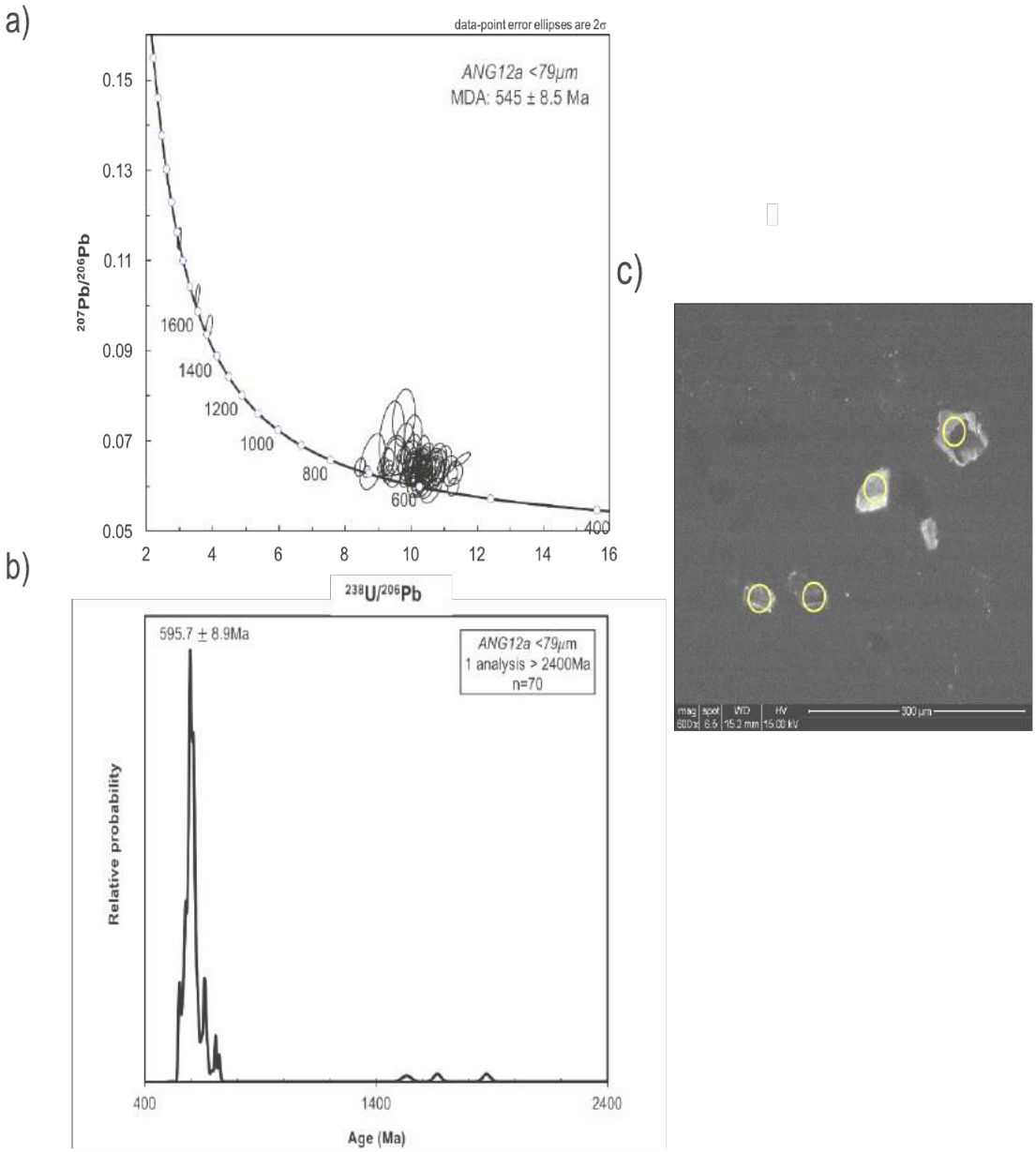

Figure 4: Detrital spectra for *ANG12a* <79*μ*m. a) Terra- Wasserburg plot, showing a cluster ~600Ma. b) Probability density estimate showing a peak at 595.7 ± 8.9Ma. c) Cathodoluminescent image of zircons, showing the scaled laser spot, and the small nature of the <79*μ*m zircons.

70 analyses ±30% concordance were dated, yielding an MDA of 545.5 ± 8.5 Ma, and the peak in Fig. 4b shows the age (595.7 ± 8.9 Ma) reflected by the highest number of zircons in the sample.

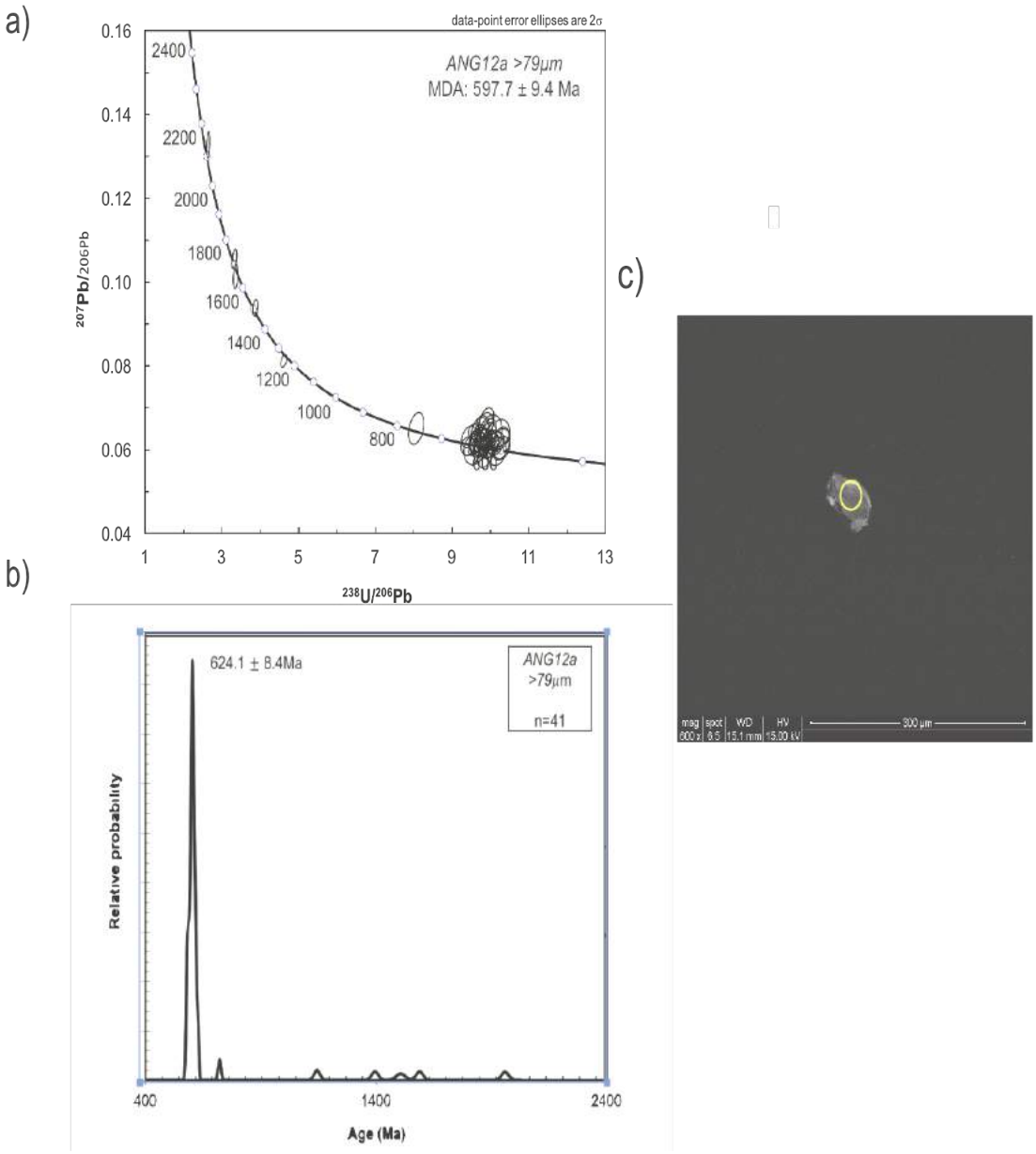

ANG12a Figure 5: U-Pb spectra of the >79μm fraction of *ANG12a.* a) Tera- Wasserburg plot, showing a cluster ~600Ma. b) Probability density estimate showing a peak at 624.1 ± 8.4Ma. c) Cathodoluminescent image of the zircon responsible for the MDA with scaled laser spot.

The >79μm fraction of *ANG12a* had 41 analyses within ± 30% concordance, with an MDA of 597.7 ± 9.4 Ma, and the peak in Fig. 5b. reflects an age of 624.1 ± 8.4 Ma.

ANG12b

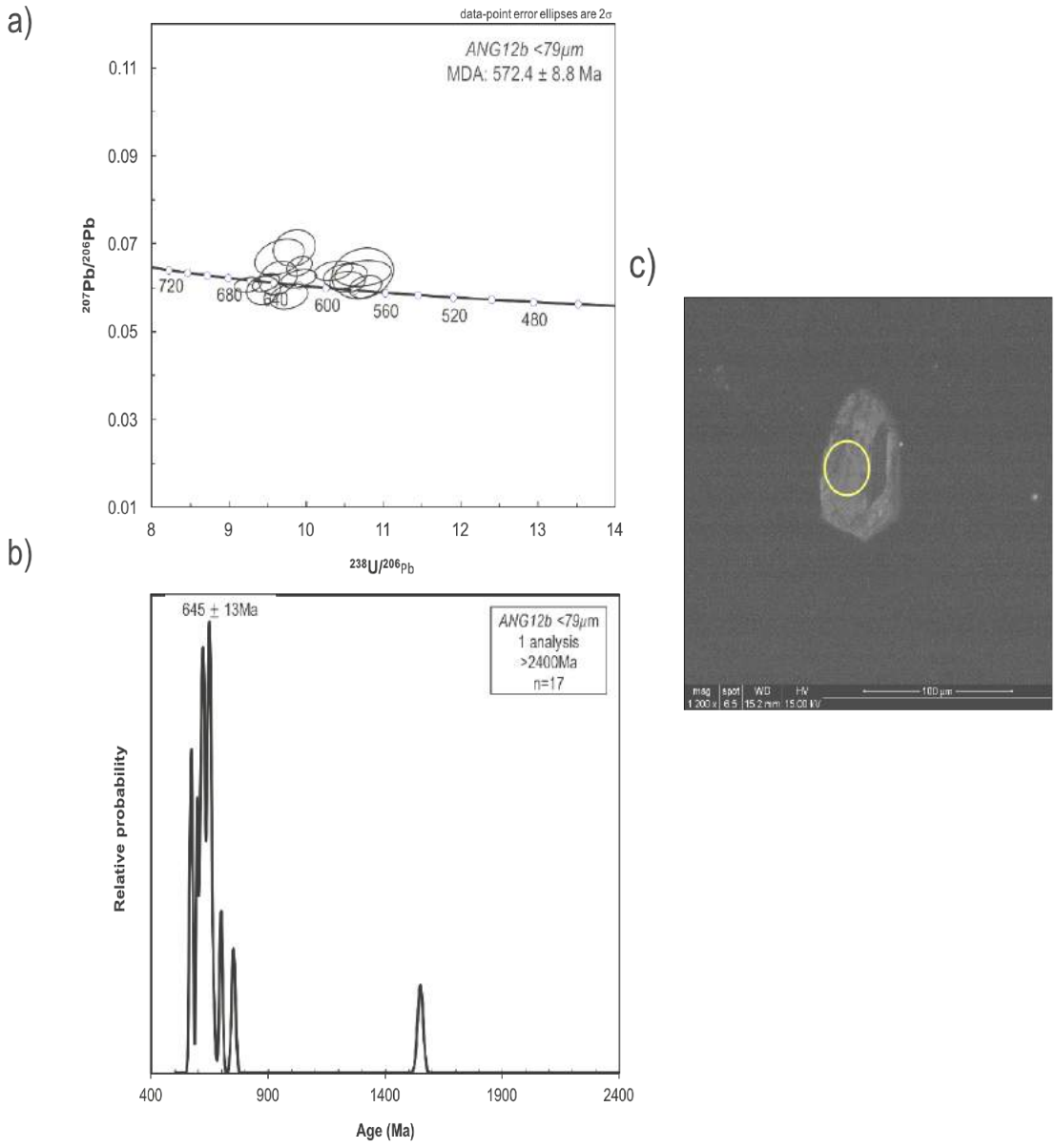

Figure 6: Detrital spectra for *ANG12b* <79µm. a) Tera- Wasserburg plot, showing a cluster ~680-600Ma. b) Probability density estimate showing a peak at 645 ± 13Ma, with a minor peak ~1500Ma. c) Cathodoluminescence image of the youngest zircon and scaled laser spot.

17 analyses ± 30% concordance yield an MDA of 572.4 ± 8.8 Ma, and the PDE in Fig. 6b shows two peaks; a major peak ~700-500Ma, and ~1500Ma. The zircon in Fig. 6c is the youngest zircon in the sample.

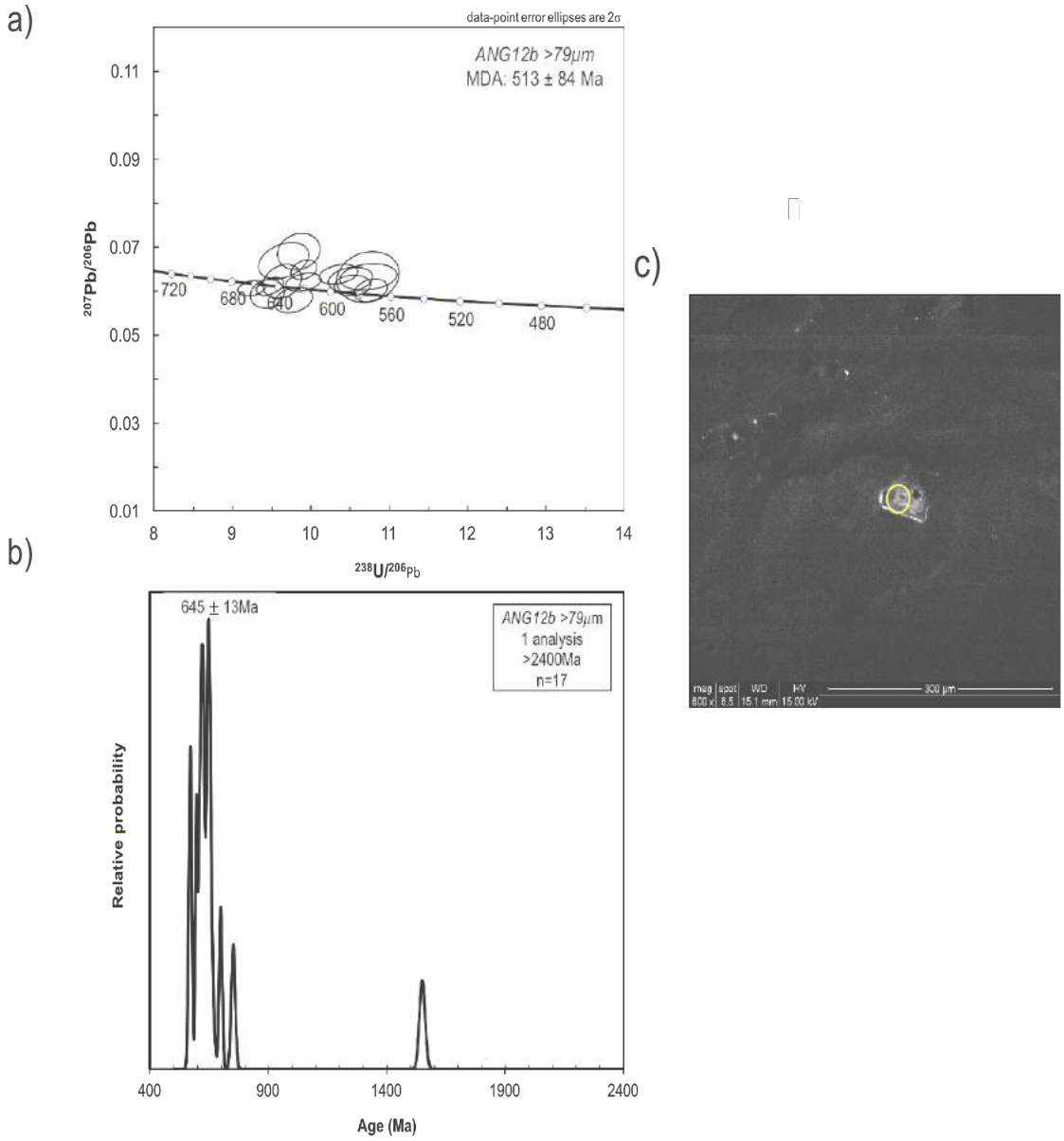

Figure 7: U-Pb spectra of the >79µm fraction of *ANG12b*. a) Terra- Wasserburg plot, showing a cluster ~680-560 Ma. b) Probability density estimate showing a peak at 645 ± 13 Ma. c) Cathodoluminescent image of the youngest zircon, showing zoning.

17 analyses ± 30% concordance were dated, with an MDA of 513 ± 84 Ma, and the peaks in Fig. 7b are similar to that of the <79μm fraction (Fig. 6b).

ANG17

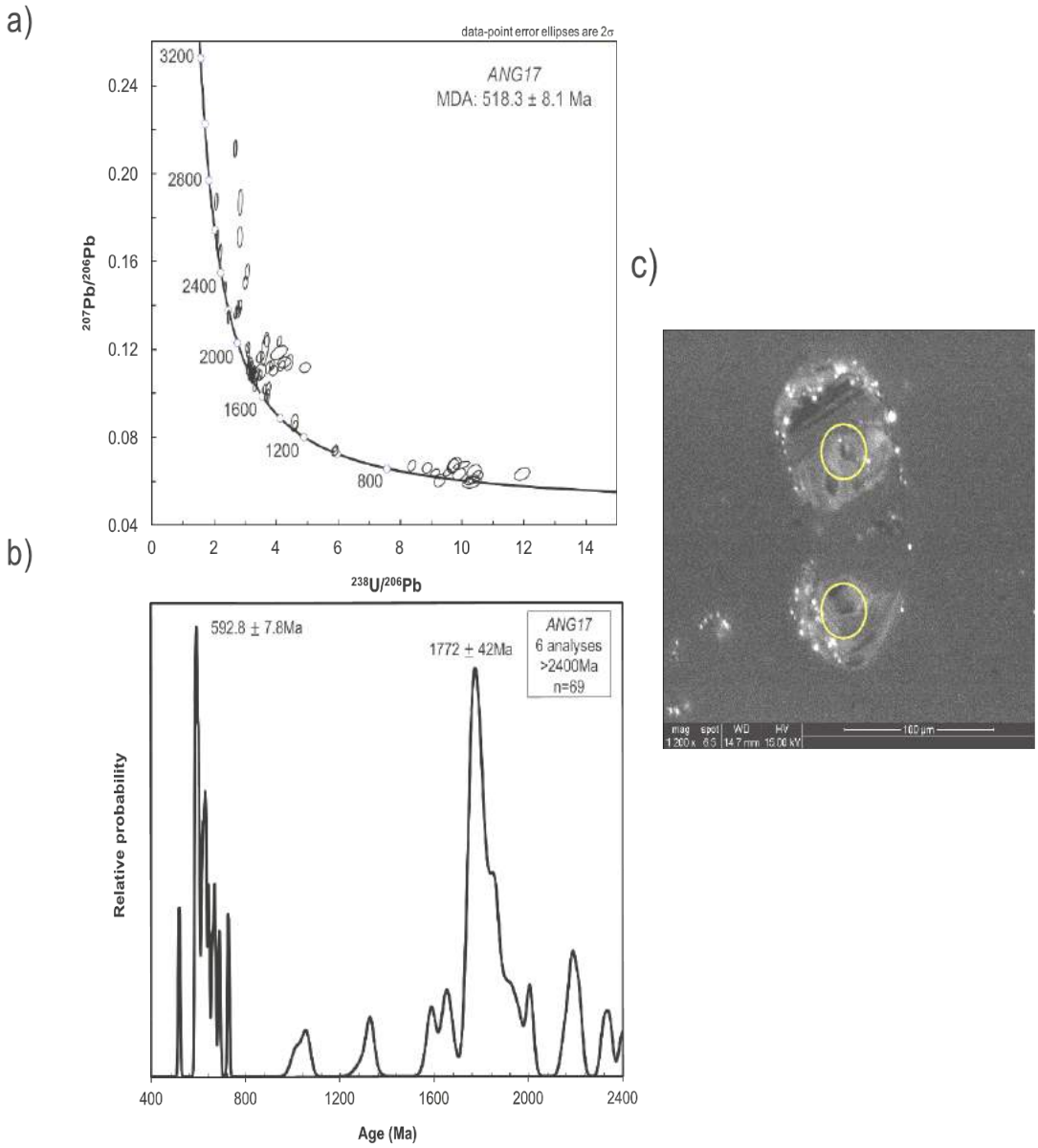

Figure 8: U-Pb analyses of *ANG17*. a) Terra-Wasserburg plot. b) Probability density estimate, showing peaks at ~592.8 ±7.8 Ma, and 1772 ±42 Ma. c) Cathodolumiscence image of youngest zircon.

69 analyses ± 30% concordance resulted in an MDA of 518.3 ± 8.1 Ma, and the peaks in Fig. 8b are different to previous samples, as the relative probability of the older peak reflects a large number of zircons of an older age. A modern lead loss trend is apparent (Fig. 8a).

ANG18

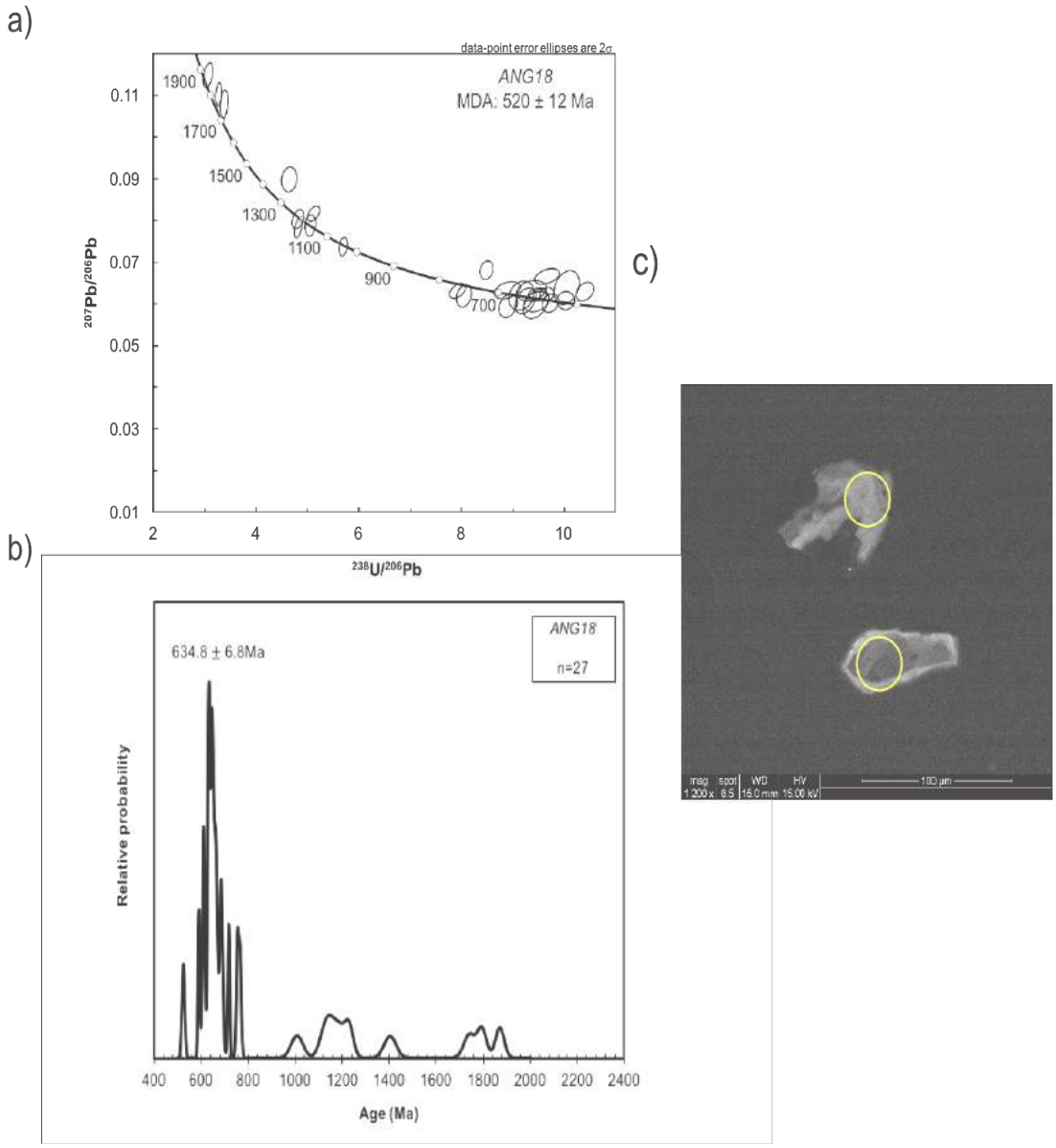

Figure 9: U-Pb analyses of *ANG18.* a) Terra-Wasserburg plot. b) Probability density estimate, showing peaks at 634.8 ± 6.8 Ma, and minor peaks between 2000-1000 Ma. c) Cathodolumiscence image of youngest zircon, with no zoning evident.

27 analyses ± 30% concordance were dated, with an MDA of 520 ± 12 Ma, and the peaks in Fig. 9b are different to previous samples, as the spread of the older peaks are not a recorded by many zircons in the sample.

ANG20

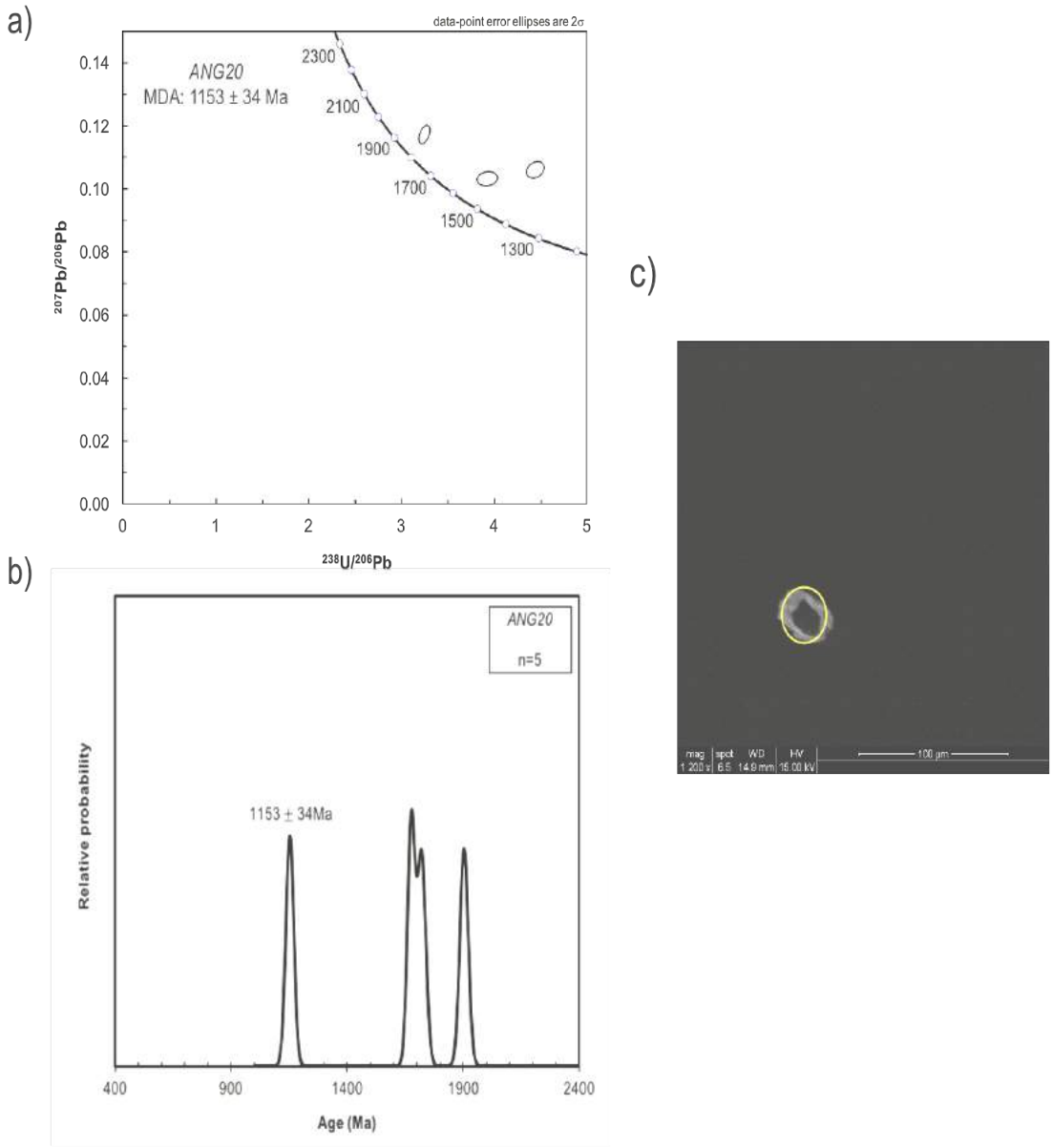

Figure 10: U-Pb analyses of *ANG20.* a) Terra-Wasserburg plot. b) Probability density estimate, showing peaks at 1153 ± 34Ma, and minor peaks between 2000-1000 Ma. c) Cathodolumiscence image of youngest zircon, with the core of the zircon unusually dark and lack of evident zoning.

ANG20 has 5 analyses within 30% concordance, and is by no means statistically robust, but substantiates the difficulty in U-Pb dating of small, fine grained zircon. The overall data from the pelitic schists suggest maximum depositional ages ~520-600Ma. Samples *8* and *20* have such little data, and *17* shows a significant lead-loss trend.

εNd evolution

Neodymium isotopes and Anglesey MDA from detrital zircon samples were used as the input age of the rock, and Figure 11 was calculated using model assumptions from Goldstein *et al.,* 1984.

Table 3: εNd whole rock values for each whole rock sample from Anglesey.

	ANG13a	ANG13b	ANG15a	ANG16
Input age of rock T (Ma)	545	545	545	545
Unmixed $^{143}/^{144}$Nd	0.512197	0.512187	0.512197	0.512231
Nd ugg-1	46.8	14.6	38.2	17.3
Sm ugg-1	10.4	3.4	8.6	4.3
147Sm/144Nd	0.1342	0.1396	0.1358	0.1511
εNd (T=0)	-8.60	-8.80	-8.61	-7.93
143Nd/144Nd (T)	.511718	.511688	.511712	.511692
εNd (T=560)	-4.26	-4.84	-4.38	-4.77
TDM (Ma)	1804	1953	1840	2199
TCHUR (Ma)	1077	1205	1105	1360
DM at age of rock (T)	.512384	.512384	.512384	.512384
CHUR at age of rock (T)	.511936	.511936	.511936	.511936

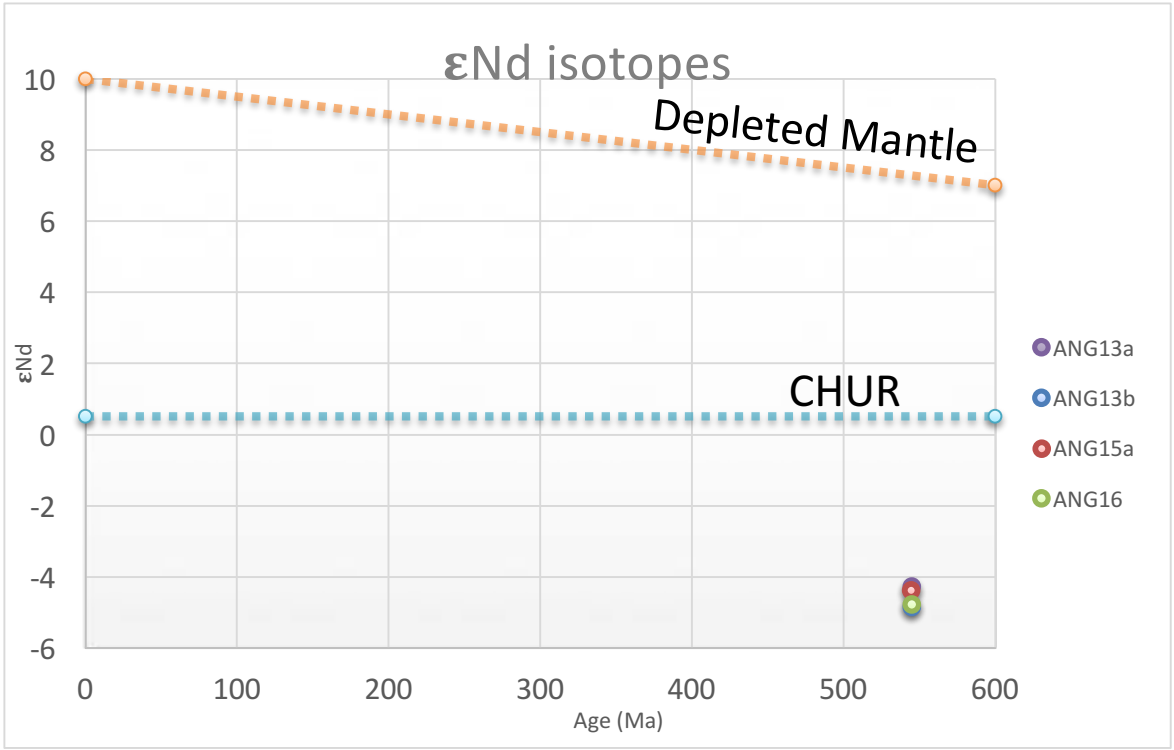

Figure 11: εNd isotope values from whole rock powders of *ANG13a, 13b, 15a* and *16*, showing deviation from CHUR and depleted mantle models, using the model assumptions from Goldstein *et al.*, (1984).

The whole rock εNd values were calculated using the maximum depositional age of 545 ± 8.5 Ma of *ANG12a >7*9μm fraction as the input age. The εNd values at T= 545Ma lie between -4 and -5, with the actual values recorded in Table 3 for each sample.

Mineral chemistry

Table 4 has selected EPMA analyses of peak minerals, where the extended mineral composition can be found in appendices. The garnet core total from *ANG13b* is low when cross-referenced with Deer, *et al.,* (1992), and the hematite shows a mixing with SiO_2 that should not be there. Table 5 shows representative analyses of peak mineral compositions. The predominant composition for garnet, is almandine (~44-57%), with ~28-29% grossular and ~1-2% spessartine. LA-ICP-MS maps of garnet (Figs. 9, 10) for samples *ANG13b* and *ANG15a* show similar enrichment patterns in major elements, and heavy rare earth elements such as dysprosium, holmium and yttrium. Both samples show prograde zonation of iron and magnesium, with enrichment to the rim. Manganese, conversely shows relative depletion to the rim. Europium, thulium, ytterbium, and lutetium show oscillatory zoning. Light rare earth elements, such as samarium and neodymium do not show any zonation, but rather inclusions that have high ppm compared to the garnet. Plagioclase is near pure endmember albite at ~98-99%. Muscovite is interpreted to be phengite, due to the high magnesium content and the proportions of celadonite and ferro-celadonite are high, at ~23-25% and ~22-27% respectively. Tables 4 and 5 were compiled and corrected against known mineral analyses from (Deer *et al.,* 1992).

Table 4: Selected electron probe microanalyses of peak minerals from thin sections *ANG13b* and *ANG15a.*

ANG13b	**Garnet Core**	**Garnet Rim**	**Muscovite**	**Albite**	**Rutile**	**Chlorite**
SiO2	36.113	37.885	48.718	66.762	0.523	23.942
TiO2	0.172	0.194	0.313	0.006	96.290	0.037
Al2O3	20.202	20.856	27.027	19.789	0.251	18.241
Cr2O3	0.000	0.000	0.000	0.000	0.003	0.000
FeO	23.240	19.927	4.673	0.023	0.317	32.453
MnO	7.511	11.209	0.000	0.000	0.000	0.389
MgO	0.566	0.394	2.489	0.005	0.006	9.334
ZnO	0.031	0.043	0.005	0.011	0.000	0.060
CaO	9.427	10.070	0.016	0.023	0.116	0.025
Na2O	0.070	0.044	0.437	11.207	0.092	0.053
K2O	0.025	0.019	10.446	0.221	0.200	0.065
Cl	0.020	0.030	0.038	0.048	0.021	0.076
F	0.000	0.000	0.025	0.000	0.000	0.000
Total	97.37	100.66	94.17	98.08	97.81	84.66
Cations:						
Si	2.979	3.022	3.339	2.973	0.007	2.752
Ti	0.011	0.012	0.016	0.000	0.986	0.003
Al	1.964	1.961	2.183	1.039	0.004	2.471
Cr	0.000	0.000	0.000	0.000	0.000	0.000
Fe3+	0.068	0.000	0.000	0.000	0.000	0.000
Fe2+	1.535	1.329	0.268	0.001	0.004	3.119
Mn2+	0.525	0.757	0.000	0.000	0.000	0.038
Mg	0.070	0.047	0.254	0.000	0.000	1.600
Zn	0.002	0.003	0.000	0.000	0.000	0.005
Ca	0.833	0.861	0.001	0.001	0.002	0.003
Na	0.011	0.007	0.058	0.968	0.002	0.012
K	0.003	0.002	0.913	0.013	0.003	0.010
Cl	0.003	0.004	0.004	0.004	0.000	0.015
F	0.000	0.000	0.005	0.000	0.000	0.000
Total Cations	8.000	8.000	7.034	4.995	1.008	10.012
ANG15a	Garnet Core	Garnet Rim	Muscovite	Albite	Titanite	Chlorite
SiO2	37.486	36.796	48.029	67.969	23.948	24.229
TiO2	0.161	0.110	0.299	0.022	31.041	0.000
Al2O3	20.651	20.406	28.002	20.185	3.141	19.682
Cr2O3	0.000	0.001	0.010	0.012	0.008	0.000
FeO	25.625	25.600	3.939	0.255	2.570	32.656
MnO	5.102	5.612	0.000	0.000	0.080	0.660
MgO	0.483	0.498	2.335	0.002	0.220	8.494
ZnO	0.000	0.050	0.000	0.000	0.000	0.041
CaO	10.042	10.494	0.001	0.111	21.460	0.000
Na2O	0.263	0.022	0.535	11.992	0.295	0.025
K2O	0.031	0.007	10.332	0.093	0.381	0.000
Cl	0.161	0.002	0.113	0.000	0.536	0.019
F	0.000	0.000	0.039	0.000	0.330	0.000
Total	99.97	99.60	93.59	100.64	83.75	85.80
Cations:						
Si	3.007	2.969	3.301	2.960	0.941	2.739
Ti	0.010	0.007	0.015	0.001	0.918	0.000
Al	1.952	1.940	2.268	1.036	0.145	2.622
Cr	0.000	0.000	0.001	0.000	0.000	0.000
Fe3+	0.036	0.113	0.000	0.000	0.000	0.000
Fe2+	1.683	1.614	0.226	0.009	0.084	3.087
Mn2+	0.347	0.383	0.000	0.000	0.003	0.063
Mg	0.058	0.060	0.239	0.000	0.013	1.431

Zn	0.000	0.003	0.000	0.000	0.000	0.003
Ca	0.863	0.907	0.000	0.005	0.904	0.000
Na	0.041	0.003	0.071	1.013	0.022	0.006
K	0.003	0.001	0.906	0.005	0.019	0.000
Cl	0.022	0.000	0.013	0.000	0.036	0.004
F	0.000	0.000	0.009	0.000	0.041	0.000
Total Cations	8.000	8.000	7.027	5.030	3.050	9.951

Table 5: Representative endmember compositions of ANG13b and ANG15a for garnet rim and core, albite, titanite and phengite. X (gt): refers to $Fe^{2+}/(Fe^{2+}+Mg)$, X (mu): $Fe^{2+}/(Fe^{2+}+Mg)$.

	ANG13b		*ANG15a*	
	Garnet Rim	Garnet Core	Garnet Rim	Garnet Core
X (gt)	0.966	0.957	0.964	0.967
Almandine	0.444	0.518	0.544	0.570
Pyrope	0.016	0.010	0.036	0.002
Grossular	0.287	0.281	0.306	0.292
Spessartine	0.253	0.177	0.129	0.117

	ANG13b	*ANG15a*
	Albite	Albite
Albite	0.986	0.990
Anorthite	0.001	0.005
Sanidine	0.013	0.005
	Phengite	Phengite
x(mu)	0.513	0.486
Paragonite	0.058	0.071
Margarite	0.001	0.000
Muscovite	0.418	0.463
Celadonite	0.255	0.239
Ferro-celadonite	0.268	0.226

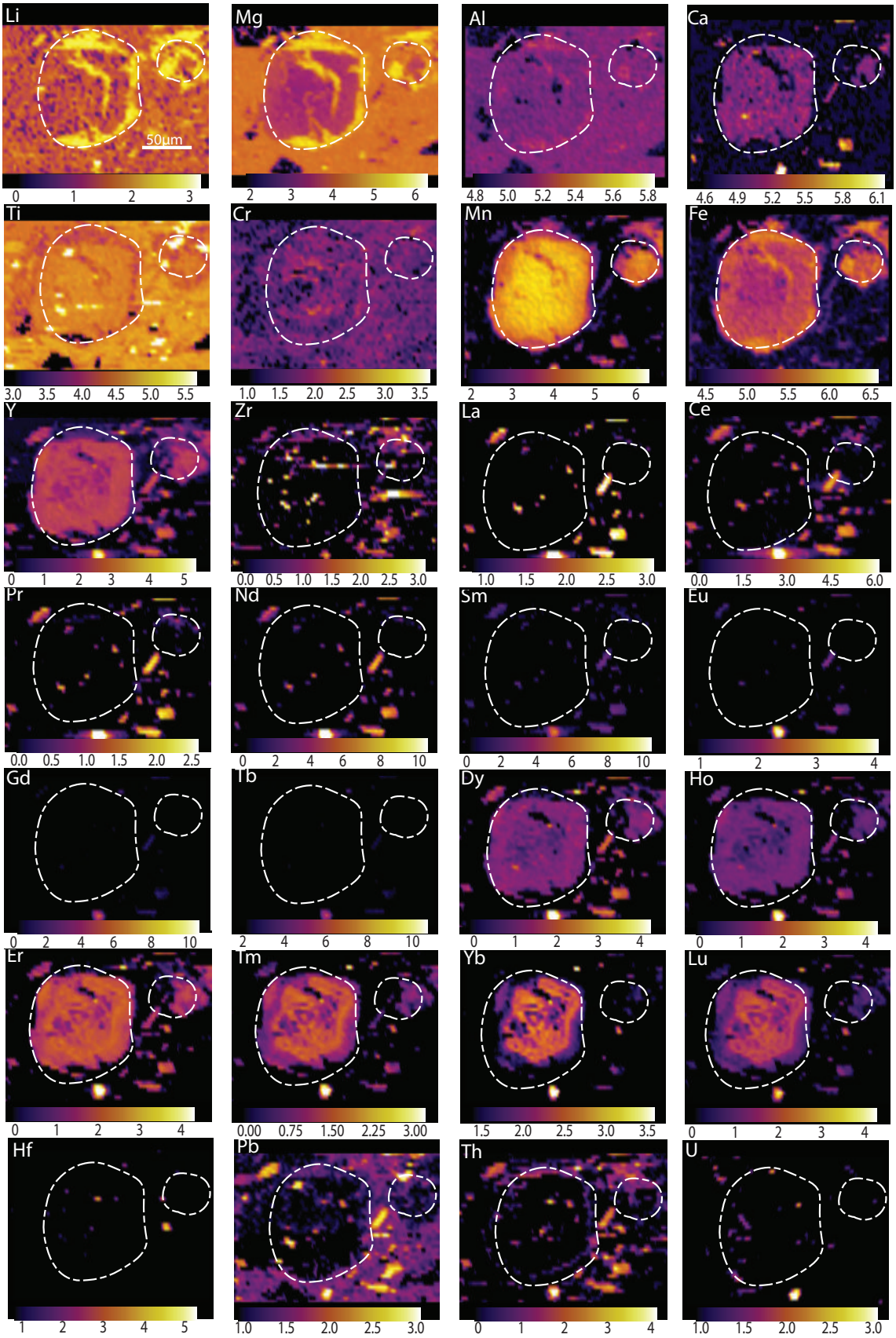

Figure 12: LA-ICP-MS garnet trace element maps of *ANG13b* with a logarithmic ppm scale.

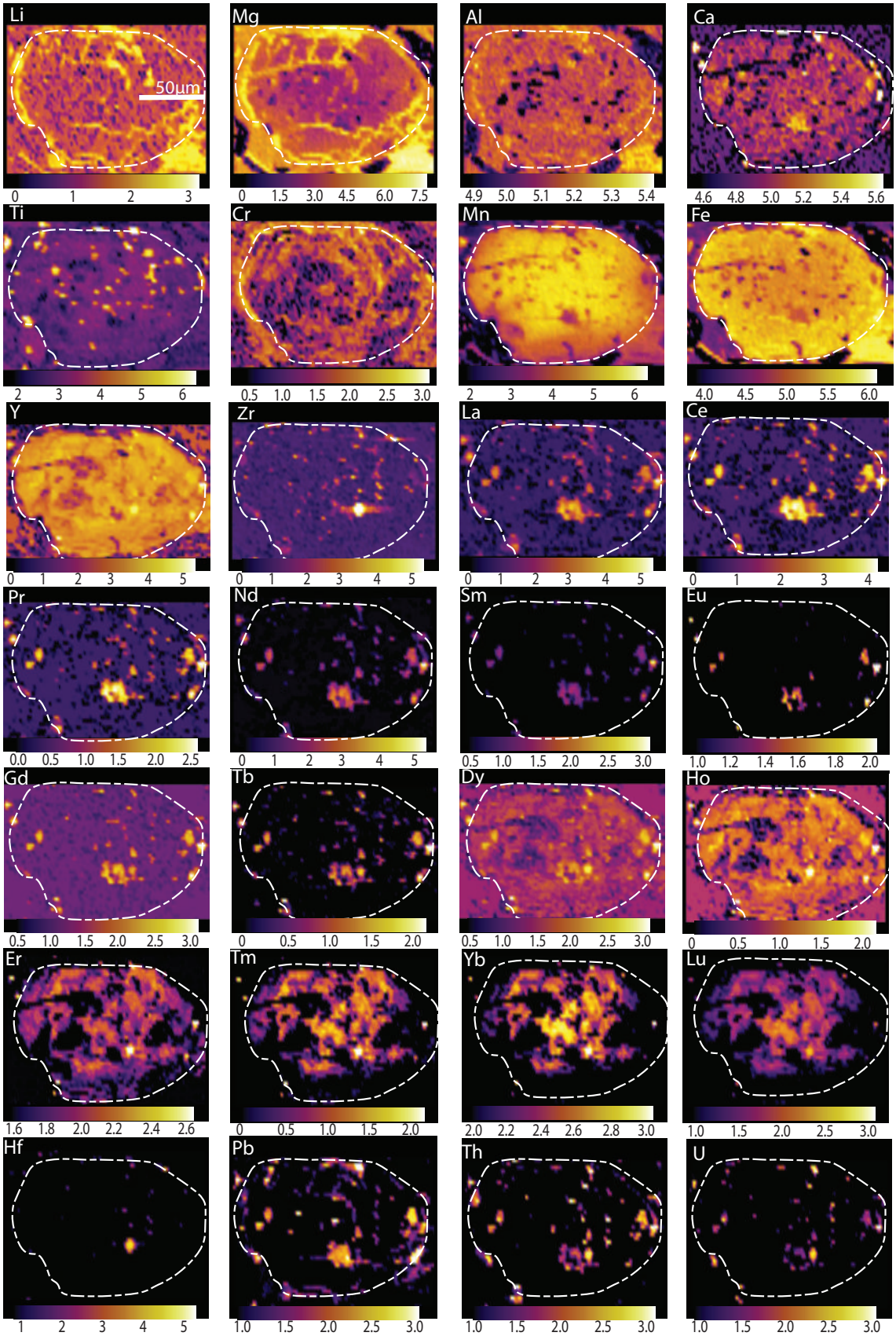

Figure 13: LA-ICP-MS maps of garnet trace elements from sample *ANG15a*, also using a logarithmic ppm scale.

Figures 12 and 13 show the trace element distributions in the garnets from *ANG13b* and *ANG15a*, a logarithmic ppm scale is used to show the rare earth elements, and shows the REE-rich inclusions.

Phase equilibria forward models

Temperature- oxidation (*T-Mo*) diagrams, where 'M' refers to the amount of an oxide component were constructed of samples *ANG13b* and *ANG15a* in order to determine the oxidation state of the rocks during the pressure- temperature evolution. The large range of temperatures and pressures stable within the peak field of the *T-Mo* diagrams led to an average composition (X=0.5 and X=0.58 respectively) taken from the stable peak assemblage to determine the composition of the P-T pseudosections of *ANG13b* and *ANG15a.* X refers to the composition at a particular point it P-T space; in this case the middle of the peak fields. P-T pseudosections (Figs. 14 and 15) have peak assemblages of garnet, chlorite, muscovite, rutile, titanite, quartz, pyrite and apatite, but pyrite and apatite are not able to be modelled. The peak field in *ANG13b* is stable from 250-450°C, and 3.5 to 12kb. The peak field in *ANG15a* is between 325- 500°C, and 6- 12kb. The geothermal gradient resulting from both pseudosections is low; low temperatures with moderately high pressures.

X=0.5	SiO2	Al2O3	CaO	MgO	FeO	K2O	Na2O	TiO2	MnO	O
	73.641	12.260	0.606	2.356	2.588	3.309	4.063	0.584	0.143	0.452

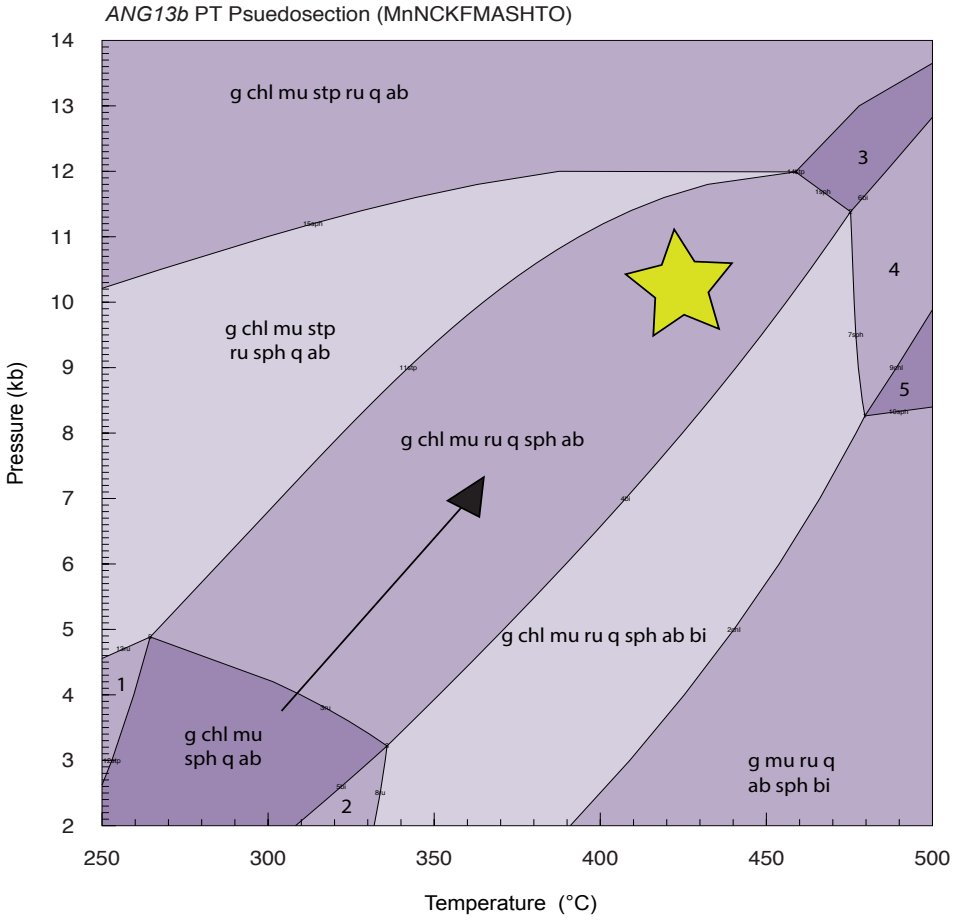

1. g chl mu stp sph q ab
2. g chl mu q ab sph bi
3. g chl mu ru q ab
4. g chl mu ru q ab bi
5. g mu ru q ab bi

Figure 14: P-T Pseudosection of *ANG13b* in the MnNCKFMASHTO system, between 250-500ºC, and 2-14kb. The peak field, indicated by the star, is stable over a large pressure and temperature interval. The star is located to the higher temperature and pressure locale as this is interpreted to best represent the modal proportions presented in Table 6. Composition used for the calculation of the diagram is provided in mol% above. Variance is between 4 and 6, with the colour of the fields increasing with variance. The arrow to the bottom of the peak assemblage represents the prograde path as rutile overgrows titanite. Small fields denoted by numbers have the corresponding assemblages below the diagram.
Abbreviations: g: garnet, chl: chlorite, mu: muscovite (phengite), ru: rutile, q: quartz, sph: sphene (titanite), bi: biotite, stp: stilpnomelane.

X=0.58	SiO2	Al2O3	CaO	MgO	FeO	K2O	Na2O	TiO2	MnO	O
	76.013	10.455	0.597	2.248	3.475	2.429	3.693	0.477	0.109	0.504

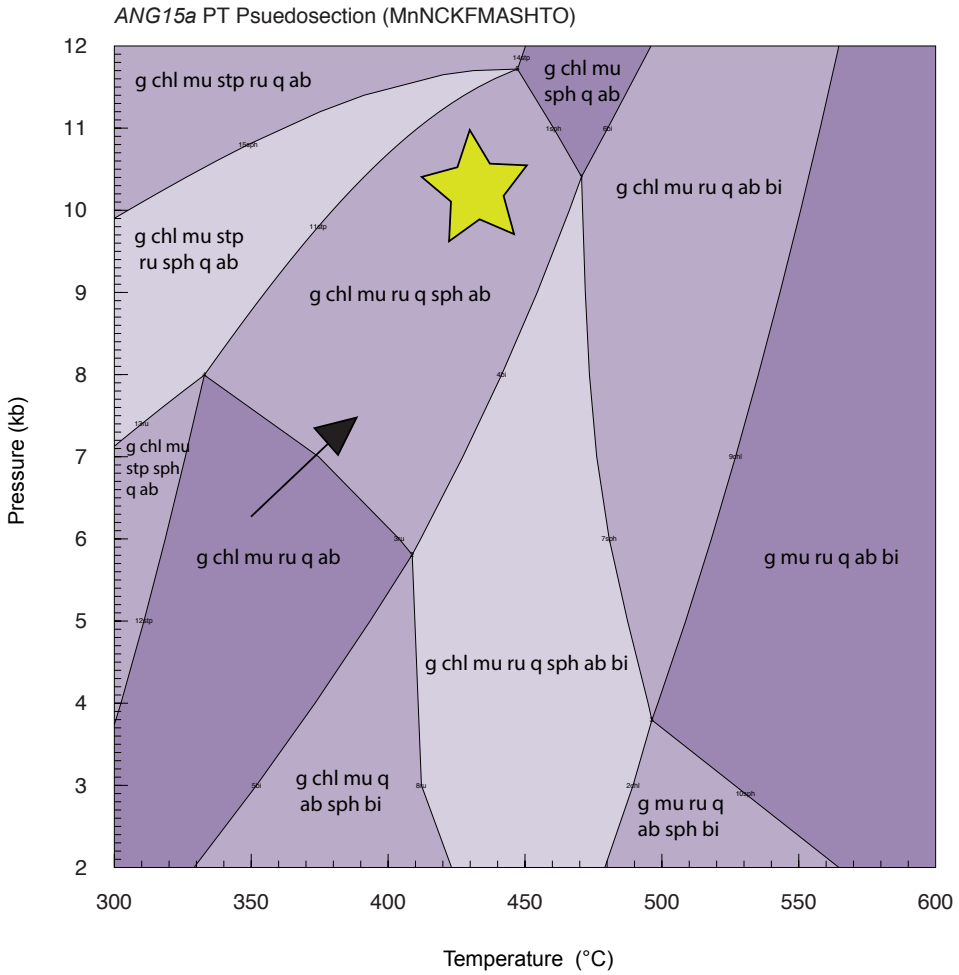

Figure 15: P-T Pseudosection of *ANG15a,* calculated using the MnNCKFMASHTO system, between 300-600ºC and 2-12kb. As above, the peak field is indicated by the star, where the peak assemblage is g-chl-mu-ru-q-sph-ab, and the arrow shows the prograde path from g-chl-mu-ru-q-ab with increasing P-T. As with the *ANG13b* pseudosection, variance is between 4 and 6, where higher variance corresponds to darker colour. Compositional information used to calculate the pressure and temperature conditions is provided above the diagram.
Abbreviations: g: garnet, chl: chlorite, mu: muscovite (phengite), ru: rutile, q: quartz, sph: sphene (titanite), bi: biotite, stp: stilpnomelane.

Phase abundance contours

TCInvestigator was used to calculate the modal abundances (mode) of peak minerals found in Figures 16 and 17.

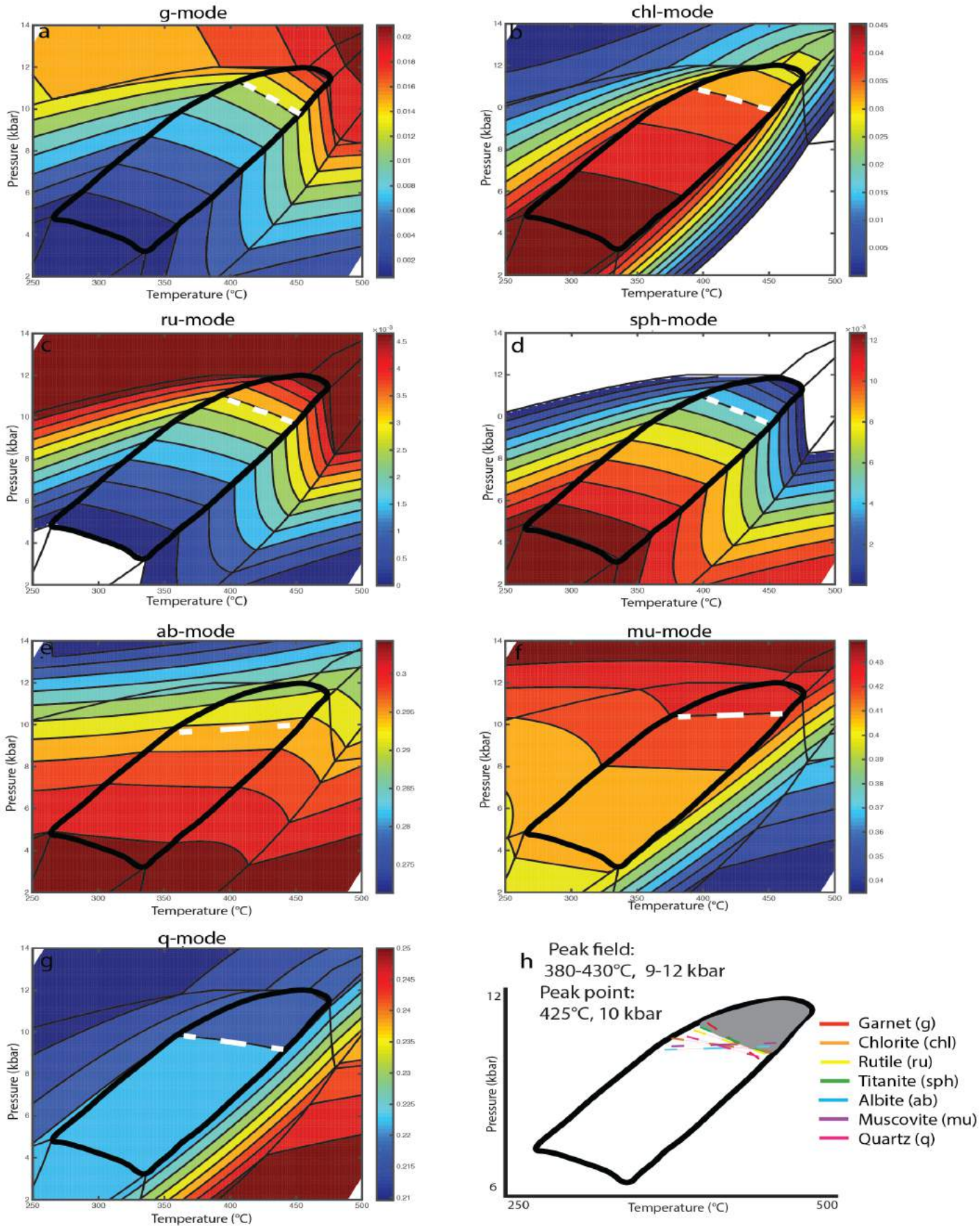

Figure 16: TCI outputs for *ANG13b* P-T, modal proportions of a) garnet, b) chlorite, c) albite, d) muscovite (phengite), e) sphene (titanite), f) rutile, g) quartz and h) further constraining the peak field by intersection of modal proportions. Bold black lines are indicative of the peak field. White dashed lines indicate the estimated modal proportion of each peak mineral (Table 6).

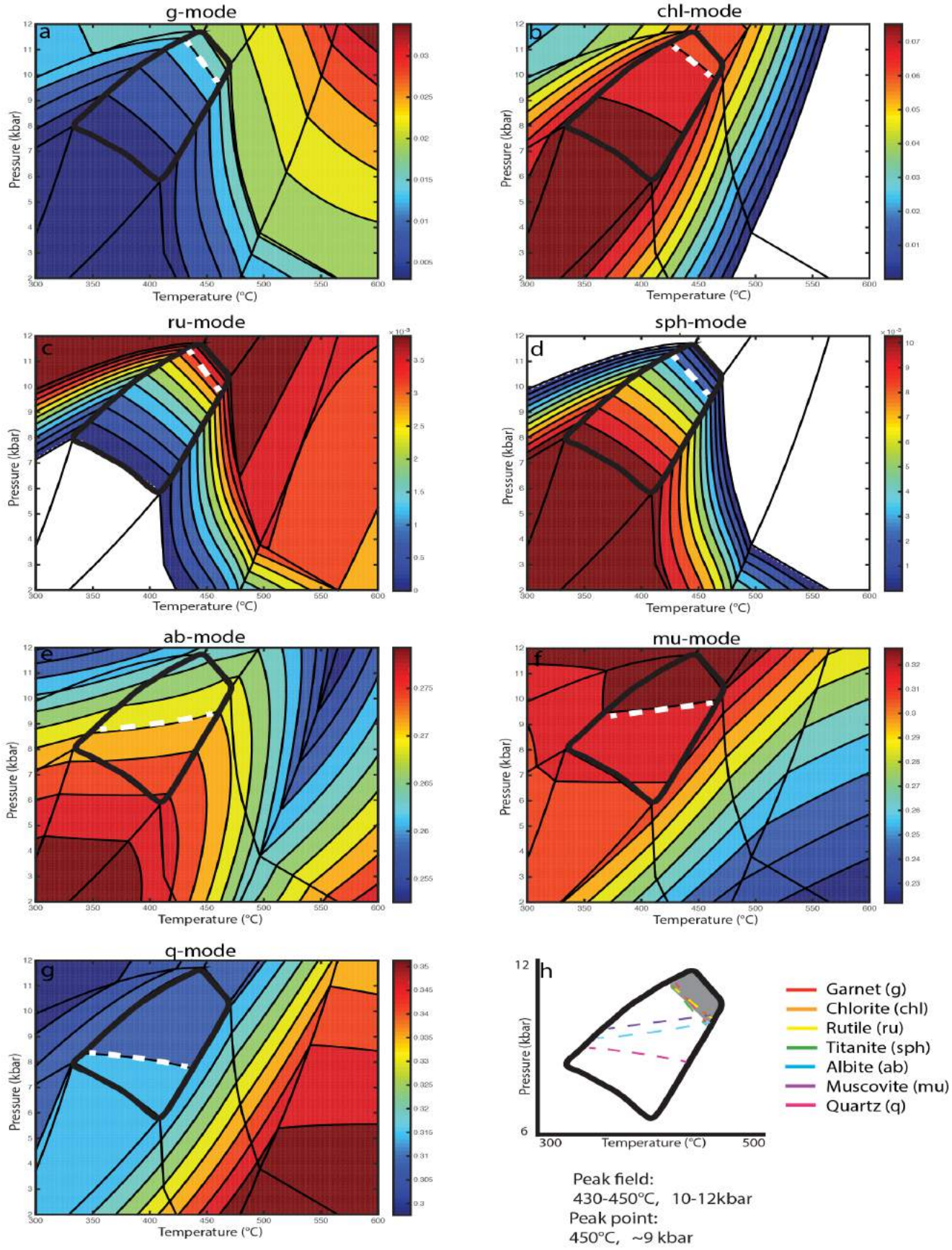

Figure 17: TCI outputs for *ANG15a* P-T, modal proportions of a) garnet, b) chlorite, c) albite, d) muscovite (phengite), e) sphene (titanite), f) rutile, g) quartz and h) further constraining the peak field by intersection of modal proportions. Bold black lines are indicative of the peak field. White dashed lines indicate the estimated modal proportion of each peak mineral, (Table 6).

Table 6: Modal proportion estimates of peak minerals within the Anglesey metapelites.

	ANG13b	*ANG15a*
Garnet	1-2%	2%
Chlorite	3-4%	5-6%
Muscovite	42%	32%
Rutile	<1%	<1%
Titanite	<1%	<1%
Albite	30%	27%
Quartz	20-22%	30%

DISCUSSION

Age of Penmynydd schists

600 million years ago marks a significant turning point in Earth history, as the emergence of lower geothermal gradients is apparent, resulting in the appearance of blueschist and eclogite facies metamorphism, shown in Figure 18. The first emergence of lawsonite blueschists occurs around the same time as the maximum depositional age of the metapelites, at ~540Ma (Tsujimori and Ernst, 2014).

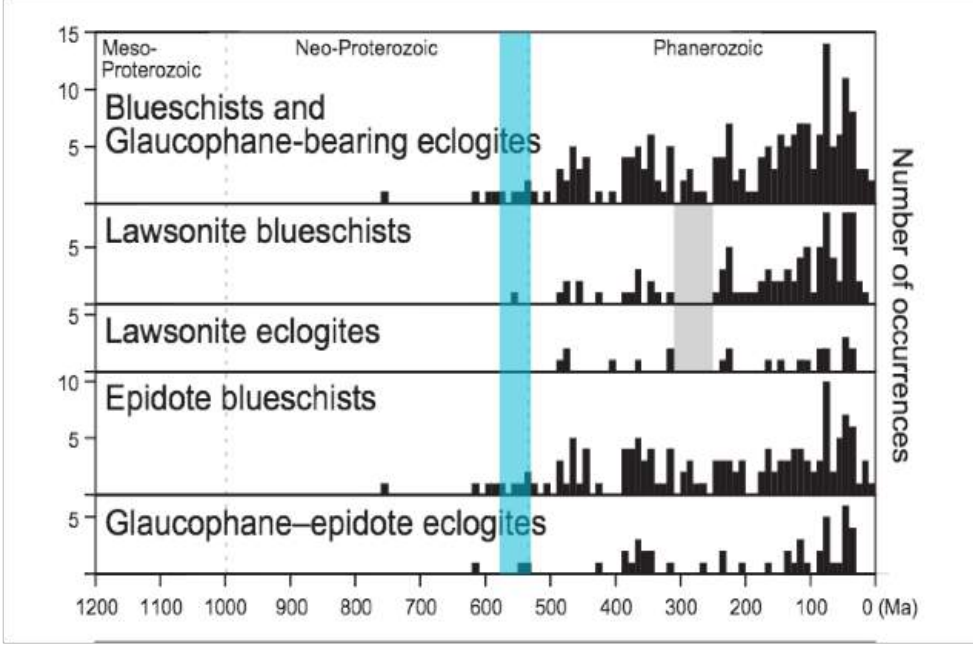

Figure 18: Figure modified from Tsujimori & Ernst, (2014), with the blue band showing the ~590-520Ma range suggested by maximum depositional ages of detrital zircon spectra. While the two ages are not mutually exclusive, we can see that the emergence of lawsonite blueschists occurs during the period of deposition of the protolith.

The maximum depositional age (MDA) purely reflects the youngest zircon in the spectra, and thus the source of the sediments that were metamorphosed into the pelitic schists are better determined through probability density estimates, such as those in Fig. 3b-10b, and Fig. 19. The MDA of the metapelites from the data given by U-Pb detrital zircon geochronology lies between ~520-590Ma. Table 2 shows that the samples are geographically quite close together, as well as the geological map in Fig. 1, and as the samples are all the same rock type, they should reflect close ages. This fits with the samples from Asanuma *et al*., (2017), and shows that therein lies a complex provenance with a comparatively evolved Late Neoproterozoic crustal source.

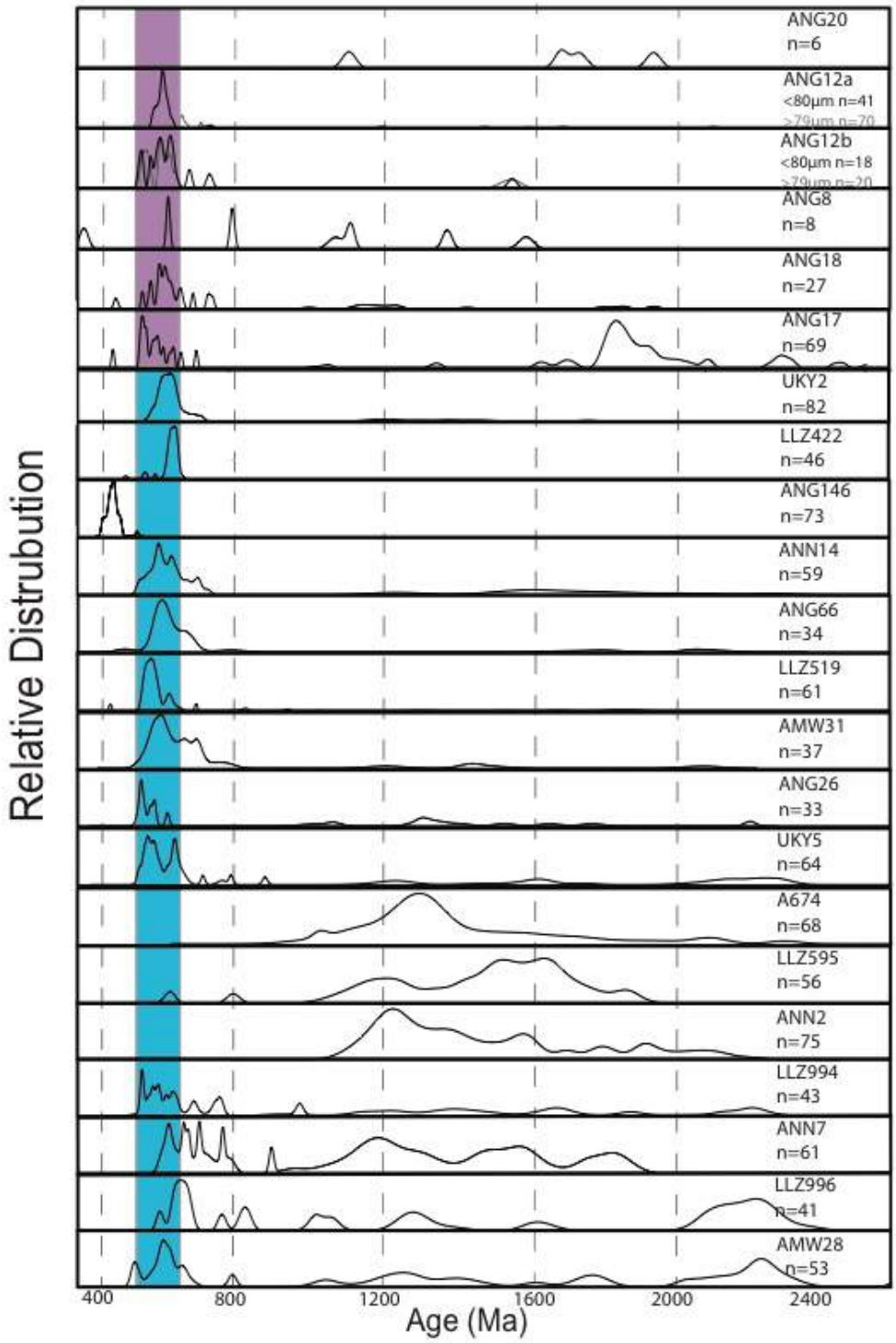

Figure 19: Detrital U-Pb zircon spectra of samples from this study (purple) and samples from Asanuma *et al.*, (2017), shown in blue, to provide a better understanding of the evolution of the island of Anglesey. Most of the samples reflect a dominant peak between ~597 and 634Ma.

Samples marked by the blue band in Figure 19 were created using the supplementary material provided by Asanuma *et al.,* (2017), as the detrital zircon spectra stated in their study encompasses the entire island of Anglesey (Fig. 20), and allows better understanding as to the evolution of the subduction system and volcanics. Arc magmatism from ~620Ma through to 600Ma may account for the source of these zircons, post arc construction and prior to the late- arc magmatism of ~577Ma (Gibbons and Horak, 1996) with a complex older source, evident in the distribution of the detrital spectra. Calc-alkaline volcanics were prevalent between ~630-600Ma (Gibbons 1996), which also coincides with the ages of the Coedana granite, at ~614Ma (Fig. 20). Evidence of this magmatism is found in Wales, England, Newfoundland and are recorded as parts of remnant Avalonia (Gibbons and Horak, 1996).

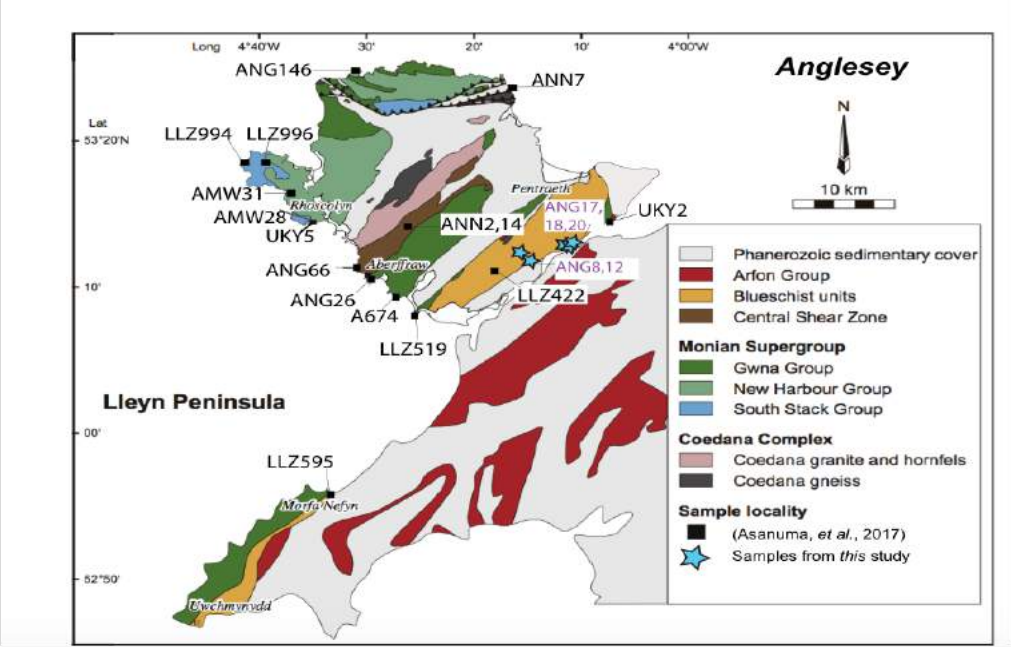

Figure 20: Map of Anglesey showing lithology and location of the Asanuma *et al.,* (2017) samples with reference to the samples from this study (purple labels).

The ages discussed by Asanuma *et al.,* (2017) reflect similar patterns to the samples in this study, with a prominent Late Neoproterozoic peak, and various minor peaks from ~2000-1000Ma, suggesting an older source, such as sediments occurring from the formation and dispersal of supercontinents such as Laurentia, Baltica and Amazonia prior to Avalonia (Fig. 19).

Neodymium isotopes (Table 3; Figure 11), with εNd values between -4 and -5 are very evolved with respect to the CHUR and Depleted Mantle models (Goldstein, *et al.,* 1984). The evolved signature of the isotopes is reflective of an older source or basement, which supports the aforementioned U-Pb detrital zircon data and provenance sources.

Ideally, the use of LA-ICP-MS trace elements maps in conjunction with Sm-Nd geochronology would be able to link evolution of garnet to a metamorphic evolution (Raimondo *et al.,* 2017; Cheng *et al*., 2016), however the maps can be used to say something about the formation of garnet, in conjunction with the pressure and temperature estimates created in figures 14 and 15. Logarithmic (ppm) LA-ICP-MS trace element maps of garnets from both samples show core-rim zonation of major elements, Li, Mg, Mn and and Fe in particular. Samarium and neodymium concentrations are quite low, with enriched heavy rare earth elements such as ytterbium, dysprosium, holmium, lutetium and thulium, suggesting that the garnets had time to fractionate rare earth elements and as such grew slowly. The non-logarithmic ppm scaled maps of garnet can be found in Appendix C.

The peak field in the *ANG13b* P-t pseudosection is g-chl-mu-ru-q-sph-ab, which has overprinted a prograde assemblage of g-chl-mu-sph-q-ab to g-chl-mu-ru-q-ab in Fig. 2. The *ANG15a* P-t pseudosection also shows the same mineral assemblage and history. The partial replacement of titanite by rutile in both samples documents a prograde burial path shown by the arrows in Figures 14 and 15. The prograde burial path passed through the g-chl-mu-sph-ab-q field, before moving into the g-chl-mu-sph-ru-ab-q field with increasing pressure and temperature. The comparatively low modal abundance of rutile with respect to titanite suggests that the peak pressures remained below the titanite-out upper pressure boundary of the peak field. However, the use of estimated modal proportions of peak minerals in thin section were used to better constrain the peak P-T conditions recorded by the rock for both samples (Table 6; Fig. 16; Fig. 17). The peak point recorded by the intersection of the modal proportions of peak minerals for *ANG13b* is at 425 °C, 10 kbar with an apparent thermal gradient of ~40°C/kbar. *ANG15a* records a similar point in P-T space, at 450°C, 9 kbar, with the same apparent thermal gradient. The close geographic location of the samples, as well as similarities in the phase equilibria forward models suggests the Anglesey metapelites experienced the same conditions (Table 2; Fig. 14; Fig. 15; Fig. 16; Fig. 17). The pressure and temperature evolution of the metapelites is indicative of moderately refrigerated subduction under a low-geothermal gradient (Brown, 2008; Tsujimori, 2006); as the temperatures are warmer that first thought. However, this is interpreted to mean that Anglesey is at the forefront of a changing thermal regime, thus supports the hypothesis that the interbedded metapelites co-exist within the Anglesey blueschist belt, and record the same characteristics.

Avalonian subduction and what this means for the emergence of cold pelites:

The geothermal gradient along a subduction zone can be used to better constrain the secular thermal evolution of the Earth (Brown, 2007; Arai *et al.,* 2015) where the age of the subducted crust controls the P-T gradients. Intermediate P-T gradients primarily result from young oceanic plates, where high P-T type gradients are experienced when older, colder subduction occurs, cooling the geothermal gradient, allowing refrigerated metamorphism, such as that experienced by the Anglesey metapelites (Arai *et al.,* 2015). Kawai *et al.,* (2006) loosely constrain the pressure and temperature evolution of the blueschist unit by conventional thermobarometry, suggesting that the minimum pressure the blueschist unit experienced was >6kbar and temperatures higher than 420°C. As the metapelites have experienced pressures and temperatures greater than the minimum conditions put forward by Kawai *et al.,* (2006), it can be inferred that the metapelites and blueschists share a pressure-temperature evolution. Therefore, based on the logic that the pelitic schists are equivalent to the blueschist unit, the subduction system required to produce such a geothermal gradient is subduction of old, cold crust (Brown, 2008; Agard *et al.,* 2009).

Many lines of evidence suggest that the Archean Earth was hotter than today, evidenced by higher geothermal gradients (Brown 2007), and Arai *et al.,* (2015) suggest that higher heat production in the Archean might have a role in driving higher mantle convection and subduction of younger oceanic plates. Intermediate P-T type geothermal gradients were more prevalent in the Archean, interpreted to be a consequence of subducting young oceanic plates (Arai, *et al.,* 2015). Therefore in order

for the emergence of refrigerated metamorphism the mode of subduction has to change from the Archean through the Neoproterozoic, in order for blueschist-facies metamorphism to be recorded in high P-T conditions in subduction zones (Brown, 2007; Brown, 2008; Brown 2009; Arai *et al.,* 2015).

Detrital zircon data from the Gwna Group on the Lleyn peninsula, and on Anglesey show similar ages with ~600Ma Avalonian calc-alkaline arc magmatism, and regional metamorphism during the late Neoproterozoic affecting the Anglesey-Lleyn complex (Moorbath and Shackleton, 1966; Gibbons and Horak, 1996; Asanuma *et al.,* 2015). Asanuma *et al.,* (2015) also suggest that the older zircon spectra results from sediments accumulated in an accretionary wedge on the western active margin of Avalonia as it subducted in the late Proterozoic. Older provenance for sediments are potentially the Amazonian, Siberian, Baltica, West African and East African cratons, with the addition of the Neoproterozoic Arfon Volcanic Group in Western Wales, which reflects a geographically closer provenance (Gibbons and Horak, 1996; Asanuma *et al.,* 2015; Asanuma *et al.,* 2017). Asanuma *et al.,* (2017) suggest that the Gwna Group ~ 578Ma-530Ma, are sources of the metasediments and blueschist unit due to the similar metamorphic age and zircon age. This does not correlate with the detrital zircon data in this study, but may indicate that the meta-sediments on Anglesey island underwent multiple metamorphic episodes throughout the Late Neoproterozoic (Asanuma *et al*., 2017). The detrital zircon spectra and Nd isotopes suggest that there is a complex, evolved provenance, likely arc related as the detritus records ages of up to ~2Ga.

The geotectonic history of Anglesey, and as such Avalonia provides insight into the evolution of similar units existing in Newfoundland, Scotland and Ireland, resulting from the closure of the Iapetus Ocean during the breakup of Gondwana, albeit recorded at different stages of ocean closure (Gibbons and Horak, 1996).

Neoproterozoic detrital zircon ages reflect quick burial from Avalonian arc, which reflects short-lived subduction (Gibbons and Horak, 1996; Asanuma *et al.,* 2017) Arc activity was widely distributed throughout Avalonia between ~570-760Ma, and Asanuma *et al.,* (2017) suggest that subduction of the Iapetus oceanic plate drove arc-related magmatism by ~711-677Ma, during the closure of the Iapetus Ocean, leading to the amalgamation of Gondwana and potential provenance to the mica schists.

CONCLUSIONS

The detrital ages of the interbedded metapelites within the Anglesey Blueschist Belt ranges from ~630-520 Ma, fitting with the existing literature and contemporaneous to where arc magmatism was interpreted to be present on the inferred margin of Avalonia (Table 1; Gibbons and Horak, 1996; Asanuma *et al.,* 2017). Dallmeyer and Gibbons (1983) show that the metamorphic age is ~550-560Ma through Ar-Ar dating (Table 1), all of which coincide with the arc magmatism, accretion and exhumation associated with a subduction system. An older detrital signal up to ~2Ga is interpreted to result from an evolved arc source, such as that of an ancient continental margin, eroded and depositing detritus as the Avalonian arc formed. This interpretation is supported by evolved εNd isotopic signatures, as the deviation from CHUR and Depleted Mantle models (Goldstein *et al.,* 1984) is indicative of a crustal source. The complex detritus and evolved Nd signature supports the hypothesis that the Anglesey metapelites and as

such the blueschist unit subscribes to an autochthonous regime. Pressure and temperature estimates resulting from the peak assemblages in the pseudosections yield a moderately cool apparent thermal gradient of ~40°C/ kbar, but cold enough so that lawsonite in the interbedded blueschists is stable. Taking into account the detrital and metamorphic ages, this suggests cold subduction emerged in the Neoproterozoic, compared to the hot geothermal gradients of the Archean (Brown 2010, Brown 2007, Brown 2008, Brown 2006). Blueschist facies-metamorphism occurs under high pressures and low-intermediate temperatures, thus it can be said that the pelitic schists on the margin of Avalonia were incorporated into the cold subduction system in the late Neoproterozoic. While Anglesey is home to the oldest-known lawsonite-bearing blueschists, the pressure and temperature environment was not truly low-T high-P with average P-T conditions of ~400-450 °C at 10-12 kbar. Thus, the interbedded blueschist and metapelite unit are interpreted to herald a changing thermal regime from a hot Archean Earth to a cold late Neoproterozoic Earth, marked by the emergence of stable lawsonite in the blueschist. In future, to constrain the metamorphic age of the garnet, Lu-Hf isotopic data could be utilized to date the garnets from the pelitic schist, and can be used to better determine the metamorphic relationship of the pelitic schists to the interbedded lawsonite-bearing blueschist unit.

ACKNOWLEDGMENTS

Firstly, gratitude and thanks are expressed to supervisors, Professor Martin Hand, and Reneé Tamblyn for their endless patience, support and knowledge. Much appreciation to Laura Morrissey and Naomi Tucker for teaching and helping with the THERMOCALC program. Thanks are expressed to staff at Curtin University for the SelFrag process, Stan Mertzmann for the geochemistry, as well as David Bruce for

performing the isotope work on the garnet. David Kelsey, Sarah Gilbert and Ben Wade are thanked for their patience and knowledge of instrumentation at Adelaide Microscopy. Thanks to Alec Walsh for help and patience with laboratory preparation and techniques. Lastly, thanks to classmates Mitchell Bockmann, Angus Nixon and Bradley Cave for their endless support this year.

REFERENCES:

AGARD, P., YAMATO, P., JOLIVET, L., & BUROV, E. 2009. Exhumation of oceanic blueschists and eclogites in subduction zones: Timing and mechanisms. *Earth-Science Reviews* **92**(1), 53-79.

ARAI, T., OMORI, S., TSUYOSHI, K. & MARUYAMA, S. 2015. Intermediate P/T-type regional metamorphism of the Isua Supracrustal Belt, southern west Greenland: The oldest Pacific-type orogenic belt? *Tectonophysics,* **662**, 22-39.

ASANUMA, H., FUJISAKI, W., SUZUKI, K., SATO, T., SAKATA, S., SAWAKI, Y., AOKI, K., OKADA, Y., MARUYAMA, S., HIRATA, T., ITAYA, T & WINDLEY, BF. 2017. New isotopic age data constrain the depositional age and accretionary history of the Neoproterozoic-Ordovician Mona Complex (Anglesey-Lleyn, Wales). *Tectonophysics* **706-707**, 164-195.

ASANUMA, H., OKADA, Y., FUJISAKI, W., SUZUKI, K., SATO, T., SAWAKI, Y., SAKATA, S, YAMAMOTO, S., HIRATA, T., MARUYAMA, S., & WINDLEY, BF. 2015. Reconstruction of ocean plate stratigraphy in the Gwna Group, NW Wales: Implications for the subduction–accretion process of a latest Proterozoic trench-forearc *Tectonophysics* **662**, 195-207.

BROWN, M. 2006. Duality of thermal regimes is the distinctive characteristic of plate tectonics since the Neoarchean. *Geology,* **34**, 961-964.

BROWN, M. 2007. Metamorphism, Plate Tectonics, and the Supercontinent Cycle. *Earth Science Frontiers* **14**(1), 1-18.

BROWN, M. 2008. Characteristic thermal regimes of plate tectonics and their metamorphic imprint throughout Earth history: When did Earth first adopt a plate tectonics mode of behaviour? *In:* Condie, K., & Pease, V. eds. *When did plate tectonics begin on planet Earth?* vol. 440, pp. 97-128 Geological Society of America.

BROWN, M. 2009. Metamorphic patterns in orogenic systems and the geological record. In CAWOOD P. A., KRONER, A. ed. Earth Accretionary Systems in Space and Time. pp. 37-74. London: The Geological Society of London.

BROWN, M. 2010. Paired metamorphic belts revisited. *Gondwana Research,* (18) 46-59.

CHENG H. L., T AND CAO, D. 2016. Coupled Lu–Hf and Sm–Nd geochronology constrains blueschist-facies metamorphism and closure timing of the Qilian Ocean in the North Qilian orogen. *Gondwana Research* **34**, 99-108.

COLLINS A. .& BUCHAN, C., 2004. Provenance and age constraints of the South Stack Group, Anglesey, UK: U-Pb SIMS detrital zircon data. *Journal of the Geological Society, London* **161**, 743-746.

DALLMEYER ,R., AND GIBBONS, W. 1987. The age of blueschist metamorphism in Anglesey, North Wales: evidence from 40Ar/39Ar mineral dates of the Penmynydd schists. *Journal of the Geological Society, London* **144**, 843-852.

DEER ,W., HOWIE, RA, AND ZUSSMAN, J. 1992. An Introduction to the Rock-Forming Minerals. (2 edition). Longman, Essex, England.

GIBBONS, W. 1983. The Monian 'Penmynydd Zone of Metamorphism' in Llŷn, North Wales. *Geological Journal* **18**, 21-41.

GIBBONS ,W., AND HORAK, J.M. 1990. Contrasting metamorphic terranes in northwest Wales. *Geological Society London Special Publications* **51**, (1) 315-327.

GIBBONS, W. & MANN, A. 1983. Pre-Mesozoic Lawsonite in Anglesey, nothern Wales: Preservation of ancient blueschists. *Geology* **11**, 3-6.

GIBBONS, W. & HORAK, J. 1996. The evolution of the Neoproterozoic Avalonian subduction system: Evidence from the British Isles. In NANCE R. A. T., MD ed. Avalonian and Related Peri-Gondwanan Terranes of the Circum-North Atlantic. pp. 269-280. Boulder, Colorado: Geological Society of America.

GOLDSTEIN, S., O'NIONS, RK, AND HAMILTON, PJ. 1984. A Sm-Nd isotopic study of atmospheric dusts and particulates from major river systems. *Earth and Planetary Science Letters,* **70**(2), 221-236.

HOLLAND, T. & POWELL, R. 2011. An improved and extended internally consistent thermodynamic dataset for phases of petrological interest, involving a new equation of state for solids, *Journal of Metamorphic Geology,* **29**(3), 333-383.

KAWAI, T., WINDLEY, B.F., TERABAYASHI, M., YAMAMOTO, H., MARUYAMA, S., ISOZAKI, Y. 2006. Mineral isograds and metamorphic zones of the Anglesey blueschist belt, UK: implications for the metamorphic development of a Neoproterozoic subduction–accretion complex. *Journal of Metamorphic Geology* **24**, 591-602.

KAWAI, T., WINDLEY, B.F., TERABAYASHI, M., YAMAMOTO, H., MARUYAMA, S., OMORI, S., SHIBUYA, T, SAWAKI, Y, AND ISOZAK,Y. 2007. Geotectonic framework of the Blueschist Unit on Anglesey–Lleyn, UK, and its role in the development of a Neoproterozoic accretionary orogen. *Precambrian Research* **153**, 11-28.

LIOU, J. G., MARUYAMA, S., WANG, X. AND GRAHAM, S. 1990. Precambrian blueschist terranes of the world, *Tectonophysics,* **181**, 97-111.

LIOU, J. G., TSUJIMORI, T., ZHANG, R.Y., KATAYAMA, I. AND MARUYAMA, S. 2010 Global UHP Metamorphism and Continental Subduction/Collision: The Himalayan Model. *International Geology Review* **46**(1) 1-27.

MARUYAMA, S., AND OKAMOTO, K. 2007. Water transportation from the subducting slab into the mantle transition zone. *Gondwana Research* **11**, 148-165.

MARUYAMA, S. & LIOU J. G. 1998. Initiation of ultrahigh-pressure metamorphism and its significance on the Proterozoic-Phanerozoic boundary, *The Island Arc* **7**, 6-35.

MOORBATH, S. & SHACKLETON, RM. 1966. Isotopic ages of the Precambrian Mona Complex of Anglesey, north Wales (Great Britain), *Earth and Planetary Science Letters* **1**, 113-117.

NANCE, R. D., MURPHY J. B., & KEPPIE J. D. 2002. A Cordilleran model for the evolution of Avalonia. *Tectonophysics* **352**(1-2), 11-31.

PALIN, R. A., & WHITE, R.W. 2015. Emergence of blueschists on Earth linked to secular changes in oceanic crust composition. *Nature Geoscience* **9** 60-65.

PATON, C., HELLSTROM, J., PAUL, B., WOODHEAD, J. AND HERGT, H. 2011. Iolite: Freeware for the visualisation and processing of mass spectrometric data. *Journal of Analytical Atomic Spectrometry **26***, (12) 2508-2518.

PAYNE, J. L., BAROVICH K. M. & HAND M. 2006. Provenance of metasedimentary rocks in the northern Gawler Craton, Australia: Implications for Palaeoproterozoic reconstructions. *Precambrian Research,* **148**(3) 275-291.

PEARCE, M., WHITE A.J.R., GAZLEY, M.F., 2015. TCInvestigator: Automated calculation of mineral mode and composition contours for THERMOCALC pseudosections. *Journal of Metamorphic Geology,* **33**(4) 331- 435.

POWELL, R. A& HOLLAND., T. 1988. An internally consistent datasetwith uncertainties and correlations: 3. Applications to geobarometry, worked examples and a computer program. *Journal of Metamorphic Geology,* **6,** 173-204.

RAIMONDO, T., PAYNE, J., WADE, B., LANARI, P., CLARK, C. AND HAND, M. 2017. Trace element mapping by LA-ICP-MS: assessing geochemical mobility in garnet. *Contributions to Mineralogy and Petrology,* **172,**(17).

SANTOSH, M. MARUYAMA, S., SAWAKI, Y AND MEERT, J.G.2014. The Cambrian Explosion: Plume-driven birth of the second ecosystem on Earth. *Gondwana Research,* **25**(3) 945-965.

SIZOVA, E., GERYA, T., BROWN, M., AND PERCHUK, L.L. 2010. Subductions styles in the Precambrian: Insight from numerical experiments. *Lithos,* **116**, 209-229.

SMYE ,A., GREENWOOD, L.V., AND HOLLAND, T.J.B. 2010. Garnet–chloritoid–kyanite assemblages: eclogite facies indicators of subduction constraints in orogenic belts. *Journal of Metamorphic Geology,* **28**(7) 753-768.

STERN, R. 2005. Evidence from ophiolites, blueschists and ultrahigh-pressure metamorphic terranes that the modern episode of subduction tectonics began in Neoproterozoic time. *Geology,* **33**(7) 557-560.

STERN, R. 2008. Modern-style plate tectonics began in Neoproterozoic time: An alternative interpretation of Earth's tectonic history, *in:*Condie, K.C., and Pease, V. pp. 265-280.

STRACHAN, R. A. 2012. Late Neoproterozoic to Cambrian Accretionary History of Eastern Avalonia and Armorica on the Active Margin of Gondwana. Geological History of Britain and Ireland. pp. 133-149. John Wiley & Sons, Ltd.

TREAGUS, J. 2007. Metamorphic zones in the Anglesey blueschist belt and implications for the development of a Neoproterozoic subduction-accretion complex: discussion, *Journal of Metamorphic Geology* **25,** 507-508.

TSUJIMORI, T., AND ERNST, W.G. 2014. Lawsonite blueschists and lawsonite eclogites as proxies for palaeo-subduction zone processes: a review. *Journal of Metamorphic Geology,* **32**(5), 437-454.

TSUJIMORI, T., SISSON, V.B., LIOU, J.G., HARLOW, G.E., AND SORENSON, S.S. 2006. Very-low-temperature record of the subduction process: A review of worldwide lawsonite eclogites. *Lithos,* **92**, 609-624.

WHITE, R. W., POWELL, R., AND JOHNSON, TE. 2014. The effect of Mn on mineral stability in metapelites revisited: new a–x relations for manganese-bearing minerals, *Journal of Metamorphic Geology,* **32,** 809-828.

ZHENG, Y., CHEN, R.X., ZHENG, X.U., AND ZHANG, S.B., 2016. The transport of water in subduction zones. *SCIENCE CHINA, Earth Sciences,* **59**(4), 651-682.

Appendix A: U-Pb Geochronological Data

Standards Session 1	Pb^{207}/Pb^{206}	2σ	Pb^{207}/U^{235}	2σ	Pb^{206}/U^{238}	2σ	%conc.	Pb^{207}/U^{235}	2σ	Pb^{206}/U^{238}	2σ	Pb^{207}/Pb^{206}	2σ
GJ	0.0598	0.0016	0.791	0.021	0.0969	0.0017	106.565	589	12	595.7	9.9	559	58
GJ1_2	0.0592	0.0015	0.807	0.019	0.0987	0.0016	109.297	598	11	606.6	9.2	555	55
GJ1_3	0.0598	0.0016	0.808	0.02	0.0984	0.0015	105.567	599	11	604.9	9	573	57
GJ1_4	0.0605	0.0016	0.799	0.019	0.0971	0.0015	102.612	594	11	597.2	8.9	582	56
GJ1_5	0.0611	0.0016	0.82	0.021	0.0974	0.0019	97.398	607	11	599	11	615	59
GJ1_6	0.0603	0.0015	0.809	0.019	0.0972	0.0015	101.494	599	11	597.8	8.7	589	55
GJ1_7	0.0603	0.0013	0.805	0.017	0.097	0.0015	101.136	597.6	9.6	596.7	9	590	50
GJ1_8	0.0604	0.0015	0.805	0.019	0.0972	0.0015	102.698	597	11	597.7	9	582	54
GJ1_9	0.0609	0.0016	0.824	0.02	0.0982	0.0016	101.258	609	11	603.5	9.1	596	57
GJ1_10	0.0601	0.0015	0.812	0.02	0.0976	0.0017	104.695	601	11	599.9	9.9	573	54
GJ1_11	0.0601	0.0015	0.809	0.019	0.0972	0.0016	103.069	600	10	597.8	9.3	580	54
GJ1_12	0.0599	0.0016	0.812	0.021	0.0977	0.0015	107.041	600	12	600.5	8.7	561	60
GJ1_13	0.061	0.0016	0.824	0.02	0.0976	0.0016	99.338	610	11	600	9.3	604	57
GJ1_14	0.0606	0.0015	0.819	0.019	0.0974	0.0016	99.933	606	11	598.6	9.5	599	51
GJ1_15	0.0599	0.0015	0.813	0.019	0.098	0.0016	106.039	602	11	602.3	9.4	568	56
GJ1_16	0.0592	0.0016	0.803	0.021	0.0976	0.0017	110.037	596	12	599.7	9.7	545	58
GJ1_17	0.0594	0.0016	0.801	0.019	0.0977	0.0015	111.429	597	11	600.6	8.8	539	60
GJ1_18	0.0593	0.0015	0.81	0.02	0.0987	0.0016	111.026	599	11	606.2	9.5	546	55
GJ1_19	0.0602	0.0016	0.814	0.02	0.0978	0.0015	103.511	601	11	601.4	9.1	581	56
GJ1_20	0.0596	0.0016	0.809	0.019	0.0978	0.0016	107.971	599	11	601.4	9.2	557	58
GJ1_21	0.0604	0.0016	0.81	0.019	0.0976	0.0013	103.806	602	11	600	7.8	578	57
GJ1_22	0.0612	0.0015	0.82	0.02	0.0967	0.0015	95.304	605	11	594.7	8.8	624	54
GJ1_23	0.0609	0.0015	0.809	0.019	0.0969	0.0016	98.823	599	11	595.9	9.1	603	52
GJ1_24	0.0593	0.0015	0.795	0.019	0.0976	0.0016	110.442	592	11	599.7	9.1	543	56
GJ1_25	0.0591	0.0018	0.796	0.021	0.0977	0.0016	113.592	592	12	600.9	9.7	529	66
GJ1_26	0.0607	0.0016	0.817	0.02	0.0976	0.0014	100.807	604	11	599.8	8.2	595	56
GJ1_27	0.059	0.0016	0.792	0.019	0.0974	0.0013	112.383	589	11	599	7.9	533	57
GJ1_28	0.0602	0.0015	0.817	0.019	0.0986	0.0014	105.759	605	11	606	8.5	573	56
GJ1_29	0.0602	0.0014	0.813	0.018	0.0974	0.0013	103.293	602.9	10	599.1	7.8	580	52
GJ1_30	0.0608	0.0015	0.816	0.018	0.0976	0.0015	99.834	604.5	10	600	9.1	601	54
GJ1_31	0.0597	0.0015	0.807	0.02	0.0977	0.0015	107.846	598	11	600.7	8.6	557	54

GJ1_32	0.0609	0.0015	0.819	0.019	0.0971	0.0014	98.694	606	11	597.1	8.4	605	54
GJ1_33	0.0599	0.0016	0.806	0.018	0.0973	0.0014	105.912	599	11	598.4	8	565	57
GJ1_34	0.061	0.0016	0.824	0.019	0.0983	0.0014	100.382	610	11	604.3	8.4	602	55
GJ1_35	0.0602	0.0015	0.811	0.021	0.0974	0.0015	104.321	600	12	598.8	8.9	574	55
GJ1_36	0.06	0.0015	0.812	0.019	0.0978	0.0014	103.316	602	11	601.3	8.4	582	53
GJ1_37	0.0594	0.0015	0.797	0.019	0.0973	0.0013	109.378	593	11	598.3	7.9	547	57
GJ1_38	0.06	0.0015	0.816	0.019	0.0986	0.0015	106.095	603	11	605.8	8.5	571	56
GJ1_39	0.0609	0.0016	0.815	0.019	0.0973	0.0015	100.201	603	11	598.2	8.7	597	56
GJ1_40	0.0594	0.0015	0.797	0.02	0.0972	0.0015	109.706	592	11	597.9	9	545	55
GJ1_41	0.0604	0.0015	0.81	0.018	0.0976	0.0015	101.506	601.1	10	599.9	8.6	591	54
GJ1_42	0.0607	0.0015	0.817	0.018	0.0978	0.0015	100.233	605.1	10	601.4	8.5	600	53
GJ1_43	0.0589	0.0014	0.796	0.018	0.0981	0.0014	112.059	593.4	9.7	604	8.4	539	54
GJ1_44	0.0606	0.0015	0.807	0.019	0.097	0.0014	100.777	599	11	596.6	8.3	592	54
GJ1_45	0.0614	0.0016	0.811	0.019	0.0964	0.0014	97.213	600	11	593	8.4	610	58
GJ1_46	0.0598	0.0015	0.808	0.019	0.0981	0.0015	105.940	600	11	602.8	8.6	569	55
GJ1_47	0.0598	0.0015	0.801	0.019	0.0975	0.0014	106.241	596	11	599.2	8.3	564	56
GJ1_48	0.0597	0.0016	0.803	0.02	0.0983	0.0015	109.025	599	11	604	8.6	554	59
GJ1_49	0.0606	0.0015	0.827	0.019	0.0984	0.0014	101.973	609	11	604.7	8.4	593	56
GJ1_50	0.0604	0.0016	0.806	0.019	0.0967	0.0013	102.041	597	11	594.9	7.7	583	58
GJ1_51	0.0598	0.0014	0.805	0.018	0.0974	0.0014	106.530	597.2	10	598.7	8	562	53
GJ1_52	0.0598	0.0016	0.809	0.019	0.0984	0.0014	109.367	600	11	604.8	7.9	553	59
GJ1_53	0.0587	0.0015	0.795	0.02	0.0976	0.0013	115.404	591	11	600.1	7.5	520	58
GJ1_54	0.0606	0.0015	0.814	0.018	0.0968	0.0013	99.866	602.3	10	595.2	7.6	596	54
GJ1_55	0.0607	0.0015	0.819	0.018	0.0977	0.0013	100.586	606	10	600.5	7.9	597	55
GJ1_56	0.0609	0.0015	0.825	0.019	0.0979	0.0015	99.439	609	11	602.6	8.5	606	54
GJ1_57	0.0598	0.0016	0.804	0.018	0.0973	0.0015	107.048	596.5	10	598.4	8.6	559	59
GJ1_58	0.0606	0.0015	0.824	0.018	0.0988	0.0014	102.411	609.7	10	607.3	8.2	593	54
GJ1_59	0.0595	0.0015	0.803	0.018	0.098	0.0014	108.755	596.9	10	602.5	8.3	554	54
GJ1_60	0.06	0.0015	0.809	0.02	0.0975	0.0013	104.860	599	11	599.8	7.8	572	54
GJ1_61	0.0603	0.0015	0.808	0.019	0.0971	0.0011	101.582	598	11	597.3	6.7	588	56
GJ1_62	0.0615	0.0015	0.819	0.017	0.0973	0.0014	95.744	605.5	9.5	598.4	8.1	625	53
GJ1_63	0.0586	0.0015	0.785	0.018	0.0978	0.0013	116.492	588	11	601.1	7.7	516	56
GJ1_64	0.0602	0.0015	0.805	0.019	0.0976	0.0014	104.764	597	11	600.3	8.2	573	56
Ples_1	0.05292	0.0012	0.3838	0.0083	0.05311	0.0009	107.929	329	6.1	333.5	5.6	309	48
Ples_2	0.05397	0.0011	0.3982	0.0078	0.05402	0.0008	97.414	339.6	5.7	339	5.4	348	46
Ples_3	0.0527	0.0012	0.3895	0.0086	0.05382	0.00083	116.886	333.1	6.3	337.8	5.1	289	51

Ples_4	0.0536	0.0012	0.3963	0.0092	0.05378	0.00089	102.614	337.9	6.7	337.6	5.5	329	49
Ples_5	0.0535	0.0012	0.4028	0.0084	0.05442	0.00088	103.485	343.4	6.2	341.5	5.4	330	51
Ples_6	0.0528	0.0012	0.3918	0.0084	0.05373	0.00084	113.953	334.8	6.1	337.3	5.1	296	51
Ples_7	0.0527	0.0012	0.3942	0.0081	0.05408	0.00086	116.233	336.6	5.9	339.4	5.3	292	50
Ples_8	0.0526	0.0012	0.3933	0.0087	0.05392	0.00088	117.909	335.8	6.3	338.4	5.4	287	52
Ples_9	0.0523	0.0012	0.395	0.0093	0.05408	0.00088	120.783	336.9	6.8	339.4	5.4	281	51
Ples_10	0.0528	0.0012	0.4003	0.0089	0.0545	0.00091	112.871	341.6	6.3	342	5.6	303	53
Ples_11	0.05324	0.0012	0.4047	0.0088	0.05485	0.00091	106.533	344.1	6.3	344.1	5.6	323	51
Ples_12	0.05349	0.0012	0.4035	0.0086	0.05466	0.0009	105.215	343.3	6.2	343	5.5	326	48
Ples_13	0.0534	0.0012	0.3997	0.0093	0.05406	0.00084	103.131	340.4	6.7	339.3	5.1	329	51
Ples_14	0.0536	0.0012	0.4051	0.0087	0.05474	0.00091	103.746	344.4	6.3	343.4	5.5	331	49
Ples_15	0.05295	0.0012	0.4026	0.0088	0.05529	0.00093	114.079	342.6	6.4	346.8	5.7	304	49
Ples_16	0.05358	0.0011	0.396	0.0086	0.05343	0.00088	99.525	338.5	6.1	335.4	5.4	337	46
Ples_17	0.05362	0.0012	0.4037	0.0083	0.05461	0.00093	103.505	344.1	6.1	342.6	5.7	331	48
Ples_18	0.05311	0.0012	0.3964	0.0078	0.05417	0.00091	109.645	338.9	5.7	339.9	5.6	310	48
Ples_19	0.0523	0.0012	0.3914	0.0088	0.05439	0.0009	122.330	334.4	6.4	341.3	5.5	279	50
Ples_20	0.05293	0.0012	0.3949	0.0086	0.05413	0.00085	111.013	337	6.2	339.7	5.2	306	49
Ples_21	0.0535	0.0013	0.4003	0.0092	0.05425	0.00086	100.740	340.8	6.7	340.5	5.3	338	52
Ples_22	0.0538	0.0013	0.4028	0.0097	0.0545	0.00088	102.703	342.5	7	342	5.4	333	54
Ples_23	0.05325	0.0012	0.4009	0.0089	0.05456	0.00087	104.360	342	6.5	342.3	5.3	328	50
Ples_24	0.05394	0.0012	0.3997	0.0084	0.05395	0.00086	98.145	340.5	6.1	338.6	5.3	345	49
Ples_25	0.05376	0.0011	0.4053	0.0081	0.05451	0.00084	99.708	344.7	5.8	342	5.2	343	48
Ples_26	0.05282	0.0011	0.3977	0.0075	0.05443	0.00084	111.967	339.9	5.3	341.5	5.1	305	45
Ples_27	0.0538	0.0012	0.3961	0.0087	0.05323	0.00087	98.006	337.9	6.3	334.2	5.4	341	48
Ples_28	0.05355	0.0011	0.3952	0.0081	0.05342	0.00082	101.024	337.3	5.9	335.4	5	332	46
Ples_29	0.0533	0.0012	0.404	0.0089	0.055	0.00086	107.477	343.6	6.4	345	5.2	321	51
Ples_30	0.0536	0.0013	0.4051	0.0089	0.05496	0.00086	104.802	344.3	6.4	344.8	5.3	329	53
Ples_31	0.0537	0.0013	0.406	0.0089	0.0553	0.00085	105.441	345	6.4	346.9	5.2	329	52
Ples_32	0.05328	0.0012	0.397	0.0082	0.05446	0.00086	107.453	338.7	5.9	341.7	5.2	318	48
91500_1	0.0725	0.0021	1.759	0.053	0.1773	0.0032	109.708	1021	19	1051	18	958	62
91500_2	0.0769	0.0024	1.877	0.055	0.1801	0.0035	100.094	1067	20	1066	19	1065	67
91500_3	0.0755	0.0023	1.838	0.056	0.178	0.0033	100.381	1051	20	1055	18	1051	61
91500_4	0.0739	0.0024	1.793	0.053	0.1773	0.0034	105.522	1040	19	1051	19	996	66
91500_5	0.074	0.0023	1.818	0.052	0.1786	0.0031	107.739	1047	19	1058	17	982	65
91500_6	0.0726	0.0021	1.825	0.052	0.1802	0.0032	110.455	1046	19	1067	18	966	60
91500_7	0.0741	0.0024	1.831	0.057	0.1778	0.0032	106.687	1046	21	1053	17	987	68

91500_8	0.0743	0.0025	1.805	0.054	0.1759	0.0034	104.930	1042	19	1043	18	994	69
91500_9	0.0755	0.0024	1.885	0.055	0.1817	0.0036	104.475	1069	19	1074	20	1028	65
91500_10	0.0755	0.0026	1.853	0.057	0.1792	0.0035	104.122	1056	21	1061	19	1019	72
91500_11	0.0744	0.0023	1.852	0.054	0.1809	0.0032	107.315	1057	19	1071	17	998	66
91500_12	0.0725	0.0024	1.783	0.055	0.1798	0.0034	113.554	1029	20	1064	19	937	70
91500_13	0.0728	0.0023	1.802	0.053	0.1796	0.0033	108.461	1041	19	1064	18	981	64
91500_14	0.0746	0.0023	1.873	0.057	0.1815	0.0035	105.397	1062	20	1074	19	1019	64
91500_15	0.0748	0.0023	1.814	0.052	0.1767	0.0033	104.382	1043	19	1048	18	1004	66
91500_16	0.0734	0.0023	1.825	0.059	0.1798	0.0035	109.804	1048	21	1064	19	969	68
91500_17	0.0748	0.0025	1.824	0.054	0.1784	0.0035	104.344	1045	20	1057	19	1013	66
91500_18	0.0737	0.0024	1.805	0.059	0.1781	0.0034	109.326	1036	21	1055	19	965	70
91500_19	0.0733	0.0024	1.785	0.056	0.1765	0.0033	107.503	1032	20	1046	18	973	69
91500_20	0.0766	0.0027	1.821	0.055	0.1759	0.0034	101.260	1049	21	1045	19	1032	73
91500_21	0.0747	0.0024	1.826	0.059	0.1777	0.0038	104.158	1046	22	1052	21	1010	66
91500_22	0.0765	0.0025	1.846	0.058	0.1758	0.0033	98.768	1056	21	1042	18	1055	68
91500_23	0.078	0.0025	1.867	0.05	0.1761	0.0033	96.584	1065	18	1046	18	1083	68
91500_24	0.0761	0.0024	1.87	0.057	0.1791	0.0035	100.569	1060	20	1061	19	1055	65
91500_25	0.0755	0.0024	1.839	0.059	0.1771	0.0032	103.346	1048	21	1050	17	1016	68
91500_26	0.075	0.0024	1.842	0.061	0.1782	0.0034	103.835	1053	22	1056	19	1017	67
91500_27	0.0761	0.0026	1.85	0.055	0.1781	0.0036	102.328	1054	20	1055	20	1031	71
91500_28	0.0754	0.0023	1.816	0.054	0.1748	0.0034	100.777	1044	20	1037	19	1029	64
91500_29	0.0745	0.0023	1.838	0.053	0.1799	0.0033	105.030	1052	19	1065	18	1014	61
91500_30	0.0765	0.0025	1.855	0.056	0.1777	0.0034	100.286	1060	20	1053	19	1050	66
91500_31	0.0766	0.0024	1.87	0.053	0.1796	0.0033	99.625	1067	19	1064	18	1068	61
91500_32	0.0754	0.0024	1.854	0.06	0.1805	0.0039	104.706	1055	22	1068	21	1020	70
Standards Session 2	Pb^{207}/Pb^{206}	2σ	Pb^{207}/U^{235}	2σ	Pb^{206}/U^{238}	2σ	%conc.	Pb^{207}/U^{235}	2σ	Pb^{206}/U^{238}	2σ	Pb^{207}/Pb^{206}	2σ
GJ1_1	0.0598	0.0015	0.805	0.02	0.0973	0.0014	105.89	598	12	598.3	8.2	565	55
GJ1_2	0.0596	0.0014	0.801	0.019	0.0975	0.0015	106.83	594.9	11	599.3	8.8	561	52
GJ1_3	0.0603	0.0014	0.814	0.019	0.0977	0.0015	102.84	603.3	11	601.6	8.7	585	51
GJ1_4	0.0603	0.0014	0.818	0.02	0.0981	0.0015	103.29	604	11	603.2	8.9	584	52
GJ1_5	0.0619	0.0014	0.823	0.02	0.0967	0.0015	91.65	608.3	11	594.8	8.9	649	48
GJ1_6	0.0592	0.0015	0.801	0.022	0.0977	0.0013	109.33	594	12	601.3	7.7	550	55
GJ1_7	0.0597	0.0015	0.797	0.019	0.0977	0.0015	107.85	593.8	11	600.7	8.7	557	54
GJ1_8	0.0608	0.0014	0.82	0.019	0.0981	0.0014	99.13	607.5	11	602.7	8	608	49
GJ1_9	0.0603	0.0015	0.815	0.021	0.0978	0.0014	103.85	602	12	601.3	8.5	579	58

GJ1_10	0.0601	0.0015	0.811	0.02	0.0977	0.0015	105.22	601	11	600.8	8.6	571	53
GJ1_11	0.0592	0.0014	0.803	0.021	0.0978	0.0015	110.13	597	11	601.3	8.8	546	53
GJ1_12	0.0596	0.0015	0.799	0.019	0.0971	0.0015	105.85	594.1	11	597	8.7	564	53
GJ1_13	0.0599	0.0016	0.804	0.021	0.0973	0.0014	105.02	598	12	598.6	7.9	570	59
GJ1_14	0.061	0.0016	0.811	0.021	0.0971	0.0015	99.53	600	12	597.2	9	600	57
GJ1_15	0.0598	0.0014	0.813	0.019	0.0984	0.0014	105.22	601.6	11	605	8.2	575	50
GJ1_16	0.0607	0.0015	0.813	0.019	0.0974	0.0015	99.97	601.9	11	598.8	8.7	599	53
GJ1_17	0.0609	0.0015	0.819	0.021	0.0977	0.0015	99.82	605	12	600.9	8.8	602	54
GJ1_18	0.0601	0.0015	0.813	0.02	0.098	0.0014	102.83	603	11	602.6	8.3	586	53
GJ1_19	0.0597	0.0015	0.807	0.021	0.0979	0.0015	108.65	597	12	601.9	8.6	554	55
GJ1_20	0.0598	0.0015	0.801	0.019	0.0969	0.0014	104.73	595	11	595.9	8.1	569	53
GJ1_21	0.06	0.0016	0.805	0.02	0.0969	0.0014	103.65	597	11	596	7.9	575	58
GJ1_22	0.0601	0.0016	0.815	0.021	0.0984	0.0014	106.07	602	12	604.6	8.1	570	59
GJ1_23	0.0599	0.0015	0.801	0.02	0.0973	0.0013	105.57	596	11	598.6	7.7	567	55
GJ1_24	0.0605	0.0015	0.812	0.02	0.0978	0.0013	103.12	600.9	11	601.2	7.8	583	54
GJ1_25	0.0594	0.0015	0.811	0.021	0.0986	0.0014	111.32	600	12	605.6	8.5	544	56
GJ1_26	0.0605	0.0017	0.81	0.022	0.0975	0.0015	104.21	599	12	599.2	8.6	575	60
GJ1_27	0.0614	0.0016	0.82	0.022	0.0968	0.0014	97.57	605	13	595.2	8	610	57
GJ1_28	0.06	0.0016	0.811	0.022	0.0978	0.0015	106.39	600	12	601.1	8.6	565	57
GJ1_29	0.059	0.0015	0.795	0.021	0.0977	0.0014	112.74	593	11	600.9	8.2	533	57
GJ1_30	0.0606	0.0015	0.812	0.021	0.0972	0.0014	101.79	601	12	597.5	8.4	587	55
GJ1_31	0.0588	0.0015	0.798	0.021	0.0979	0.0014	114.39	593	12	601.7	8	526	55
GJ1_32	0.0611	0.0015	0.822	0.02	0.0977	0.0014	98.60	607	11	600.5	8.3	609	53
GJ1_33	0.0601	0.0015	0.81	0.021	0.0978	0.0013	103.83	601	12	601.2	7.8	579	56
GJ1_34	0.0605	0.0016	0.809	0.02	0.0975	0.0014	102.65	600	12	599.5	8.3	584	58
GJ1_35	0.0606	0.0016	0.807	0.021	0.0971	0.0015	101.20	599	12	597.1	9	590	55
GJ1_36	0.0604	0.0015	0.812	0.021	0.0978	0.0015	103.51	601	12	601.4	8.6	581	54
GJ1_37	0.0601	0.0015	0.815	0.02	0.0982	0.0014	105.32	602	11	603.5	8.4	573	57
GJ1_38	0.0596	0.0016	0.807	0.02	0.0978	0.0013	108.77	600	11	601.5	7.9	553	57
GJ1_39	0.0604	0.0016	0.808	0.02	0.0971	0.0014	102.59	598.6	11	597.1	8.1	582	56
GJ1_40	0.0597	0.0014	0.806	0.021	0.0974	0.0014	105.39	597	12	598.6	8	568	54
GJ1_41	0.0591	0.0016	0.79	0.021	0.0974	0.0015	113.82	588	12	598.7	8.6	526	59
GJ1_42	0.0614	0.0015	0.832	0.02	0.0984	0.0014	96.61	613.6	11	604.8	8	626	54
GJ1_43	0.06	0.0016	0.805	0.021	0.0978	0.0015	107.71	598	12	601	8.7	558	59
GJ1_44	0.0603	0.0015	0.808	0.021	0.0969	0.0014	100.85	599	12	596	8.2	591	54
GJ1_45	0.0604	0.0015	0.815	0.02	0.0981	0.0015	100.63	603	12	602.8	8.9	599	55

GJ1_46	0.061	0.0016	0.82	0.022	0.0975	0.0014	99.27	605	12	599.6	8.5	604	57
GJ1_47	0.0597	0.0016	0.795	0.02	0.0966	0.0014	107.12	591	11	594.5	8.1	555	58
GJ1_48	0.0596	0.0014	0.808	0.019	0.0982	0.0014	107.25	599.2	11	603.8	8.1	563	49
GJ1_49	0.0606	0.0015	0.821	0.021	0.0981	0.0013	101.86	607	12	603	7.9	592	55
GJ1_50	0.0602	0.0015	0.81	0.02	0.0975	0.0014	103.04	602	11	599.7	8.1	582	56
GJ1_51	0.0595	0.0015	0.8	0.02	0.0974	0.0014	109.73	595	11	599.1	8.4	546	55
GJ1_52	0.0606	0.0017	0.812	0.023	0.0974	0.0013	102.36	603	13	598.8	7.8	585	58
GJ1_53	0.0598	0.0016	0.799	0.022	0.0972	0.0016	107.27	593	12	597.5	9.4	557	58
GJ1_54	0.0599	0.0014	0.808	0.02	0.0979	0.0014	104.81	600	12	601.6	8.3	574	53
GJ1_55	0.0602	0.0015	0.812	0.02	0.0977	0.0012	104.89	602	11	601	7.3	573	55
GJ1_56	0.0603	0.0016	0.809	0.02	0.0976	0.0013	104.37	600	11	600.1	7.6	575	56
GJ1_57	0.0605	0.0017	0.808	0.022	0.0969	0.0015	103.10	598	12	595.9	8.7	578	60
GJ1_58	0.0604	0.0016	0.812	0.021	0.0974	0.0014	101.89	602	11	599.1	8	588	56
GJ1_59	0.0608	0.0016	0.825	0.021	0.0982	0.0013	100.95	608	11	603.7	7.9	598	56
GJ1_60	0.0599	0.0015	0.807	0.02	0.0977	0.0013	105.20	601	11	600.7	7.7	571	56
GJ1_61	0.0592	0.0015	0.797	0.019	0.0977	0.0012	111.71	592.9	11	601	7	538	55
GJ1_62	0.0589	0.0015	0.801	0.021	0.098	0.0014	112.85	595	12	602.6	8.1	534	58
GJ1_63	0.0606	0.0015	0.815	0.02	0.0974	0.0013	101.82	603	11	599.7	7.6	589	55
GJ1_64	0.0606	0.0017	0.81	0.021	0.0971	0.0014	102.05	599	12	597	8.4	585	60
GJ1_65	0.0613	0.0017	0.836	0.022	0.0991	0.0014	101.13	614	12	609.8	8.4	603	59
GJ1_66	0.0606	0.0016	0.81	0.02	0.0972	0.0013	102.36	600	11	597.8	7.4	584	58
GJ1_67	0.0598	0.0015	0.803	0.019	0.0976	0.0013	106.11	596.3	11	600.6	7.5	566	54
GJ1_68	0.0603	0.0015	0.803	0.02	0.097	0.0012	102.32	595.9	11	596.5	7	583	53
GJ1_69	0.0604	0.0016	0.809	0.021	0.0974	0.0015	103.78	600	12	598.8	8.7	577	58
GJ1_70	0.0603	0.0015	0.812	0.021	0.0974	0.0014	102.53	601	12	598.8	8	584	56
GJ1_71	0.0594	0.0015	0.806	0.02	0.0978	0.0013	107.99	598	11	601.5	7.8	557	55
GJ1_72	0.0601	0.0016	0.807	0.021	0.0979	0.0014	106.86	599	12	601.6	8.4	563	59
Ples_1	0.0535	0.0012	0.3977	0.0098	0.05372	0.00082	103.44	338.9	7.1	337.2	5	326	51
Ples_2	0.0536	0.0012	0.3961	0.0095	0.05359	0.00074	102.87	337.8	7	336.4	4.5	327	51
Ples_3	0.0527	0.0013	0.3973	0.0097	0.05479	0.00077	119.38	338.7	7	343.8	4.7	288	53
Ples_4	0.0541	0.0012	0.4027	0.0095	0.05395	0.00071	97.05	342.6	6.9	338.7	4.3	349	49
Ples_5	0.05381	0.0012	0.3993	0.0087	0.05382	0.00072	98.63	340.4	6.3	338.3	4.5	343	48
Ples_6	0.0536	0.0012	0.4053	0.009	0.05507	0.00073	105.34	345.3	6.4	345.5	4.5	328	50
Ples_7	0.0535	0.0012	0.3984	0.0092	0.05394	0.00074	102.30	339.6	6.7	338.6	4.5	331	49
Ples_8	0.0527	0.0012	0.3927	0.0093	0.05417	0.00078	118.47	335.4	6.8	340	4.7	287	51
Ples_9	0.0538	0.0012	0.3974	0.009	0.05363	0.00078	99.03	338.9	6.5	336.7	4.8	340	49

Ples_10	0.0532	0.0012	0.3947	0.0084	0.05423	0.0008	109.81	338.3	5.9	340.4	4.9	310	51
Ples_11	0.05378	0.0011	0.4028	0.0083	0.0542	0.00072	97.48	343.5	5.9	340.2	4.4	349	46
Ples_12	0.05339	0.0011	0.4003	0.0085	0.05435	0.00069	105.28	341.1	6.2	341.1	4.2	324	45
Ples_13	0.0596	0.0015	0.447	0.012	0.05433	0.00081	60.55	373.9	8.3	340.9	5	563	54
Ples_14	0.0564	0.0014	0.418	0.011	0.05368	0.00077	76.24	353.1	7.9	337	4.7	442	57
Ples_15	0.0532	0.0012	0.396	0.0092	0.054	0.0008	109.32	337.9	6.7	338.9	4.9	310	50
Ples_16	0.0533	0.0012	0.4073	0.0088	0.0554	0.00085	107.92	346.2	6.3	347.5	5.2	322	49
Ples_17	0.05326	0.001	0.4012	0.0084	0.05459	0.00077	106.73	341.8	6	342.6	4.7	321	43
Ples_18	0.0555	0.0012	0.4188	0.0093	0.0546	0.0008	83.56	354.4	6.6	342.6	4.9	410	50
Ples_19	0.0535	0.0012	0.4005	0.0094	0.05387	0.00074	101.53	341	6.8	338.1	4.5	333	51
Ples_20	0.0532	0.0011	0.3965	0.009	0.05387	0.00079	106.02	338.8	6.4	338.2	4.9	319	48
Ples_21	0.0541	0.0012	0.4041	0.0092	0.05436	0.00074	98.02	343.8	6.6	341.1	4.5	348	50
Ples_22	0.0533	0.0012	0.3959	0.0087	0.05404	0.00074	106.67	337.9	6.3	339.2	4.5	318	50
Ples_23	0.0525	0.0012	0.3875	0.0089	0.05363	0.0007	117.73	331.7	6.6	336.7	4.3	286	49
Ples_24	0.054	0.0013	0.4069	0.0098	0.05477	0.00076	99.88	345.6	7	343.6	4.7	344	53
Ples_25	0.0516	0.0013	0.3907	0.0099	0.05471	0.00077	135.16	334.4	7.4	343.3	4.7	254	55
Ples_26	0.0536	0.0009	0.4014	0.0079	0.05409	0.00079	99.27	342.6	5.6	339.5	4.8	342	42
Ples_27	0.05284	0.0009	0.3966	0.0078	0.05433	0.00072	110.36	338.6	5.7	341	4.4	309	43
Ples_28	0.05304	0.001	0.4004	0.0084	0.05477	0.00076	108.77	341.2	6.1	343.7	4.7	316	43
Ples_29	0.0566	0.0015	0.433	0.014	0.05501	0.00079	76.86	363.6	9.4	345.1	4.8	449	59
Ples_30	0.0526	0.001	0.3999	0.0076	0.05496	0.00074	115.70	341.1	5.5	344.8	4.5	298	43
Ples_31	0.0528	0.0014	0.395	0.011	0.05424	0.00087	114.61	336.8	8	340.4	5.3	297	60
Ples_32	0.053	0.0012	0.3964	0.0088	0.05417	0.00066	108.97	338.3	6.4	340	4	312	51
Ples_33	0.0604	0.002	0.466	0.017	0.05603	0.00087	61.96	385	11	351.3	5.3	567	68
Ples_34	0.05351	0.0009	0.4075	0.0076	0.05554	0.00074	103.97	346.6	5.5	348.3	4.5	335	40
Ples_35	0.05306	0.001	0.4062	0.0081	0.05495	0.00067	108.77	345.5	5.8	344.8	4.1	317	42
Ples_36	0.05328	0.0009	0.4057	0.0078	0.05457	0.00069	104.07	345.2	5.7	342.4	4.2	329	41
91500_1	0.0754	0.0024	1.807	0.063	0.1736	0.0029	101.88	1036	23	1031	16	1012	68
91500_2	0.0759	0.0025	1.837	0.058	0.1765	0.003	101.65	1051	20	1047	16	1030	70
91500_3	0.0747	0.0025	1.814	0.057	0.1764	0.0033	103.87	1047	20	1046	18	1007	71
91500_4	0.0764	0.0025	1.823	0.056	0.1746	0.0032	98.48	1046	21	1036	18	1052	67
91500_5	0.0766	0.0026	1.846	0.056	0.178	0.0032	101.25	1056	21	1055	17	1042	73
91500_6	0.076	0.0024	1.851	0.057	0.1778	0.0031	101.15	1056	21	1055	17	1043	66
91500_7	0.0747	0.0023	1.83	0.058	0.1777	0.0029	103.84	1046	21	1054	16	1015	64
91500_8	0.0728	0.0025	1.766	0.057	0.1761	0.0031	111.78	1023	22	1044	17	934	76
91500_9	0.0748	0.0024	1.823	0.057	0.1774	0.0031	102.43	1049	21	1052	17	1027	65

91500_10	0.0744	0.0024	1.828	0.061	0.1781	0.003	105.18	1049	21	1056	16	1004	68
91500_11	0.0763	0.0026	1.837	0.059	0.1749	0.003	99.05	1048	21	1038	17	1048	67
91500_12	0.077	0.0029	1.849	0.063	0.1757	0.0029	101.07	1051	23	1042	16	1031	80
91500_13	0.0756	0.0023	1.818	0.056	0.1752	0.0028	100.00	1045	21	1040	15	1040	61
91500_14	0.0739	0.0024	1.781	0.057	0.1757	0.0029	106.54	1029	21	1042	16	978	68
91500_15	0.0734	0.0026	1.733	0.06	0.1727	0.0029	106.76	1014	23	1026	16	961	72
91500_16	0.0743	0.0026	1.803	0.064	0.1764	0.0031	105.44	1039	23	1046	17	992	75
91500_17	0.074	0.0025	1.8	0.059	0.1769	0.003	107.48	1037	22	1049	16	976	71
91500_18	0.0745	0.0027	1.775	0.057	0.1745	0.0032	105.40	1029	21	1035	18	982	73
91500_19	0.0773	0.0026	1.828	0.056	0.173	0.003	95.54	1048	21	1028	16	1076	68
91500_20	0.0753	0.0027	1.813	0.063	0.1754	0.0031	104.41	1043	22	1041	17	997	73
91500_21	0.0765	0.0026	1.824	0.06	0.1742	0.0028	98.01	1050	22	1034	15	1055	71
91500_22	0.0744	0.0025	1.8	0.06	0.1765	0.0031	106.84	1034	22	1047	17	980	74
91500_23	0.074	0.0024	1.801	0.059	0.1759	0.0028	105.67	1037	22	1043	15	987	70
91500_24	0.0752	0.0024	1.812	0.056	0.1756	0.0029	102.46	1043	21	1042	16	1017	67
91500_25	0.0755	0.0025	1.842	0.062	0.1759	0.0029	100.29	1054	22	1044	16	1041	69
91500_26	0.0764	0.0025	1.859	0.058	0.1764	0.0029	99.71	1059	21	1046	16	1049	69
91500_27	0.0725	0.0026	1.763	0.059	0.1775	0.0029	111.56	1028	21	1052	16	943	73
91500_28	0.0746	0.0025	1.833	0.063	0.1777	0.0027	105.71	1048	22	1055	15	998	69
91500_29	0.0725	0.0026	1.765	0.06	0.1778	0.0029	115.32	1022	22	1054	16	914	76
91500_30	0.0743	0.0027	1.778	0.061	0.1736	0.0027	103.93	1028	22	1031	15	992	73
91500_31	0.0761	0.0024	1.836	0.057	0.1761	0.0029	99.62	1053	21	1044	16	1048	63
91500_32	0.0752	0.0023	1.851	0.058	0.1771	0.0027	100.48	1058	21	1050	15	1045	62
91500_33	0.0767	0.0027	1.853	0.062	0.1768	0.0031	99.90	1055	22	1048	17	1049	72
91500_34	0.0751	0.0025	1.813	0.059	0.1769	0.0031	102.34	1046	21	1049	17	1025	67
91500_35	0.0756	0.0026	1.832	0.059	0.1751	0.0029	101.17	1051	21	1039	16	1027	68
91500_36	0.0774	0.0025	1.878	0.061	0.1746	0.0028	96.73	1064	22	1036	15	1071	66

Anglesey Samples, italicized: not used

Sample Session 1	Pb^{207}/Pb^{206}	2σ	Pb^{207}/U^{235}	2σ	Pb^{206}/U^{238}	2σ	%conc.	Pb^{207}/U^{206}	2σ	Pb^{207}/U^{235}	2σ	Pb^{206}/Pb^{238}	2σ
ANG8_1	0.0963	0.002	2.914	0.051	0.2194	0.0031	83.0	1540	39	1383	13	1278	16
ANG8_6	0.772	0.082	11.9	1.9	0.128	0.021	16.6	4890	220	2450	140	750	110
ANG8_10	0.1219	0.0023	1.116	0.059	0.0672	0.0038	55.1	1972	34	742	28	417	23
ANG8_11	0.791	0.097	54	11	0.52	0.11	65.7	4930	230	4000	190	2630	460
ANG8_12	*0.843*	*0.016*	*2580*	*160*	*22.1*	*1.3*	*2621.6*	*5059*	*36*	*7936*	*59*	*20040*	*370*
ANG8_14	0.685	0.024	38.3	1.3	0.415	0.014	60.6	4685	58	3700	34	2221	64
ANG8_15	0.66	0.17	37.6	9.1	0.421	0.081	63.8	4620	420	3670	270	2250	370
ANG8_17	*0.814*	*0.026*	*204*	*26*	*1.79*	*0.24*	*219.9*	*5001*	*62*	*5020*	*190*	*5950*	*580*
ANG8_18	0.198	0.0033	5.049	0.097	0.1854	0.0037	93.6	2803	27	1823	16	1095	20
ANG8_19	0.1899	0.0032	2.697	0.048	0.1029	0.0016	54.2	2734	28	1325	13	631.1	9.3
ANG8_21	*0.1133*	*0.0021*	*3.613*	*0.079*	*0.2315*	*0.0049*	*204.3*	*1845*	*33*	*1545*	*18*	*1340*	*25*
ANG8_22	*0.1245*	*0.0022*	*3.06*	*0.12*	*0.1794*	*0.0072*	*144.1*	*2012*	*31*	*1397*	*33*	*1057*	*40*
ANG8_27	*0.788*	*0.015*	*389*	*74*	*3.49*	*0.66*	*442.9*	*4934*	*35*	*5280*	*200*	*7320*	*850*
ANG8_32	*0.835*	*0.021*	*503*	*48*	*4.34*	*0.4*	*519.8*	*5040*	*47*	*6206*	*93*	*10440*	*470*
ANG8_33	0.1661	0.0034	1.977	0.04	0.0866	0.0015	52.1	2505	35	1104	14	535.3	8.6
ANG8_35	*0.834*	*0.044*	*339*	*36*	*2.98*	*0.32*	*357.3*	*5039*	*99*	*5890*	*100*	*8790*	*510*
ANG8_37	*0.845*	*0.017*	*2670*	*100*	*23.3*	*1*	*2757.4*	*5064*	*38*	*8000*	*43*	*20420*	*280*
ANG8_38	*0.846*	*0.018*	*1450*	*220*	*13*	*2*	*1536.6*	*5065*	*40*	*7230*	*120*	*15970*	*740*
ANG8_39	0.1819	0.004	1.48	0.036	0.0601	0.0019	33.0	2660	36	919	15	375	11
ANG8_40	0.1403	0.0026	2.525	0.043	0.1311	0.0022	93.4	2223	32	1277	12	794	12
ANG12_1	0.0631	0.0028	0.871	0.036	0.1006	0.0018	99.7	620	93	627	20	618	11
ANG12_2	0.0637	0.0029	0.851	0.038	0.0976	0.002	96.6	622	98	614	21	601	12
ANG12_4	0.062	0.0022	0.854	0.031	0.0993	0.0018	97.1	628	78	622	17	610	10
ANG12_5	0.08125	0.0012	2.431	0.033	0.2171	0.0028	103.6	1222	29	1250.8	9.5	1266	15
ANG12_6	0.0742	0.003	1.076	0.041	0.1057	0.0021	66.7	970	81	734	20	647	12
ANG12_7	0.0614	0.0013	0.864	0.017	0.1021	0.0013	98.1	639	44	630.2	9.1	626.7	7.4
ANG12_8	0.0576	0.0028	0.809	0.037	0.1018	0.0022	142.5	438	100	595	22	624	13
ANG12_9	0.0674	0.0021	0.931	0.027	0.101	0.0015	77.8	797	66	666	14	619.8	8.8
ANG12_10	0.0597	0.0028	0.802	0.037	0.0984	0.0019	122.5	494	96	589	21	605	11
ANG12_11	0.062	0.0017	0.852	0.022	0.0996	0.0014	95.5	641	61	624	12	612.1	8.3
ANG12_12	0.0622	0.0021	0.883	0.03	0.1036	0.0018	102.1	622	73	638	16	635	10
ANG12_13	0.06249	0.001	0.873	0.012	0.1011	0.0012	89.7	692	35	636.5	6.5	620.8	7.2

ANG12_14	0.1056	0.0019	4.379	0.071	0.3012	0.0045	98.9	1714	33	1705	13	1695	22
ANG12_16	0.0639	0.0017	0.904	0.022	0.1028	0.0013	89.4	705	57	651	12	630.3	7.7
ANG12_17	0.0638	0.0033	0.897	0.044	0.1028	0.002	105.0	600	110	636	24	630	12
ANG12_18	0.0731	0.0036	1.031	0.048	0.1037	0.0023	71.3	890	100	713	25	635	14
ANG12_21	0.809	0.047	427	40	3.94	0.44	202.4	4980	110	6112	97	10080	570
ANG12_22	0.0631	0.0021	0.918	0.029	0.1061	0.0017	99.5	653	72	656	15	649.6	9.6
ANG12_23	0.0612	0.002	0.882	0.026	0.1044	0.0015	109.0	587	71	637	14	639.7	8.6
ANG12_24	0.1013	0.0024	4.15	0.089	0.2983	0.0043	103.6	1623	44	1659	18	1681	21
ANG12_25	0.0618	0.0029	0.877	0.041	0.1031	0.0021	114.5	552	100	628	22	632	12
ANG12_26	0.0602	0.0023	0.85	0.03	0.1028	0.0016	119.1	530	81	618	16	631.2	8.9
ANG12_27	0.0586	0.0022	0.814	0.028	0.1015	0.0017	129.5	481	81	600	16	623	10
ANG12_28	0.0644	0.0014	0.927	0.019	0.1045	0.0013	86.9	737	44	664.9	9.7	640.4	7.7
ANG12_29	0.061	0.0014	0.857	0.019	0.1017	0.0014	99.9	625	50	626.9	10	624.1	8.4
ANG12_30	0.0623	0.0021	0.871	0.028	0.1018	0.0015	98.2	636	71	634	16	624.5	9
ANG12_31	0.0632	0.0042	0.857	0.054	0.1002	0.0026	113.9	540	140	613	30	615	15
ANG12_32	0.825	0.023	179.3	5.9	1.597	0.057	121.6	5016	52	5262	34	6100	140
ANG12_34	0.0655	0.0022	0.926	0.032	0.102	0.0015	84.2	744	72	660	18	626.1	8.5
ANG12_35	0.847	0.038	127	16	1.12	0.15	91.0	5067	85	4810	140	4610	440
ANG12_36	0.0651	0.0031	1.103	0.049	0.1241	0.0025	116.2	650	100	741	24	755	14
ANG12_37	0.0613	0.0027	0.86	0.039	0.1005	0.002	110.8	557	97	619	21	617	11
ANG12_38	0.0617	0.0028	0.861	0.036	0.1019	0.0019	109.6	570	98	625	20	625	11
ANG12_39	0.0638	0.003	0.878	0.037	0.1006	0.0018	96.6	640	99	632	20	618	11
ANG12_40	0.0605	0.0022	0.811	0.028	0.0972	0.0016	109.3	547	78	597	16	597.7	9.4
ANG12_41	0.0685	0.0028	0.823	0.032	0.088	0.0021	68.4	794	88	602	18	543	12
ANG12_42	0.0939	0.0016	3.367	0.058	0.2585	0.004	98.7	1500	33	1494	14	1481	20
ANG12_43	0.136	0.019	2.49	0.44	0.1083	0.0033	48.0	1380	200	988	95	663	19
ANG12_44	0.0659	0.0025	0.913	0.032	0.1013	0.0017	85.1	730	79	657	17	621.4	9.6
ANG12_45	0.0602	0.003	0.856	0.042	0.1044	0.0025	127.8	500	100	620	24	639	14
ANG12_46	0.0616	0.0032	0.82	0.039	0.0974	0.0018	113.0	530	110	600	23	599	11
ANG12_47	0.8	0.023	505	30	4.56	0.25	222.6	4963	52	6302	63	11050	280
ANG12_48	0.0621	0.0024	0.875	0.031	0.1039	0.0017	102.8	619	78	633	17	636.6	9.7
ANG12_49	0.0614	0.0022	0.873	0.028	0.1026	0.0016	107.2	587	76	633	15	629.1	9.4
ANG12_50	0.0609	0.0018	0.898	0.026	0.1063	0.0016	110.4	590	67	646	14	651.2	9.5
ANG12_51	0.0599	0.0013	0.843	0.016	0.1017	0.0012	107.1	583	49	619	8.6	624.2	6.9
ANG12_52	0.0615	0.0023	0.834	0.028	0.0987	0.0017	102.0	594	79	612	16	606.1	9.8
ANG12_53	0.07	0.0027	0.862	0.031	0.0905	0.0021	66.6	838	82	625	17	558	12

ANG12_54	0.0629	0.0018	0.851	0.024	0.0978	0.002	89.6	671	64	621	13	601	12
ANG12_55	0.1329	0.0026	6.97	0.13	0.3796	0.0052	97.6	2123	34	2102	16	2072	24
ANG12b_1	0.058	0.0039	0.802	0.051	0.1014	0.0026	172.8	360	140	579	30	622	15
ANG12b_2	0.0604	0.0048	0.843	0.063	0.1029	0.003	157.5	400	160	596	37	565	11
ANG12b_4	0.064	0.0044	0.881	0.059	0.0988	0.0024	99.5	610	150	628	32	625	12
ANG12b_5	0.815	0.023	201.5	9.9	1.787	0.091	130.4	4993	54	5359	48	1562	23
ANG12b_7	0.0644	0.0037	0.93	0.05	0.1045	0.002	100.0	640	120	658	27	624	18
ANG12b_8	0.0642	0.0039	0.95	0.066	0.1075	0.0034	96.6	680	120	672	35	1997	89
ANG12b_9	0.0656	0.0019	1.124	0.032	0.1235	0.0029	97.5	769	64	762	15	622	12
ANG12b_10	0.0643	0.0029	0.811	0.036	0.0916	0.0018	85.5	661	97	596	20	630	18
ANG12b_11	0.0591	0.0023	0.824	0.027	0.1018	0.002	121.8	513	84	607	15	593.9	8.6
ANG12b_12	0.0965	0.0017	3.648	0.067	0.2745	0.0046	100.8	1549	34	1559	14	7310	370
ANG12b_13	0.058	0.0033	0.816	0.044	0.1017	0.003	132.8	470	120	600	24	614	11
ANG12b_18	0.621	0.027	30.8	1.5	0.367	0.019	44.0	4540	72	3488	50	697	13
ANG12b_19	0.0662	0.0025	0.925	0.035	0.1013	0.002	82.8	751	83	660	18	645	13
ANG12b_20	0.0626	0.0022	0.828	0.026	0.0966	0.0015	96.1	618	74	608	15	572	10
ANG12b_21	0.815	0.019	265	19	2.37	0.18	146.4	4994	45	5470	99	331	11
ANG12b_22	0.0622	0.0033	0.851	0.041	0.1	0.0019	115.8	530	110	614	22	651	12
ANG12b_23	0.0629	0.0018	0.989	0.028	0.1142	0.0023	101.9	684	61	698	14	3510	160
ANG12b_24	0.0637	0.0021	0.927	0.029	0.1054	0.0022	93.6	689	73	663	15	607	14
ANG12b_25	0.062	0.0017	0.792	0.023	0.0928	0.0018	86.9	658	56	590	13	6510	210
ANG12b_26	0.0796	0.0019	0.569	0.013	0.0527	0.0018	28.2	1175	47	456.6	8.6	640	12
ANG12b_27	0.0621	0.0018	0.897	0.028	0.1064	0.002	104.0	626	63	648	15	657	20
ANG12b_30	*0.569*	*0.02*	*57.2*	*3.1*	*0.731*	*0.04*	*79.2*	*4431*	*51*	*4082*	*63*	*750*	*17*
ANG17_1	0.1141	0.0029	3.546	0.099	0.2266	0.0059	70.7	1861	44	1534	23	1315	31
ANG17_2	0.1098	0.003	4.33	0.18	0.287	0.013	91.3	1794	46	1691	36	1638	60
ANG17_3	0.1711	0.0027	11.26	0.16	0.4778	0.0061	98.0	2566	27	2544	13	2515	26
ANG17_4	0.1129	0.0021	3.998	0.067	0.2588	0.0037	80.7	1837	35	1630	14	1482	19
ANG17_5	0.1274	0.0023	2.871	0.079	0.1648	0.0048	47.6	2062	33	1368	21	981	27
ANG17_6	0.0669	0.0026	0.946	0.034	0.103	0.0016	80.6	784	84	672	18	631.9	9.1
ANG17_7	0.1103	0.0019	4.816	0.073	0.3178	0.0036	99.0	1796	32	1785	13	1778	18
ANG17_8	0.1113	0.0022	4.856	0.079	0.3179	0.0039	98.4	1806	37	1791	14	1778	19
ANG17_9	0.1199	0.0029	1.982	0.054	0.121	0.0036	37.7	1953	41	1107	19	736	21
ANG17_10	0.1136	0.0023	4.92	0.11	0.3157	0.0063	95.4	1852	35	1805	19	1766	31
ANG17_11	0.1022	0.0025	3.735	0.085	0.2667	0.0043	92.8	1642	46	1575	18	1523	22
ANG17_12	0.121	0.0021	5.4	0.1	0.3243	0.0059	92.1	1963	32	1880	17	1808	29

ANG17_13	0.1742	0.0029	3.214	0.066	0.134	0.0023	31.2	2594	27	1459	16	810	13
ANG17_14	0.0609	0.0016	0.807	0.02	0.0964	0.0013	97.8	606	58	600	11	592.8	7.8
ANG17_15	0.1203	0.0061	4.43	0.12	0.2748	0.0074	82.3	1895	63	1704	28	1560	38
ANG17_16	0.1078	0.0022	4.45	0.083	0.3007	0.0052	96.7	1751	37	1720	15	1693	26
ANG17_17	0.1078	0.0022	4.582	0.088	0.3082	0.0046	98.9	1750	38	1742	16	1730	23
ANG17_18	0.0638	0.0013	0.923	0.016	0.1051	0.0012	89.9	716	45	662.4	8.6	643.9	7.3
ANG17_19	0.1084	0.0019	4.317	0.072	0.2879	0.0039	92.5	1765	33	1693	14	1632	20
ANG17_20	0.1086	0.0022	4.398	0.089	0.2936	0.0055	93.9	1766	38	1708	17	1658	27
ANG17_21	0.1195	0.0022	1.411	0.029	0.0853	0.0019	27.2	1942	34	892	12	528	11
ANG17_22	0.1288	0.0026	0.96	0.028	0.0524	0.0028	15.8	2078	38	663	21	328	17
ANG17_23	0.1185	0.0025	3.98	0.19	0.244	0.013	72.5	1928	40	1606	42	1398	67
ANG17_24	0.0864	0.0032	2.596	0.093	0.2182	0.0049	97.2	1307	69	1290	26	1270	26
ANG17_25	0.1104	0.0036	4.78	0.15	0.3127	0.0066	98.8	1772	62	1773	25	1751	33
ANG17_26	0.0736	0.0016	1.733	0.038	0.1697	0.0027	99.4	1016	46	1017	14	1010	15
ANG17_27	0.07493	0.0013	1.757	0.024	0.1692	0.0019	95.2	1058	34	1028.3	9	1007	11
ANG17_28	0.2114	0.0033	10.95	0.16	0.3734	0.0048	70.1	2914	25	2517	15	2044	23
ANG17_29	0.1711	0.0037	8.41	0.26	0.3538	0.0094	76.1	2559	36	2261	29	1947	45
ANG17_30	0.1119	0.0022	4.37	0.1	0.2658	0.006	83.4	1819	36	1652	18	1517	31
ANG17_31	0.1067	0.0018	4.59	0.069	0.3082	0.0038	99.4	1740	33	1744	13	1730	19
ANG17_32	0.1161	0.0022	2.205	0.06	0.137	0.0039	43.8	1888	34	1176	19	826	22
ANG17_33	0.1456	0.0024	2.583	0.053	0.1566	0.0065	40.9	2291	29	1441	35	938	36
ANG17_34	0.1251	0.0021	1.947	0.033	0.112	0.0016	33.8	2022	30	1094	12	684	9.5
ANG17_35	0.1228	0.0023	2.231	0.053	0.1445	0.0034	43.8	1986	33	1252	17	869	19
ANG17_36	0.102	0.0019	3.907	0.069	0.2753	0.0038	95.1	1649	35	1610	14	1568	19
ANG17_37	0.13	0.0023	1.371	0.02	0.0759	0.0011	22.5	2095	29	875.5	8.9	471.7	6.5
ANG17_38	0.1208	0.0032	1.167	0.038	0.0689	0.0019	22.0	1955	46	785	17	430	12
ANG17_39	0.0633	0.0021	0.883	0.027	0.1009	0.0017	92.4	670	71	640	14	619	10
ANG17_40	0.0634	0.0023	0.732	0.027	0.0838	0.0014	77.4	670	76	557	13	518.3	8.1
ANG17_41	0.1693	0.0029	11.32	0.19	0.4808	0.007	99.4	2543	29	2545	17	2527	31
ANG17_42	0.1665	0.003	6.68	0.11	0.2887	0.0045	64.9	2517	30	2067	15	1634	23
ANG17_43	0.0594	0.002	0.802	0.026	0.0969	0.0022	108.0	552	73	596	15	596	13
ANG17_44	0.1365	0.0023	7.048	0.098	0.3707	0.0048	93.3	2178	30	2116	13	2031	22
ANG17_45	0.1348	0.0025	7.64	0.13	0.4051	0.0046	101.8	2153	33	2180	14	2191	21
ANG17_46	0.1872	0.0032	13.17	0.22	0.4851	0.0093	93.8	2710	29	2641	20	2543	41
ANG17_47	0.1095	0.0025	4.65	0.11	0.3057	0.0039	97.0	1772	42	1753	16	1718	19
ANG17_48	0.1167	0.0021	2.715	0.066	0.1757	0.0025	55.1	1894	33	1366	14	1043	14

ANG17_49	0.1553	0.0029	7.32	0.24	0.3259	0.0059	75.7	2398	31	2110	18	1815	29
ANG17_50	0.1296	0.0022	1.332	0.036	0.07	0.0023	20.7	2097	32	820	16	435	14
ANG17_51	0.0642	0.0027	0.876	0.047	0.0963	0.0018	87.2	680	96	627	20	593	10
ANG17_52	0.1239	0.002	1.625	0.041	0.0982	0.0018	30.0	2009	29	1003	11	603	10
ANG17_53	0.1098	0.002	4.617	0.069	0.3033	0.0034	95.6	1786	32	1750	12	1707	17
ANG17_54	0.1092	0.0021	4.758	0.088	0.3134	0.004	99.2	1773	35	1774	15	1758	19
ANG17_55	0.1869	0.0049	9.17	0.24	0.3525	0.0069	71.7	2707	42	2354	25	1942	33
ANG17_56	0.1417	0.0023	2.525	0.082	0.217	0.01	55.9	2242	28	1649	39	1253	53
ANG17_57	0.1523	0.0024	2.014	0.056	0.0837	0.0019	21.9	2366	27	1031	16	518	11
ANG17_58	0.121	0.002	5.113	0.076	0.1465	0.005	44.7	1965	30	1248	24	878	28
ANG17_59	0.1145	0.002	2.228	0.062	0.3216	0.004	96.3	1865	32	1835	13	1796	20
ANG17_60	0.1211	0.0022	0.972	0.023	0.2058	0.0092	60.9	1964	32	1482	33	1197	49
ANG17_61	0.0639	0.0013	1.785	0.031	0.1095	0.0014	93.0	720	42	687.7	8.6	669.6	7.9
ANG17_62	0.1239	0.0021	1.138	0.05	0.1108	0.0014	33.8	2005	30	1079	11	677.1	8
ANG17_63	0.0672	0.0021	10.02	0.36	0.1193	0.0015	91.9	790	69	752	16	726.4	8.4
ANG17_64	0.1638	0.0036	2.968	0.075	0.4559	0.0072	97.4	2481	38	2455	19	2417	32
ANG17_65	0.1166	0.0019	0.905	0.046	0.2088	0.005	64.3	1902	30	1494	19	1223	27
ANG17_66	0.0603	0.0022	2.304	0.056	0.1078	0.0017	118.0	559	82	647	18	659.5	9.9
ANG17_67	0.1281	0.0022	4.36	0.13	0.1427	0.0036	41.6	2064	30	1273	18	858	20
ANG17_68	0.1466	0.0053	7.06	0.11	0.2078	0.0049	54.0	2251	59	1649	18	1215	26
ANG17_69	0.1371	0.0022	7.08	0.14	0.3594	0.0058	90.4	2186	27	2084	15	1976	28
ANG17_70	0.1396	0.0022	4.89	0.098	0.3527	0.0065	87.7	2216	28	2083	17	1944	31
ANG17_71	0.1237	0.0022	4.655	0.09	0.2701	0.0051	76.8	2005	32	1748	19	1539	26
ANG17_72	0.1103	0.0019	6.54	0.19	0.2556	0.0076	81.2	1799	32	1600	25	1461	39
ANG17_73	0.1389	0.0025	0.812	0.022	0.3621	0.0049	90.3	2203	32	2108	15	1990	23
ANG17_74	0.0604	0.0015	0.949	0.02	0.0979	0.0011	103.4	582	55	605	10	602	6.4
ANG17_76	0.0673	0.0014	2.472	0.049	0.1001	0.0022	73.8	833	43	664.4	8.3	615	13
ANG17_77	0.0858	0.0015	4.312	0.076	0.2169	0.0025	95.3	1328	32	1291	12	1266	14
ANG17_78	0.1083	0.0021	4.649	0.07	0.2878	0.0043	92.5	1761	35	1692	14	1629	22
ANG17_79	0.1093	0.0019	4.272	0.093	0.3075	0.004	97.1	1779	31	1754	13	1727	20
ANG17_81	0.0675	0.0026	1.344	0.043	0.1025	0.0017	74.8	840	80	681	18	628	10
ANG17_82	0.1142	0.0021	4.77	0.076	0.2347	0.0093	72.6	1859	32	1543	36	1349	50
ANG17_83	0.1226	0.0022	5.296	0.084	0.1127	0.0066	34.4	1987	32	1053	32	683	37
ANG17_84	0.1081	0.002	1.649	0.027	0.318	0.0037	101.0	1762	34	1775	13	1779	18
ANG17_85	0.1195	0.0026	3.662	0.081	0.322	0.0045	93.1	1930	39	1864	14	1797	22
ANG17_86	0.1254	0.002	2.051	0.04	0.0972	0.0014	29.5	2030	27	1002.9	9.7	598	8.1

ANG17_87	0.0989	0.0024	4.18	0.069	0.2683	0.0039	96.7	1583	47	1563	17	1530	20
ANG17_88	0.1273	0.002	1.027	0.035	0.1069	0.0017	31.9	2055	27	1072	11	654.6	9.9
ANG17_89	0.1234	0.002	1.791	0.043	0.2394	0.0031	69.1	2001	30	1651	12	1382	16
ANG17_90	0.0661	0.0019	8.82	0.21	0.1127	0.0016	89.3	770	62	716	15	687.9	9.3
ANG17_91	0.129	0.0022	2.616	0.042	0.0876	0.0026	26.0	2076	29	945	18	540	15
ANG17_92	0.1502	0.0026	2.213	0.034	0.293	0.018	69.5	2342	32	1913	61	1628	88
ANG17_93	0.1325	0.0022	2.687	0.036	0.1422	0.0016	40.3	2124	28	1300.4	10	856.6	8.9
ANG17_94	0.1316	0.0022	7.22	0.16	0.1214	0.0017	35.0	2112	29	1183	11	738.3	9.7
ANG17_95	0.1293	0.0021	2.8	0.1	0.1494	0.0016	43.1	2084	28	1320.6	9.8	897.2	8.9
ANG17_96	0.1503	0.0024	2.662	0.067	0.3318	0.0054	78.7	2343	27	2095	16	1845	26
ANG17_97	0.1163	0.002	3.227	0.059	0.1819	0.0066	56.7	1891	30	1367	28	1072	36
ANG17_98	0.1158	0.002	3.813	0.063	0.1707	0.0045	53.8	1882	32	1329	18	1013	25
ANG17_99	0.126	0.0021	4.174	0.064	0.1866	0.0028	54.2	2035	29	1467	13	1102	15
ANG17_100	0.1125	0.002	3.119	0.042	0.2394	0.0048	75.5	1830	32	1572	16	1381	25
ANG17_101	0.1237	0.002	1.337	0.03	0.2438	0.0034	70.1	2004	29	1667	13	1405	18
ANG17_102	0.1248	0.002	3.54	0.085	0.1827	0.0022	53.5	2022	28	1447.6	11	1081	12
ANG17_103	0.1276	0.002	4.305	0.076	0.0628	0.0019	19.0	2060	27	751	17	392	11
ANG17_104	0.1228	0.0023	3.739	0.076	0.1715	0.0073	51.0	1988	34	1354	32	1014	40
ANG17_105	0.1032	0.0021	4.93	0.098	0.3009	0.0036	101.3	1672	40	1693	14	1694	18
ANG17_106	0.1119	0.0018	0.816	0.029	0.2031	0.0058	65.2	1823	30	1432	22	1188	31
ANG17_108	0.111	0.0024	3.677	0.079	0.3224	0.0042	99.9	1802	39	1806	17	1800	20
ANG17_109	0.0625	0.002	8.68	0.12	0.0952	0.0012	92.6	633	68	605	13	586.3	7.3
ANG17_110	0.0985	0.0018	3.818	0.084	0.2727	0.0029	97.9	1588	35	1576	13	1554	15
ANG17_111	0.148	0.0024	3.677	0.079	0.4245	0.0049	98.4	2318	28	2304	13	2282	22
ANG17_112	0.1165	0.002	8.68	0.12	0.2866	0.0081	85.3	1896	32	1737	25	1618	41
ANG17_113	0.1241	0.002	3.818	0.084	0.1953	0.0046	57.1	2011	29	1486	19	1148	25
Sample	Pb^{207}/Pb^{206}	2σ	Pb^{207}/U^{235}	2σ	Pb^{206}/U^{238}	2σ	%conc.	Pb^{207}/U^{206}	2σ	Pb^{207}/U^{235}	2σ	Pb^{206}/Pb^{238}	2σ
Session 2													
ANG12aD_2	0.0642	0.002	0.874	0.027	0.0991	0.0017	86.0	708	67	634	14	609	10
ANG12aD_5	0.0954	0.0021	3.404	0.079	0.2574	0.0055	96.3	1531	41	1502	19	1475	28
ANG12aD_7	0.0695	0.0037	0.978	0.052	0.1021	0.0025	77.3	810	110	683	27	626	14
ANG12aD_8	0.0648	0.0024	0.892	0.033	0.0997	0.0025	84.0	729	80	644	18	612	15
ANG12aD_9	0.791	0.042	145	10	1.33	0.11	110.5	4930	100	5065	71	5450	320
ANG12aD_10	0.0638	0.002	0.847	0.026	0.0959	0.0016	86.4	683	69	619	14	590	9.2
ANG12aD_12	0.0827	0.0015	0.495	0.012	0.04291	0.0009	21.6	1256	35	407.4	8.2	270.7	6.1
ANG12aD_13	0.0655	0.0035	0.907	0.046	0.1014	0.0021	98.7	630	110	645	25	622	12

ANG12aD_14	0.0628	0.0029	0.831	0.037	0.0964	0.002	96.4	615	97	607	20	593	12
ANG12aD_15	0.0625	0.0012	0.819	0.016	0.0947	0.0013	86.9	671	42	606.2	8.8	583.3	7.5
ANG12aD_16	0.067	0.0036	0.905	0.048	0.0995	0.0022	82.6	740	110	647	26	611	13
ANG12aD_17	0.1149	0.002	5.302	0.097	0.3343	0.0047	99.2	1877	33	1867	16	1862	22
ANG12aD_18	0.075	0.0047	1.104	0.072	0.1078	0.0031	67.3	980	130	748	34	660	18
ANG12aD_19	0.0638	0.003	0.858	0.037	0.0995	0.0021	91.1	671	99	627	20	611	12
ANG12aD_20	0.0671	0.002	0.878	0.025	0.0959	0.0019	73.7	801	65	637	14	590	11
ANG12aD_21	0.0652	0.0044	0.946	0.063	0.1053	0.003	89.6	720	140	671	32	645	17
ANG12aD_22	0.0752	0.0052	1.044	0.074	0.1022	0.0029	67.4	930	150	714	37	627	17
ANG12aD_23	0.0602	0.0024	0.797	0.035	0.0961	0.002	102.4	577	89	591	20	591	12
ANG12aD_25	0.126	0.023	1.94	0.44	0.114	0.013	39.2	1770	300	1010	130	693	78
ANG12aD_26	0.0653	0.0024	0.86	0.029	0.0967	0.0013	83.5	712	76	625	16	594.8	7.9
ANG12aD_27	0.0623	0.0019	0.763	0.023	0.0894	0.0013	85.3	647	66	573	13	551.8	7.7
ANG12aD_28	0.0598	0.0016	0.725	0.02	0.0887	0.0011	97.4	562	61	552	12	547.5	6.5
ANG12aD_29	0.0801	0.0028	1.225	0.042	0.1115	0.0023	58.2	1171	68	809	19	681	13
ANG12aD_31	0.847	0.067	323	41	2.82	0.37	168.2	5070	150	5840	130	8530	620
ANG12aD_33	0.0627	0.0016	0.932	0.022	0.1074	0.0013	98.0	671	53	667	12	657.7	7.7
ANG12aD_34	0.0654	0.0051	1.021	0.077	0.1134	0.004	106.3	650	170	698	38	691	23
ANG12aD_36	0.0727	0.0036	0.781	0.039	0.0778	0.0021	51.8	932	100	581	22	483	13
ANG12aD_37	0.0633	0.0026	0.86	0.032	0.098	0.0018	89.3	674	85	626	18	602	10
ANG12aD_38	0.6609	0.011	30.7	2.7	0.331	0.028	38.9	4650	24	3393	92	1810	140
ANG12aD_39	0.064	0.0014	0.956	0.021	0.1078	0.0016	90.5	729	50	680.1	11	659.7	9.5
ANG12aD_40	0.0655	0.0014	0.888	0.021	0.0977	0.0016	77.6	774	47	644	12	600.5	9.2
ANG12aD_41	0.0642	0.0033	0.81	0.039	0.0924	0.0016	94.9	600	100	593	22	569.4	9.4
ANG12aD_42	0.0633	0.0029	0.858	0.038	0.0979	0.0019	92.2	653	98	624	21	602	11
ANG12aD_43	0.0618	0.0021	0.809	0.025	0.0946	0.0017	91.1	639	72	601	15	582	10
ANG12aD_44	0.0648	0.0029	0.841	0.037	0.0934	0.0018	79.4	724	97	613	20	575	11
ANG12aD_45	0.0631	0.0032	0.832	0.04	0.0959	0.0023	93.7	630	100	610	22	590	14
ANG12aD_46	0.0654	0.0024	0.972	0.036	0.1076	0.0019	88.6	743	76	685	18	658	11
ANG12aD_47	0.0635	0.002	0.818	0.024	0.0935	0.0012	86.1	669	69	603	14	575.8	7.1
ANG12aD_48	0.0647	0.0031	0.884	0.042	0.0994	0.002	88.6	690	100	637	23	611	12
ANG12aD_49	0.0651	0.0022	0.864	0.03	0.0974	0.0015	82.4	727	73	633	16	599	9
ANG12aD_50	0.0603	0.0023	0.808	0.027	0.0976	0.0015	105.4	569	79	601	15	600	8.7
ANG12aD_51	0.726	0.029	166	16	1.65	0.14	128.7	4793	66	5111	93	6170	360
ANG12aD_52	0.0648	0.0016	0.798	0.02	0.0898	0.0016	74.7	742	54	594	11	554.4	9.2
ANG12aD_53	0.0667	0.0017	0.874	0.025	0.0965	0.0017	73.3	809	53	637	13	593.4	9.9

ANG12aD_54	0.0616	0.0015	0.838	0.02	0.0988	0.0013	94.4	643	53	616	11	607.2	7.8
ANG12aD_55	0.0668	0.0036	0.975	0.058	0.1047	0.0031	79.3	810	110	683	30	642	18
ANG12aD_56	0.06349	0.0012	0.871	0.016	0.0995	0.0013	85.2	718	40	635.3	8.8	611.6	7.8
ANG12aD_57	0.729	0.02	28.7	1.9	0.283	0.016	33.3	4802	45	3421	62	1599	78
ANG12aD_58	0.06326	0.0011	1.01	0.019	0.1156	0.0011	99.6	708	40	708.4	9.5	705.2	6.6
ANG12aD_59	0.0727	0.0018	0.569	0.018	0.0567	0.0014	36.0	988	50	455	11	355.3	8.4
ANG12aD_60	0.077	0.0032	1.017	0.044	0.0957	0.0017	56.0	1051	90	705	23	589	10
ANG12aD_61	0.0632	0.0023	0.844	0.031	0.0969	0.0015	90.0	662	83	616	18	595.7	8.9
ANG12aD_63	0.06594	0.0012	0.7845	0.013	0.0866	0.0015	67.4	794	36	587.5	7.4	535	8.8
ANG12aD_64	0.0639	0.0019	0.822	0.023	0.0931	0.0012	81.7	702	63	607	13	573.6	7.4
ANG12aD_65	0.0652	0.003	0.816	0.036	0.0911	0.0017	83.4	674	98	596	20	561.8	9.9
ANG12aD_66	0.0704	0.0023	0.969	0.031	0.0994	0.0015	67.9	900	71	684	16	610.9	8.5
ANG12aD_67	0.063	0.0021	0.768	0.026	0.0883	0.0014	82.3	663	74	576	15	545.5	8.5
ANG12aD_68	0.0583	0.0033	0.792	0.045	0.098	0.002	130.9	460	120	583	25	602	12
ANG12aD_69	0.0623	0.0036	0.828	0.046	0.096	0.0018	100.2	590	130	604	26	591	10
ANG12aD_70	0.0639	0.0021	0.853	0.028	0.0971	0.0013	85.9	695	71	623	15	597.3	7.6
ANG12aD_71	0.0751	0.0029	1.065	0.038	0.1045	0.0017	63.6	1007	81	733	19	640.3	9.9
ANG12aD_72	0.0634	0.0021	0.802	0.024	0.0914	0.0014	80.6	699	68	596	13	563.7	8.4
ANG12aD_73	0.0667	0.0028	0.917	0.037	0.1001	0.0024	77.5	792	90	658	19	614	14
ANG12aD_74	0.0658	0.0027	0.931	0.037	0.1024	0.0017	85.2	737	84	662	20	628	10
ANG12aD_75	0.0705	0.0068	0.995	0.094	0.1062	0.0035	89.0	730	200	685	49	650	20
ANG12aD_76	0.062	0.0018	0.868	0.024	0.1015	0.0017	97.6	638	66	632	13	622.9	9.9
ANG12aD_78	0.0714	0.0032	0.964	0.043	0.0982	0.0022	63.7	948	89	681	22	604	13
ANG12aD_79	0.0621	0.0025	0.841	0.031	0.0985	0.0016	98.0	619	88	615	17	606.4	9.4
ANG12aD_80	0.0675	0.003	0.892	0.037	0.0965	0.0016	78.7	754	91	642	20	593.5	9.3
ANG12aD_81	0.0713	0.0036	0.968	0.048	0.0994	0.0022	67.8	900	100	686	26	610	13
ANG12aD_83	0.0647	0.004	0.827	0.048	0.093	0.0022	89.5	640	130	602	27	573	13
ANG12aD_84	0.0642	0.0017	1.054	0.028	0.1183	0.0018	99.7	722	57	728	14	720	10
ANG12aD_86	0.0775	0.0041	1.001	0.054	0.0937	0.0026	54.4	1060	100	695	28	577	15
ANG12aD_87	0.0633	0.0026	0.872	0.036	0.1	0.0016	94.6	649	90	631	20	614	9.5
ANG12aD_88	0.0727	0.0049	1.002	0.063	0.1004	0.0026	66.2	930	140	695	30	616	15
ANG12aD_89	0.0697	0.0028	0.915	0.034	0.0949	0.0018	66.0	885	86	659	19	584	11
ANG12aD_91	0.799	0.055	215	20	2.11	0.31	144.4	4960	130	5434	96	7160	600
ANG12aD_92	0.7	0.11	173	30	1.89	0.36	141.2	4710	260	5180	200	6650	850
ANG12aD_93	0.0615	0.0043	0.787	0.051	0.0941	0.0027	105.3	550	150	581	29	579	16
ANG12aD_94	0.0614	0.0022	0.817	0.029	0.0969	0.0016	98.7	604	77	602	16	595.9	9.5

ANG12aD_95	0.0633	0.0035	0.815	0.044	0.0936	0.0023	91.6	630	120	599	24	577	13
ANG12aD_96	0.0751	0.0021	0.852	0.022	0.0833	0.0018	49.7	1036	58	625	12	515	11
ANG12aD_97	0.0631	0.0023	0.832	0.031	0.0957	0.0016	87.8	671	82	613	18	588.9	9.4
ANG12aD_98	0.0653	0.0025	0.873	0.033	0.097	0.002	78.6	760	78	636	18	597	12
ANG12aD_99	0.0753	0.0017	0.775	0.016	0.0751	0.0015	44.1	1059	45	581.2	9.1	466.7	8.7
ANG12aD_100	0.0643	0.0016	0.964	0.025	0.1092	0.0016	92.7	722	54	684	13	669	9
ANG12aD_101	0.1025	0.0018	3.992	0.076	0.2824	0.0045	96.3	1664	33	1631	15	1602	23
ANG12aD_102	0.2408	0.0037	17.61	0.28	0.5292	0.0065	87.6	3122	25	2966	15	2736	28
ANG12aD_105	0.123	0.015	2.15	0.35	0.113	0.0032	44.1	1570	180	1014	85	692	19
ANG12aD_106	0.0624	0.0019	0.851	0.025	0.099	0.0013	93.8	648	66	622	14	608.1	7.7
ANG12aD_109	0.0608	0.0027	0.826	0.037	0.0989	0.0017	105.0	579	94	606	20	608	10
ANG12aD_111	0.0918	0.0016	0.714	0.014	0.05685	0.0008	24.5	1456	33	546.4	8.5	356.3	5.4
ANG12aD_113	0.181	0.037	4.3	1.1	0.143	0.016	40.4	2170	320	1440	200	877	99
ANG12aD_114	0.0754	0.0045	1.038	0.064	0.0998	0.002	60.1	1020	120	715	33	613	12
ANG12aD_115	0.0617	0.0019	0.82	0.025	0.0963	0.0013	92.9	638	66	605	14	592.6	7.7
ANG12aD_116	0.0621	0.0018	0.852	0.023	0.0998	0.0013	95.5	642	61	623	13	613.2	7.3
ANG12aD_117	0.0751	0.0028	1.09	0.039	0.1072	0.0019	66.1	992	77	746	19	656	11
ANG12aD_118	0.768	0.027	226	32	1.95	0.26	130.5	4889	61	5180	200	6380	610
ANG12bD_1	0.0602	0.0021	0.767	0.026	0.0929	0.0015	104.1	550	77	575	15	572.4	8.8
ANG12bD_2	0.0638	0.0018	0.852	0.026	0.0966	0.0019	83.4	712	64	623	14	594	11
ANG12bD_3	0.0594	0.0026	0.869	0.04	0.1059	0.002	125.5	517	97	631	22	649	12
ANG12bD_4	0.0633	0.0047	0.805	0.056	0.0932	0.0028	95.7	600	150	590	32	574	16
ANG12bD_5	0.0649	0.0018	0.905	0.024	0.1009	0.0014	83.6	741	57	652	13	619.2	8.4
ANG12bD_6	0.0607	0.0014	0.91	0.022	0.1082	0.0017	108.5	610	50	655	12	662	9.7
ANG12bD_7	0.0611	0.0016	0.891	0.023	0.1055	0.0016	103.7	623	55	646	12	646.2	9.3
ANG12bD_8	0.0613	0.0019	0.807	0.027	0.095	0.0017	94.5	619	68	598	16	585	10
ANG12bD_9	0.058	0.0023	0.819	0.032	0.1023	0.0021	133.4	470	85	603	18	627	12
ANG12bD_10	0.0621	0.0017	0.864	0.024	0.101	0.0019	95.5	649	60	630	13	620	11
ANG12bD_11	0.0709	0.0015	0.438	0.013	0.0422	0.0011	28.1	947	41	367.9	8.9	266.2	6.6
ANG12bD_13	0.069	0.0034	0.969	0.049	0.1016	0.0023	77.9	800	100	677	26	623	13
ANG12bD_14	0.0696	0.0033	0.457	0.021	0.0477	0.0014	35.8	838	98	379	15	300.1	8.3
ANG12bD_15	0.0626	0.0023	0.828	0.033	0.0952	0.0021	89.5	655	80	608	18	586	12
ANG12bD_16	0.826	0.025	0.007	0.001	67	13	529.9	5020	57	9020	230	26660	1800
ANG12bD_17	0.132	0.01	1.69	0.15	0.0916	0.0024	30.2	1870	140	953	53	565	14
ANG12bD_19	0.0712	0.0029	0.856	0.032	0.088	0.0018	60.9	892	86	624	18	543	11
ANG12bD_20	0.771	0.015	79	5.7	0.741	0.05	71.5	4897	34	4408	69	3500	190

ANG12bD_21	0.7972	0.013	134.7	4.1	1.224	0.037	103.5	4956	29	4977	31	5130	110
ANG12bD_22	0.0669	0.0034	0.966	0.05	0.1036	0.0028	80.4	790	110	682	25	635	16
ANG12bD_23	0.0622	0.0031	0.881	0.043	0.1038	0.0022	107.8	590	110	636	24	636	13
ANG12bD_24	0.0961	0.0024	3.41	0.11	0.2582	0.0062	96.2	1537	47	1503	24	1478	32
ANG12bD_25	0.0958	0.0024	3.342	0.1	0.2531	0.0062	94.5	1537	45	1489	25	1453	32
ANG12bD_27	0.0633	0.0024	0.804	0.03	0.0932	0.0026	83.3	689	82	599	18	574	15
ANG12bD_29	0.0974	0.002	3.064	0.077	0.2282	0.0052	84.6	1565	37	1420	19	1324	27
ANG12bD_30	0.849	0.035	216	22	1.87	0.2	129.7	5073	80	5380	130	6580	510
ANG12bD_31	0.698	0.045	78	14	0.78	0.12	73.4	4700	120	4070	240	3450	440
ANG12bD_34	0.825	0.035	67.6	6.2	0.574	0.043	57.6	5017	79	4252	89	2890	170
ANG12bD_35	0.862	0.037	1301	95	11.02	0.78	311.6	5102	83	7256	75	15900	410
ANG18_1	0.0812	0.0014	0.5777	0.011	0.05168	0.0007	26.6	1219	34	463.4	6.7	324.8	4.6
ANG18_4	0.0605	0.002	0.88	0.03	0.1057	0.0022	108.4	598	75	640	17	648	13
ANG18_5	0.0629	0.0018	0.825	0.023	0.0961	0.0013	87.9	673	63	611	13	591.3	7.6
ANG18_6	0.0611	0.0018	0.759	0.023	0.0849	0.002	84.4	622	65	572	13	525	12
ANG18_11	0.0686	0.0015	0.679	0.024	0.0723	0.0024	51.4	873	45	523	14	449	15
ANG18_13	0.0639	0.0033	0.869	0.043	0.0995	0.002	94.0	650	120	627	24	611	12
ANG18_14	0.0607	0.0025	0.901	0.034	0.1082	0.0019	115.7	572	90	651	19	662	11
ANG18_16	0.0762	0.0024	0.67	0.023	0.0639	0.0014	37.3	1069	65	521	13	399.2	8.4
ANG18_18	0.0596	0.0023	0.925	0.035	0.1123	0.0018	130.9	524	86	659	19	686	11
ANG18_19	0.0608	0.0017	0.837	0.026	0.0997	0.0014	103.4	592	65	617	14	612.2	8.1
ANG18_20	0.068	0.0013	0.885	0.021	0.0945	0.0019	67.8	858	41	642.2	11	582	11
ANG18_21	0.0624	0.0013	0.896	0.02	0.1035	0.0012	92.5	686	44	649.7	11	634.8	6.8
ANG18_22	0.0789	0.0021	2.153	0.063	0.1979	0.0034	101.2	1152	52	1166	19	1166	18
ANG18_23	0.0781	0.0019	2.249	0.051	0.2076	0.0026	107.7	1128	49	1195	16	1215	14
ANG18_24	0.0632	0.002	0.941	0.034	0.1068	0.0027	92.5	707	67	670	18	654	16
ANG18_25	0.1102	0.0023	4.694	0.1	0.3063	0.0041	96.0	1793	39	1763	18	1722	20
ANG18_26	0.0815	0.0034	0.88	0.034	0.0789	0.0019	41.8	1169	89	639	19	489	11
ANG18_27	0.0633	0.0017	0.982	0.028	0.1125	0.0026	98.8	695	58	693	15	687	15
ANG18_28	0.0622	0.0013	0.908	0.021	0.1055	0.0017	97.5	663	46	655	12	646.5	9.9
ANG18_29	0.1148	0.0024	5.17	0.13	0.3262	0.008	97.3	1869	37	1844	22	1818	39
ANG18_30	0.0899	0.0024	2.691	0.094	0.2155	0.0057	89.5	1403	52	1317	27	1256	30
ANG18_31	0.1079	0.0028	4.42	0.12	0.2968	0.0052	96.3	1740	48	1705	23	1675	27
ANG18_32	0.06	0.0029	0.873	0.039	0.1058	0.0022	111.5	581	96	636	20	648	13
ANG18_33	0.0666	0.0015	0.945	0.021	0.1035	0.0021	78.2	812	46	675.8	12	635	12
ANG18_34	0.0709	0.0013	0.788	0.021	0.0808	0.0024	53.0	946	38	588	12	501	14

ANG18_35	0.062	0.0028	0.929	0.04	0.1091	0.0024	107.9	618	95	663	21	667	14
ANG18_36	0.0737	0.0018	1.781	0.045	0.1756	0.0021	103.4	1008	51	1033	16	1042	12
ANG18_38	0.0619	0.0022	1.061	0.039	0.1243	0.0018	119.1	634	82	731	20	755	10
ANG18_39	0.0631	0.0015	1.098	0.025	0.1262	0.002	108.7	705	50	751	12	766	11
ANG18_40	0.0681	0.0018	1.104	0.03	0.1178	0.0015	85.0	844	56	753	14	717.7	8.4
ANG18_41	0.0602	0.0018	0.846	0.025	0.1028	0.0014	111.2	567	66	619	14	630.6	8
ANG18_42	0.0816	0.0015	2.189	0.046	0.1953	0.0036	93.5	1229	37	1176	14	1149	20
ANG18_43	0.0803	0.0019	2.301	0.058	0.2079	0.004	102.3	1190	47	1210	18	1217	22
ANG20D_1	0.0927	0.0027	0.989	0.026	0.0782	0.0015	33.4	1450	56	696	13	484.9	9
ANG20D_2	0.1438	0.0069	2.94	0.16	0.1539	0.0084	41.4	2218	81	1369	43	918	48
ANG20D_4	0.1461	0.004	0.888	0.022	0.04447	0.0008	12.3	2280	49	643	12	280.4	5.1
ANG20D_5	0.0749	0.0058	1.037	0.083	0.101	0.0028	69.9	890	160	703	41	622	17
ANG20D_6	0.827	0.021	609	21	4.98	0.2	229.3	5023	46	6505	34	11520	230
ANG20D_8	0.8385	0.012	2810	110	24.24	0.95	410.2	5049	27	8049	41	20710	240
ANG20D_9	0.834	0.017	2120	120	18.5	1.1	378.5	5038	38	7756	62	19070	360
ANG20D_10	0.1033	0.0018	3.657	0.11	0.255	0.0059	87.2	1676	32	1554	25	1461	30
ANG20D_12	0.8269	0.011	2382	94	20.93	0.82	392.6	5023	25	7870	40	19720	240
ANG20D_13	0.84	0.02	1780	120	15.6	1.2	356.6	5051	44	7601	65	18010	410
ANG20D_14	0.83	0.02	2520	140	22	1.3	400.8	5030	44	7945	63	20160	400
ANG20D_17	0.1173	0.0024	5	0.1	0.3083	0.0048	90.9	1904	36	1816	17	1731	24
ANG20D_18	0.1061	0.0021	3.302	0.076	0.2252	0.0039	76.0	1721	37	1477	18	1308	21
ANG20D_20	0.823	0.018	1830	140	16	1.2	360.2	5014	40	7595	74	18060	440
ANG20D_22	0.1137	0.0042	1.85	0.1	0.1186	0.0037	39.3	1836	58	1058	34	722	21
ANG20D_23	0.804	0.05	1000	110	9.5	1.4	295.2	4970	120	6960	120	14670	780
ANG20D_24	0.8392	0.013	7360	390	63.6	3.3	528.8	5051	30	9018	52	26710	330
ANG20D_26	0.848	0.016	2700	220	23	1.9	398.7	5071	37	7994	84	20220	550
ANG20D_30	0.0749	0.0035	0.845	0.041	0.0827	0.002	50.4	1015	90	620	22	512	12
ANG20D_31	0.819	0.021	1000	140	8.8	1.2	283.2	5004	49	6900	150	14170	820
ANG20D_32	0.826	0.016	3440	220	30.9	2.1	442.1	5021	37	8267	67	22200	420
ANG20D_33	0.839	0.019	4030	220	35.1	2	456.1	5049	42	8416	56	23030	360
ANG20D_35	0.756	0.015	76.5	3.1	0.727	0.028	72.4	4862	34	4401	41	3520	110
ANG20D_37	0.817	0.016	1315	84	11.73	0.73	319.6	5009	33	7232	67	16010	370
ANG20D_38	0.764	0.012	85.6	1.8	0.81	0.016	78.2	4881	26	4523	21	3816	56
ANG20D_41	0.845	0.022	7180	740	62.2	6.8	523.3	5064	50	8980	100	26500	700
ANG20D_42	0.0786	0.0014	1.943	0.037	0.1808	0.0031	92.8	1153	34	1096	13	1070	17
ANG20D_44	0.8376	0.013	1372	40	11.96	0.35	325.1	5044	30	7325	30	16400	180

Note: “D” after analyses refers to the ‘dust’ portion, <79μm zircons.

U/Pb standard information: GJ was the primary standard used, with a 1% uncertainty. (TIMS normalisation data: 207Pb/206Pb = 608.3 Ma, 206Pb/238U = 600.7Ma and 207Pb/235U = 602.2 Ma; (Payne *et al*. 2006). Secondary standards used were the Plesovice zircon and 91500 standards.

Appendix B: Representative electron probe microanalyses

ANG13b	Quartz	Quartz (Inclusion)	Hematite
SiO_2	93.344	94.357	2.484
TiO_2	0.001	0.042	0.000
Al_2O_3	0.303	1.677	0.008
Cr_2O_3	0.021	0.000	0.000
FeO	0.104	2.882	70.778
MnO	0.000	0.330	0.000
MgO	0.048	0.266	0.505
ZnO	0.000	0.010	0.000
CaO	0.000	0.268	0.327
Na_2O	0.093	0.048	0.035
K_2O	0.155	0.131	0.026
Cl	0.018	0.032	0.036
F	0.000	0.000	0.000
Total	94.08	100.04	74.19
Cations			
Si	0.995	0.966	0.114
Ti	0.000	0.000	0.000
Al	0.004	0.020	0.000
Cr	0.000	0.000	0.000
Fe^{3+}	0.000	0.000	0.000
Fe^{2+}	0.001	0.025	2.717
Mn^{2+}	0.000	0.003	0.000
Mg	0.001	0.004	0.035
Zn	0.000	0.000	0.000
Ca	0.000	0.003	0.016
Na	0.002	0.001	0.003
K	0.002	0.002	0.002
Cl	0.000	0.001	0.003
F	0.000	0.000	0.000
Total Cations	1.005	1.024	2.887

ANG15a	Quartz	Titanite	Quartz (Inclusion)	Hematite
SiO_2	101.037	23.948	98.808	2.484
TiO_2	0.000	31.041	0.000	0.000
Al_2O_3	0.032	3.141	0.360	0.008
Cr_2O_3	0.000	0.008	0.000	0.000
FeO	0.462	2.570	0.452	70.778
MnO	0.067	0.080	0.020	0.000
MgO	0.001	0.220	0.009	0.505
ZnO	0.016	0.000	0.000	0.000
CaO	0.014	21.460	0.014	0.327
Na_2O	0.023	0.295	0.049	0.035
K_2O	0.009	0.381	0.024	0.026
Cl	0.000	0.536	0.048	0.036
F	0.000	0.330	0.000	0.000
Total	101.66	83.75	99.77	74.19
Cations				
Si	0.997	0.941	0.994	0.099
Ti	0.000	0.918	0.000	0.000
Al	0.000	0.145	0.004	0.001
Cr	0.000	0.000	0.000	0.000
Fe^{3+}	0.000	0.000	0.004	1.804
Fe^{2+}	0.004	0.084	0.000	0.066
Mn^{2+}	0.001	0.003	0.000	0.000
Mg	0.000	0.013	0.000	0.015
Zn	0.000	0.000	0.000	0.000
Ca	0.000	0.904	0.001	0.011
Na	0.000	0.022	0.000	0.004
K	0.000	0.019	0.001	0.000
Cl	0.000	0.036	0.000	0.001
F	0.000	0.041	0.994	0.000
Total Cations	1.003	3.050	1.004	2.000

APPENDIX C: EXTENDED LASER TRACE ELEMENT DATA

ANG13b

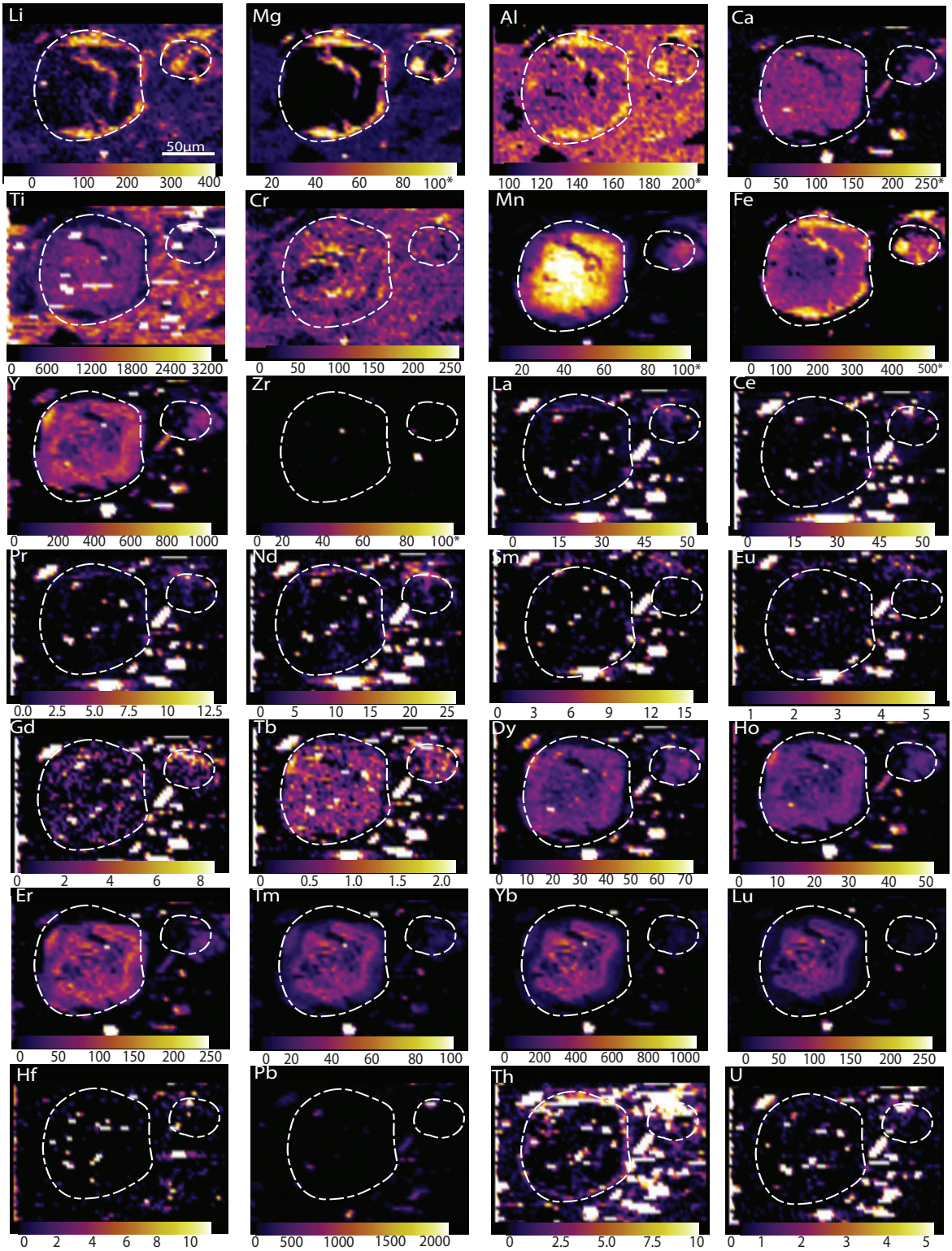

ANG15a

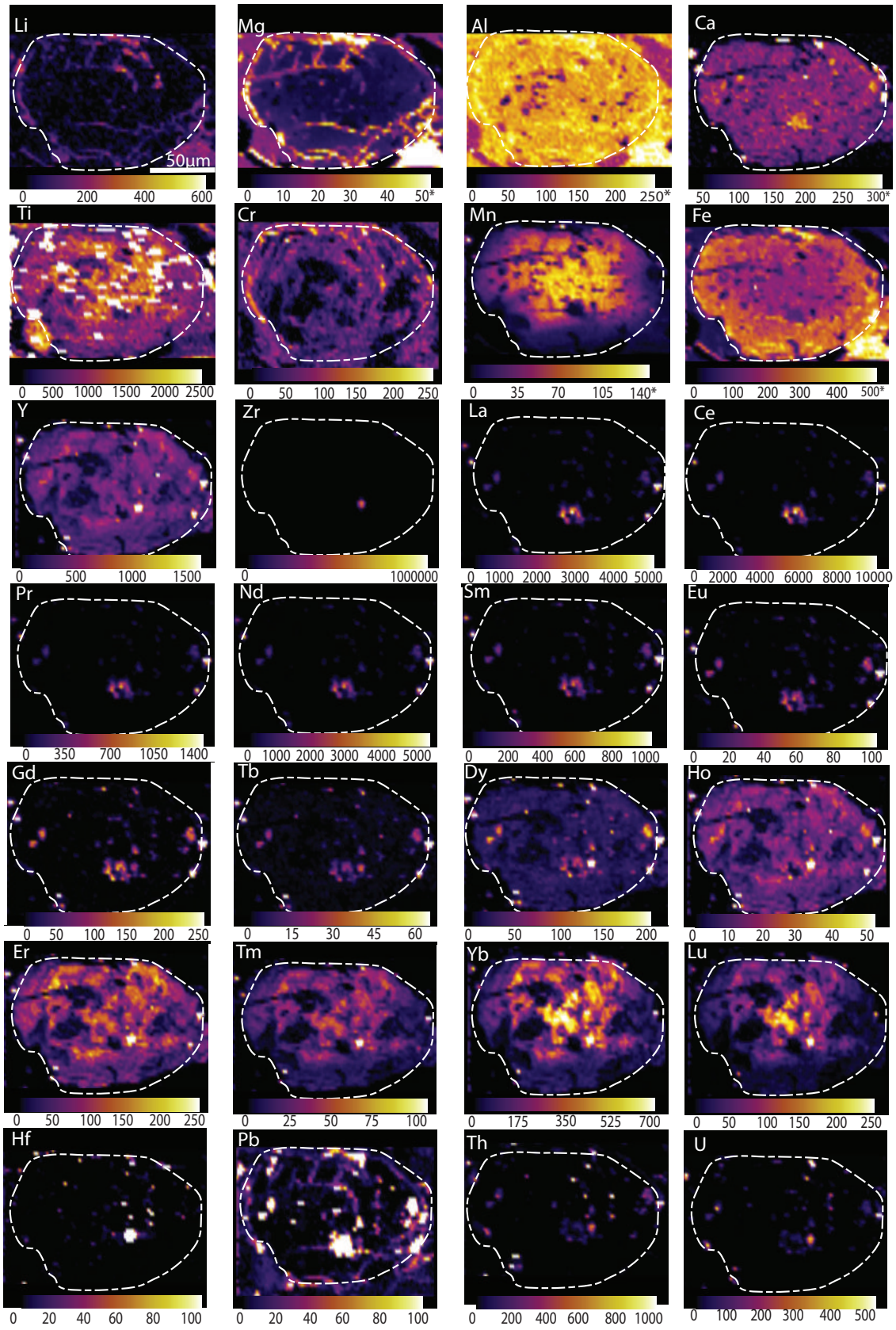
Li
50µm
0 200 400 600
Mg
0 10 20 30 40 50*
Al
0 50 100 150 200 250*
Ca
50 100 150 200 250 300*
Ti
0 500 1000 1500 2000 2500
Cr
0 50 100 150 200 250
Mn
0 35 70 105 140*
Fe
0 100 200 300 400 500*
Y
0 500 1000 1500
Zr
0 1000000
La
0 1000 2000 3000 4000 5000
Ce
0 2000 4000 6000 8000 10000
Pr
0 350 700 1050 1400
Nd
0 1000 2000 3000 4000 5000
Sm
0 200 400 600 800 1000
Eu
0 20 40 60 80 100
Gd
0 50 100 150 200 250
Tb
0 15 30 45 60
Dy
0 50 100 150 200
Ho
0 10 20 30 40 50
Er
0 50 100 150 200 250
Tm
0 25 50 75 100
Yb
0 175 350 525 700
Lu
0 50 100 150 200 250
Hf
0 20 40 60 80 100
Pb
0 20 40 60 80 100
Th
0 200 400 600 800 1000
U
0 100 200 300 400 500

APPENDIX D: WHOLE ROCK GEOCHEMISTRY RESULTS

Specimen	ANG12B	ANG13A	ANG13B	ANG15A	ANG16	ANG7-18
SiO_2	68.18	68.58	65.69	69.58	61.53	71.84
TiO_2	0.63	0.62	0.69	0.58	0.77	0.61
Al2O3	17.37	16.56	18.56	16.24	21.14	14.44
Fe2O3T	4.42	4.82	4.37	4.23	5.56	4.42
MnO	0.08	0.11	0.15	0.12	0.10	0.17
MgO	1.50	1.50	1.41	1.38	1.89	1.36
CaO	0.23	0.53	0.35	0.64	0.23	0.12
Na2O	3.60	3.39	3.74	3.49	2.62	2.10
K2O	3.88	3.80	4.63	3.49	6.00	4.56
P2O5	0.13	0.12	0.09	0.10	0.13	0.09
Total	**100.02**	**100.03**	**99.68**	**99.85**	**99.97**	**99.71**
LOI	2.75	2.91	2.98	2.79	3.50	2.65
FeO	2.25	2.47	1.62	2.56	2.78	1.36
Fe2O3	1.92	2.07	2.57	1.38	2.47	2.91
Rb	177.3	162.7	215.1	153.4	270.7	178.5
Sr	46	47	48	59	48	24
Y	26.8	45.2	15.9	39.1	26.3	33.7
Zr	314	324	369	285	360	303
V	77	72	74	70	89	80
Ni	25	22	21	20	26	13
Cr	79	72	81	26	30	24
Nb	20.0	19.0	20.9	17.7	24.8	19.1
Ga	22.9	23.3	26.0	22.9	30.6	21.0
Cu	30	22	30	29	34	17
Zn	95	94	99	95	100	75
Co	6	7	5	6	7	4
Ba	796	837	976	798	1144	578
La	16	53	19	43	23	34
Ce	97	97	84	70	119	73
U	2.3	<0.5	0.6	<0.5	<0.5	<0.5
Th	25.2	26.7	29.7	28.0	30.0	23.1
Sc	8	9	9	7	12	5
Pb	<1	6	4	<1	<1	<1

Geochemical results from samples used in this study. Total Fe is presented as Ferric iron.

APPENDIX E: GEOCHEMICAL PLOTS